

Rochester Institute of Technology

## RIT Digital Institutional Repository

---

### Theses

---

1-2013

## Photophysical and Photochemical Effects of UV and VUV Photo-Oxidation and Photolysis on PET and PEN

Andrew Morgan

Follow this and additional works at: <https://repository.rit.edu/theses>

---

### Recommended Citation

Morgan, Andrew, "Photophysical and Photochemical Effects of UV and VUV Photo-Oxidation and Photolysis on PET and PEN" (2013). Thesis. Rochester Institute of Technology. Accessed from

This Thesis is brought to you for free and open access by the RIT Libraries. For more information, please contact [repository@rit.edu](mailto:repository@rit.edu).

**PHOTOPHYSICAL AND PHOTOCHEMICAL EFFECTS  
OF UV AND VUV PHOTO-OXIDATION AND  
PHOTOLYSIS ON PET AND PEN**

A Thesis Presented to the School  
of  
Chemistry and Materials Science and Engineering  
College of Science  
At Rochester Institute of Technology  
Rochester, New York 14623

In Partial Fulfillment of  
the Requirement for the Degree  
of Masters of Science in Materials Science & Engineering

By:  
Andrew Morgan

January 2013

**CERTIFICATION OF APPROVAL**

**PHOTOPHYSICAL AND PHOTOCHEMICAL EFFECTS  
OF UV AND VUV PHOTO-OXIDATION AND  
PHOTOLYSIS ON PET AND PEN**

By:

Andrew Morgan

_____ Research Advisor	_____ Date
Dr. Gerald A. Takacs	
Professor of Chemistry and Materials Science & Engineering	

_____ Director D. KSV Santhanam	_____ Date
Professor of Chemistry and Materials Science & Engineering	

**COPYRIGHT RELEASE FORM**

**PHOTOPHYSICAL AND PHOTOCHEMICAL EFFECTS  
OF UV AND VUV PHOTO-OXIDATION AND  
PHOTOLYSIS ON PET AND PEN**

I, Andrew Morgan, hereby grant permission to the Wallace Memorial Library of the Rochester Institute of Technology to reproduce this thesis in its entirety or in part. Any reproduction will be with the intent to contribute to the proliferation of knowledge and understanding in the scientific community and will not be for commercial use or profit.

---

Andrew Morgan

---

Date

## **DEDICATIONS**

I appreciatively dedicate my work to my family and friends. A genuine obliged sincerity to my loving and supportive parents, Maher and Hanaa Morgan for their care and provisions that led me to ultimately start and finish my Master's degree. A special feeling of appreciation to my sister, Heidi Morgan for her great emotional support. I would also like to thank my brother and my sister-in-law for their words of encouragement. I earnestly also appreciate the emotional and spiritual support of my friends and my church.

## ACKNOWLEDGMENT

I would like to express my deepest and most sincere gratitude to my research advisor as well as my committee member, Dr. Gerald Takacs, whose patience and intelligence made my thesis possible. His support and accessibility allowed me to successfully finish my research. The advice and assistance facilitated my completion of this thesis, manuscript, and seminar presentation.

I would also like to thank Dr. Matt Miri for his support and advice during my proposal. A special regards to the rest of my thesis committee members, Dr. Kalathur Santhanam and Dr. Alan Entenberg, for their honesty and integrity as well as their willingness to clear up their busy schedules to assess my research and thesis.

A much deserved feelings of appreciation and regards to Dr. Tom Debies, Michael Mehan, Greg Thompson, and Xerox Corp. for their concise and timely XPS and SEM analysis. I would like to express my sincere gratitude for Tom Allston for his very important guidance with instrumentation and methods of analysis.

I would finally like to thank all my research colleagues, Ryan Divens, Lisa Andrews, Ameya Khot, and Algis Naujokas for all their support and encouragement during my research.

## TABLE OF CONTENTS

	PAGE
<b>CERTIFICATION OF APPROVAL</b> .....	i
<b>COPYRIGHT RELEASE FORM</b> .....	ii
<b>DEDICATION</b> .....	iii
<b>ACKNOWLEDGMENT</b> .....	iv
<b>TABLE OF CONTENTS</b> .....	v
<b>LIST OF TABLES</b> .....	xiii
<b>LIST OF FIGURES</b> .....	xvii
<b>ABSTRACT</b> .....	xxvi
<b>1 INTRODUCTION</b> .....	1
<b>1.1</b> Surface modification versus bulk region reactions .....	1
<b>1.2</b> Poly(Ethylene Terephthalate) (PET) .....	1
<b>1.3</b> Poly(Ethylene 2,6-Napthalate) (PEN).....	3
<b>1.4</b> UV photo-oxidation reactions.....	4
<b>1.5</b> UV photolysis reactions.....	6
<b>1.6</b> Vacuum UV (VUV) plasma phase photo-oxidation .....	6
<b>1.7</b> Vacuum UV plasma phase photoreactions .....	7
<b>1.8</b> Remote oxygen atom reactions.....	8
<b>1.9</b> Implications of bulk modifications of PET and PEN.....	9
<b>1.10</b> Implications of surface modification for PET and PEN.....	9
<b>2 RESEARCH OBJECTIVES</b> .....	11
<b>3 EXPERIMENTAL</b> .....	13

<b>3.1</b>	<b>Materials.....</b>	<b>13</b>
3.1.1	Poly(ethylene terephthalate).....	13
3.1.2	Poly(ethylene 2,6-naphthalate).....	13
<b>3.2</b>	<b>UV photoreactions.....</b>	<b>14</b>
3.2.1	Atmospheric pressure UV photo-oxidation.....	14
3.2.2	Atmospheric pressure UV photo-ozonation.....	17
3.2.3	Atmospheric pressure UV photolysis.....	20
<b>3.3</b>	<b>Plasma photoreactions.....</b>	<b>21</b>
3.3.1	VUV photo-oxidation.....	21
3.3.2	VUV photolysis.....	23
<b>3.4</b>	<b>Remote oxygen reaction.....</b>	<b>23</b>
3.4.1	MW discharge of Ar and O <sub>2</sub> mixture.....	23
3.4.2	MW discharge of Ar.....	25
<b>3.5</b>	<b>Analysis techniques.....</b>	<b>25</b>
3.5.1	X-Ray Photoelectron Spectroscopy (XPS).....	25
3.5.2	Scanning Electron Microscopy (SEM).....	28
3.5.3	UV Absorption Spectroscopy.....	29
3.5.4	FTIR.....	32
3.5.5	Contact angle goniometry.....	35
<b>4</b>	<b>RESULTS.....</b>	<b>37</b>
<b>4.1</b>	<b>XPS.....</b>	<b>37</b>
4.1.1	Untreated controls.....	37
I	PET control.....	37



<b>II</b>	PEN control.....	38
<b>4.1.2</b>	UV photo-oxidation.....	39
<b>I.</b>	Atmospheric pressure 300 nm broad spectrum UV photo-oxidation of PET.....	39
<b>II.</b>	Atmospheric pressure 253.7 nm UV photo-oxidation of PET.....	41
<b>4.1.3</b>	Atmospheric pressure 184.9/253.7 nm UV photo-ozonation of PET.....	43
<b>4.1.4</b>	UV photolysis.....	46
<b>I.</b>	Atmospheric pressure 300 nm broad spectrum UV photolysis of PET in nitrogen.....	46
<b>II.</b>	Atmospheric pressure 253.7 nm UV photolysis of PET in nitrogen.....	49
<b>III.</b>	Atmospheric pressure 184.9/253.7 nm UV photolysis of PET in nitrogen.....	52
<b>4.1.5</b>	VUV photo-oxidation.....	54
<b>I.</b>	VUV photo-oxidation of PET using Ar plasma.....	54
<b>II.</b>	VUV photo-oxidation of PEN using Ar plasma.....	56
<b>4.1.6</b>	VUV photolysis.....	59
<b>I.</b>	VUV photolysis of PET using Ar plasma.....	59
<b>II.</b>	VUV photolysis of PEN using Ar plasma.....	61
<b>4.1.7</b>	Remote O and/or Ar radical exposure in the absence of photons.....	64
<b>I.</b>	MW discharge of Ar/O <sub>2</sub> and Ar plasma on PET.....	64
<b>II.</b>	MW discharge of Ar/O <sub>2</sub> and Ar plasma on PEN.....	67
<b>4.2</b>	Contact angle.....	71
<b>4.2.1</b>	UV photo-oxidation.....	71

I.	Atmospheric pressure 300 nm broad spectrum UV photo-oxidation of PET.....	71
II.	Atmospheric pressure 253.7 nm UV photo-oxidation of PET.....	71
4.2.2	Atmospheric pressure 184.9/253.7 nm UV photo-ozonation of PET.....	72
4.2.3	UV photolysis.....	73
I.	Atmospheric pressure 300 nm broad spectrum UV photolysis of PET in nitrogen.....	73
II.	Atmospheric pressure 253.7 nm UV photolysis of PET in nitrogen.....	73
III.	Atmospheric pressure 184.9/253.7 nm UV photolysis of PET in nitrogen.....	74
4.2.4	VUV photo-oxidation.....	75
I.	VUV photo-oxidation of PET using Ar plasma.....	75
II.	VUV photo-oxidation of PEN using Ar plasma.....	75
4.2.5	VUV photolysis.....	76
I.	VUV photolysis of PET using Ar plasma.....	76
II.	VUV photolysis of PEN using Ar plasma.....	77
4.2.6	Remote O and/or Ar radical exposure in the absence of photons.....	78
I.	Remote MW discharge of Ar/O <sub>2</sub> plasma on PET.....	78
II.	MW discharge of Ar/O <sub>2</sub> plasma on PEN.....	78
4.3	SEM.....	79
4.3.1	UV photo-oxidation.....	79
I.	Atmospheric pressure 300 nm broad spectrum UV photo-oxidation of PET.....	79

II.	Atmospheric pressure 253.7 nm UV photo-oxidation of PET.....	80
4.3.2	Atmospheric pressure 184.9/253.7 nm UV photo-ozonation of PET.....	81
4.4	UV absorption spectroscopy.....	81
4.4.1	UV photo-oxidation.....	82
I.	Atmospheric pressure 300 nm broad spectrum UV photo-oxidation of PET.....	82
II.	Atmospheric pressure 253.7 nm UV photo-oxidation of PET.....	83
4.4.2	Atmospheric pressure 184.9/253.7 nm UV photo-ozonation of PET.....	84
4.4.3	UV Photolysis.....	85
I.	Atmospheric pressure 300 nm broad spectrum UV photolysis of PET in nitrogen.....	85
II.	Atmospheric pressure 253.7 nm UV photolysis of PET in nitrogen.....	86
III.	Atmospheric pressure 184.9/253.7 nm UV photolysis of PET in nitrogen.....	87
4.4.4	VUV photo-oxidation.....	88
I.	VUV photo-oxidation of PET using Ar plasma.....	88
II.	VUV photo-oxidation of PEN using Ar plasma.....	89
4.4.5	VUV photolysis.....	90
I.	VUV photolysis of PET using Ar plasma.....	90
II.	VUV photolysis of PEN using Ar plasma.....	91
4.4.6	Remote oxygen exposure in the absence of photons.....	92
I.	MW discharge of Ar/O <sub>2</sub> plasma on PET in vacuum.....	92

II.	MW discharge of Ar/O <sub>2</sub> plasma on PEN in vacuum.....	93
<b>4.5</b>	<b>FTIR.....</b>	<b>94</b>
<b>4.5.1</b>	<b>UV photo-oxidation.....</b>	<b>94</b>
I.	Atmospheric pressure 300 nm broad spectrum UV photo-oxidation of PET.....	94
II.	Atmospheric pressure 253.7 nm UV photo-oxidation of PET.....	95
<b>4.5.2</b>	<b>Atmospheric pressure 184.9/253.7 nm UV photo-ozonation of PET.....</b>	<b>97</b>
<b>4.5.3</b>	<b>UV photolysis.....</b>	<b>99</b>
I.	Atmospheric pressure 300 nm broad spectrum UV photolysis of PET in nitrogen.....	99
II.	Atmospheric pressure 253.7 nm UV photolysis of PET in nitrogen.....	99
III.	Atmospheric pressure 184.9/253.7 nm UV photolysis of PET in nitrogen.....	100
<b>4.5.4</b>	<b>VUV photo-oxidation.....</b>	<b>103</b>
I.	VUV photo-oxidation of PET using Ar plasma.....	103
II.	VUV photo-oxidation of PEN using Ar plasma.....	103
<b>4.5.5</b>	<b>VUV photolysis.....</b>	<b>106</b>
I.	VUV photolysis of PET using Ar plasma.....	106
II.	VUV photolysis of PEN using Ar plasma.....	107
<b>4.5.6</b>	<b>Remote oxygen exposure in the absence of photons.....</b>	<b>109</b>
I.	MW discharge of Ar/O <sub>2</sub> plasma on PET in vacuum.....	109
II.	MW discharge of Ar/O <sub>2</sub> plasma on PEN in vacuum.....	109
<b>5</b>	<b>DISCUSSION.....</b>	<b>112</b>

<b>5.1</b>	Extent of light penetration.....	112
<b>5.2</b>	Photophysical and photochemical aspects of UV photo-oxidized PET.....	115
<b>I.</b>	Effect of UV photo-oxidation at the surface.....	115
<b>II.</b>	Effect of UV photo-oxidation at the transitional-bulk layers.....	125
<b>III.</b>	Comparison of the treatments to each other and to the available literature...	130
<b>5.3</b>	Photophysical and photochemical aspects of atmospheric pressure UV photo- ozonation treated PET.....	131
<b>I.</b>	Effect of UV photo-ozonation at the surface.....	131
<b>II.</b>	Effect of UV photo-ozonation at the transitional-bulk layers.....	133
<b>III.</b>	Comparison of UV photo-ozonation to UV photo-oxidation and to the available literature.....	135
<b>5.4</b>	Photophysical and photochemical aspects of atmospheric pressure UV photolysis treated PET in nitrogen.....	136
<b>I.</b>	Effect of UV photolysis at the surface.....	136
<b>II.</b>	Effect of UV photolysis at the transitional-bulk layers.....	137
<b>III.</b>	Comparison of UV photolysis to UV photo-oxidation and to the available literature.....	138
<b>5.5</b>	Photophysical and photochemical aspects of VUV photo-oxidation treated PET and PEN.....	140
<b>I.</b>	Effect of VUV photo-oxidation at the surface.....	140
<b>II.</b>	Effect of VUV photo-oxidation at the transitional-bulk layers.....	141
<b>III.</b>	Comparison of the VUV photo-oxidation on each polymer and to the available literature.....	142

<b>5.6</b>	Photophysical and photochemical aspects of VUV photolysis treated PET and PEN.....	143
<b>I.</b>	Effect of VUV photolysis at the surface.....	143
<b>II.</b>	Effect of VUV photolysis at the transitional-bulk layers.....	144
<b>III.</b>	Comparison of VUV photolysis on each polymer with the VUV photo-oxidation treatment and to the available literature.....	145
<b>5.7</b>	Photophysical and photochemical aspects of remote oxygen and/or argon reaction with PET and PEN.....	146
<b>I.</b>	Effect of the remote oxygen and argon at the surface.....	146
<b>II.</b>	Effect of the remote oxygen at the transitional-bulk layers.....	148
<b>III.</b>	Comparison of the remote oxygen treatment to VUV photo-oxidation treatment and to the available literature.....	149
<b>6</b>	<b>FUTURE WORK.....</b>	<b>151</b>
<b>7</b>	<b>CONCLUSION.....</b>	<b>152</b>
	<b>REFERENCES.....</b>	<b>154</b>

## LIST OF TABLES

	PAGE
<b>Table 1:</b> XPS literature assignment of various functional groups in a C 1s peak [52].....	27
<b>Table 2:</b> IR spectra peak assignment for functional groups on PET and PEN [51, 55-59].....	35
<b>Table 3:</b> XPS elemental percent composition of PET exposed to the 300 nm broad spectrum UV photo-oxidation treatment.....	40
<b>Table 4:</b> XPS C 1s functional group analysis for the 300 nm broad spectrum UV photo-oxidation of PET.....	41
<b>Table 5:</b> XPS elemental percent composition of PET exposed to the 253.7 nm UV photo-oxidation treatment.....	42
<b>Table 6:</b> XPS C 1s functional groups analysis for the 253.7 nm UV Photo-oxidation of PET.....	43
<b>Table 7:</b> XPS elemental percent composition of PET exposed to the 184.9/253.7 nm UV photo-ozonation treatment.....	44
<b>Table 8:</b> XPS C 1s functional groups analysis for the 184.9/253.7 nm UV photo-ozonation of PET.....	45
<b>Table 9:</b> XPS elemental percent composition of PET exposed to a 300 nm broad spectrum UV photolysis in nitrogen.....	47
<b>Table 10:</b> XPS C 1s functional groups analysis for the 300 nm broad spectrum UV photolysis of PET in nitrogen.....	49
<b>Table 11:</b> XPS elemental percent composition of PET exposed to a 253.7 nm UV photolysis in nitrogen.....	50

<b>Table 12:</b> XPS C 1s functional groups analysis for the 253.7 nm UV photolysis of PET in nitrogen.....	51
<b>Table 13:</b> XPS elemental percent composition of PET exposed to a 184.9/253.7 nm UV photolysis in nitrogen.....	52
<b>Table 14:</b> XPS C 1s functional groups analysis for the 184.9/253.7 nm UV photolysis of PET in nitrogen.....	54
<b>Table 15:</b> XPS elemental percent composition of PET exposed to VUV photo-oxidation.....	55
<b>Table 16:</b> XPS C 1s functional groups analysis for the VUV photo-oxidation of PET.....	56
<b>Table 17:</b> XPS elemental percent composition of PEN exposed to VUV photo-oxidation.....	57
<b>Table 18:</b> XPS C 1s functional groups analysis for the VUV photo-oxidation of PEN.....	59
<b>Table 19:</b> XPS elemental percent composition of PET exposed to VUV photolysis.....	60
<b>Table 20:</b> XPS C 1s functional groups analysis for the VUV photolysis of PET.....	61
<b>Table 21:</b> XPS elemental percent composition of PEN exposed to VUV photolysis.....	62
<b>Table 22:</b> XPS C 1s functional groups analysis for the VUV photolysis of PEN.....	64
<b>Table 23:</b> XPS elemental percent composition of PET exposed to remote oxygen atoms in the absence of photons.....	65



<b>Table 24:</b> XPS C 1s functional groups analysis for PET exposed to remote oxygen atoms in the absence of photons.....	67
<b>Table 25:</b> XPS elemental percent composition of PEN exposed to remote oxygen or argon atoms in the absence of photons.....	68
<b>Table 26:</b> XPS C 1s functional groups analysis for PEN exposed to remote oxygen or argon atoms in the absence of photons.....	70
<b>Table 27:</b> Percent change in the total UV absorption of PET due to the 300 nm broad spectrum UV photo-oxidation treatment.....	82
<b>Table 28:</b> Percent change in the total UV absorption of PET due to the 253.7 nm UV photo-oxidation treatment.....	83
<b>Table 29:</b> Percent change in the total UV absorption of PET due to the 184.9/253.7 nm UV photo-ozonation.....	84
<b>Table 30:</b> Percent change in the total UV absorption of PET due to the 300 nm broad spectrum UV photolysis in nitrogen.....	85
<b>Table 31:</b> Percent change in the total UV absorption of PET due to the 253.7 nm UV photolysis in nitrogen.....	86
<b>Table 32:</b> Percent change in the total UV absorption of PET due to the 184.9/253.7 nm UV photolysis in nitrogen.....	87
<b>Table 33:</b> Percent change in the total UV absorption of PET due to VUV photo-oxidation.....	88
<b>Table 34:</b> Percent change in the total UV absorption of PEN due to VUV photo-oxidation.....	89
<b>Table 35:</b> Percent change in the total UV absorption of PET due to VUV photolysis.....	90

<b>Table 36:</b> Percent change in the total UV absorption of PEN due to VUV photolysis.....	91
<b>Table 37:</b> Percent change in the total UV absorption of PET due to remote oxygen atom exposure in the absence of photons.....	92
<b>Table 38:</b> Percent change in the total UV absorption of PEN due to remote oxygen atom exposure in the absence of photons.....	93
<b>Table 39:</b> IR functional group analysis of the 300 nm broad spectrum and 253.7 nm UV photo-oxidized PET film.....	96
<b>Table 40:</b> FTIR functional group analysis of the 184.9/253.7 nm UV photo-ozonated PET.....	98
<b>Table 41:</b> IR functional group analysis of the 300 nm broad spectrum, 253.7 nm, and 184.9/253.7nm UV photolysis of PET.....	102
<b>Table 42:</b> IR functional group analysis of the VUV photo-oxidation treated PET and PEN.....	105
<b>Table 43:</b> IR functional group analysis of the VUV photolysis treated PET and PEN...	108
<b>Table 44:</b> IR functional group analysis of the remote oxygen reaction with PET and PEN.....	111

## LIST OF FIGURES

	PAGE
<b>Figure 1:</b> Poly(Ethylene Terephthalate) (PET) structure.....	2
<b>Figure 2:</b> Poly(Ethylene 2,6-Naphthalate) (PEN) structure.....	3
<b>Figure 3:</b> The UV photo-absorption spectrum of PET and PEN, where the identifiable peaks are labeled from I to VII [28].....	4
<b>Figure 4:</b> The emission spectrum of the medium pressure mercury lamp, labeled as RPR-3000 and is shown in blue [46].....	15
<b>Figure 5:</b> Custom made quartz glass UV sample holder/chamber. The polymer film is placed horizontally with the notch in the upper left corner as shown in the figure.....	16
<b>Figure 6:</b> The quartz chamber is placed in the middle of the photoreactor. The gas supply line is connected (shown on right) to one side and the other side (left) is an outlet.....	16
<b>Figure 7:</b> The UV absorption spectrum of oxygen (O <sub>2</sub> ) gas [47].....	18
<b>Figure 8:</b> Nitrogen gas absorption spectrum is located mainly in VUV region [49].....	19
<b>Figure 9:</b> A Rayonet photo-reactor chamber.....	20
<b>Figure 10:</b> Ar plasma pointing down towards the sample inside the vacuum chamber....	21
<b>Figure 11:</b> Schematic of the VUV photo-oxidation setup [50].....	22
<b>Figure 12:</b> Schematic of the remote oxygen atom reaction setup [50].....	24
<b>Figure 13:</b> Schematic of the parallel placement of the plasma source, to remove the interaction of photons with the sample while still being downstream.....	24
<b>Figure 14:</b> Simulation of 50 primary electron scattering into a material [51].....	29
<b>Figure 15:</b> Schematics of the ISR-2200 Integrating Spherical attachment [53].....	31
<b>Figure 16:</b> Depth of ATR analysis as a function of the wavenumber for PET [51, 54]...	33

<b>Figure 17:</b> Depth of ATR analysis as function of the wavenumber for PEN [51, 54].....	33
<b>Figure 18:</b> The increase in contact angle from a hydrophilic to a more hydrophobic surface [60].....	36
<b>Figure 19:</b> The C 1s spectrum of an untreated and washed PET sample.....	38
<b>Figure 20:</b> The C 1s spectrum of an untreated and washed PEN sample.....	39
<b>Figure 21:</b> Overlapped C1s spectra of the 300 nm broad spectrum UV photo-oxidized PET per the exposure times; where 1-5 are 30, 60, 90, 120, and 150 min, respectively...	40
<b>Figure 22:</b> C 1s spectra of 253.7 nm UV photo-oxidized PET samples; where red, blue, cyan , green, and magenta are the 0, 60, 90, 120, and 150 min treated samples, respectively.....	42
<b>Figure 23:</b> C 1s spectra of 184.9/253.7 nm UV photo-ozonated PET samples; where 1-4 shown on z axis are the 4, 8, 15, and 30 min treated samples, respectively.....	44
<b>Figure 24:</b> Depth profile XPS analysis of a 15 min 184.9/253.7 nm UV photo-ozonation treated PET sample.....	46
<b>Figure 25:</b> The overlapped C 1s spectrum of each of the 300 nm broad spectrum UV photolysis treated PET samples; where red, green, blue, cyan, magenta, and yellow are the 30, 60, 90, 120, 150, and 180 min treated samples, respectively.....	48
<b>Figure 26:</b> The C 1s spectrums of the 253.7 nm UV photolysis treated PET samples in nitrogen; where red, blue, green, cyan, magenta, and yellow are the 15, 33, 45, 60, 90, and 120 min treated samples, respectively.....	51
<b>Figure 27:</b> The overlapped C 1s spectra of the 184.9/253.7 nm UV photolysis treated PET samples in nitrogen; where red, blue, yellow, green, magenta, and cyan are the 5, 10, 15, 25, 45, and 60 min treatment times, respectively.....	53

<b>Figure 28:</b> The overlapped C 1s spectrum of the VUV photo-oxidized PET samples; where 1-5 in the z-axis are the 30, 60, 90, 120, and 150 min treatment times, respectively.....	55
<b>Figure 29:</b> The overlapped C 1s spectrum of the VUV photo-oxidized PEN samples; where 1-5 are the 5, 10, 15, 20, and 25 min treatment times, respectively.....	58
<b>Figure 30:</b> The C 1s spectrums of the VUV photo-oxidized PEN samples; where 1-5 are the 30, 60, 90, 120, and 150 min treatment times, respectively.....	58
<b>Figure 31:</b> The C 1s spectrums of the VUV photolysis treated PET samples; where yellow, magenta, green, pale green, cyan, and blue are the 15, 30, 60, 90, 120, and 150 min treatment times, respectively.....	60
<b>Figure 32:</b> The overlapped C 1s spectra of the VUV photolysis treated PEN samples; where 1-7 on the z axis are the 5, 15, 30, 60, 90, 120, and 150 min treated samples, respectively.....	63
<b>Figure 33:</b> The overlapped C 1s spectrum of the remote argon treated PET samples; where red, blue, and cyan are the 30, 60, and 90 min treated samples, respectively.....	66
<b>Figure 34:</b> The C 1s spectrums of the remote oxygen treated PET samples; where 2-6 on the z-axis are the 30, 60, 90, 120, and 150 min treated samples, respectively. Plot #1 is the 60 min remote argon treated sample as a comparison.....	66
<b>Figure 35:</b> The overlapped C 1s spectrum of the remote oxygen and remote argon treated stabled; where 1-3 are the 0, 10, and 60 min remote argon treated samples while the 4-14 are the 5, 10, 15, 20, 25, 30, 60, 90, 120, and 150 min remote oxygen treated samples, respectively.....	69

<b>Figure 36:</b> Percent change in the advancing contact angle on PET due to the 300 nm broad spectrum UV photo-oxidation treatment.....	71
<b>Figure 37:</b> Percent change in the advancing contact angle on PET due to 253.7 nm UV photo-oxidation.....	72
<b>Figure 38:</b> Percent change in the advancing contact angle on PET due to the 184.9/253.7 nm UV photo-ozonation treatment.....	72
<b>Figure 39:</b> Percent change in the advancing contact angle on PET due to the 300 nm broad spectrum UV photolysis in nitrogen.....	73
<b>Figure 40:</b> Percent change in the advancing contact angle on PET due to the 253.7 nm UV photolysis in nitrogen.....	74
<b>Figure 41:</b> Percent change in the advancing contact angle on PET due to the 184.9/253.7 nm UV photolysis in nitrogen.....	74
<b>Figure 42:</b> Percent change in the advancing contact angle on PET due to VUV photo-oxidation.....	75
<b>Figure 43:</b> Percent change in the advancing contact angle on PEN due to VUV photo-oxidation.....	76
<b>Figure 44:</b> Percent change in the advancing contact angle on PET due to VUV photolysis.....	77
<b>Figure 45:</b> Percent change in the advancing contact angle on PEN due to VUV photolysis.....	77
<b>Figure 46:</b> Percent change in the advancing contact angle on PET due to remote oxygen atom exposure in the absence of photons.....	78

<b>Figure 47:</b> Percent change in the advancing contact angle on PEN due to remote oxygen atom exposure in the absence of photons.....	79
<b>Figure 48:</b> SEM scans of 10, 50, and 100kX (left to right) magnification of untreated (top) and 90 min 300 nm broad spectrum UV photo-oxidation treated (bottom) PET films.....	80
<b>Figure 49:</b> SEM scans of 10, 50, and 100kX (left to right) magnification of untreated (top) and 90 min 253.7 nm UV photo-oxidation treated (bottom) PET films.....	80
<b>Figure 50:</b> SEM scans of 10, 50, and 100kX (left to right) magnification of untreated (top) and 15 min 184.9/253.7 nm UV photo-ozonation treated (bottom) PET films.....	81
<b>Figure 51:</b> Percent change in the UV absorption of PET per wavelength due the 300 nm broad spectrum UV photo-oxidation treatment.....	82
<b>Figure 52:</b> Percent change in the UV absorption of PET per wavelength due 253.7 nm UV photo-oxidation.....	83
<b>Figure 53:</b> Percent change in the UV absorption of PET per wavelength due the 184.9/253.7 nm UV photo-ozonation treatment.....	84
<b>Figure 54:</b> Percent change in the UV absorption of PET per wavelength due the 300 nm broad spectrum UV photolysis in nitrogen.....	85
<b>Figure 55:</b> Percent change in the UV absorption of PET per wavelength due the 253.7 nm UV photolysis in nitrogen.....	86
<b>Figure 56:</b> Percent change in the UV absorption of PET per wavelength due the 184.9/253.7 nm UV photolysis in nitrogen.....	87
<b>Figure 57:</b> Percent change in the UV absorption of PET per wavelength due to VUV photo-oxidation.....	88

<b>Figure 58:</b> Percent change in the UV absorption of PEN per wavelength due VUV photo-oxidation.....	89
<b>Figure 59:</b> Percent change in the UV absorption of PET per wavelength due VUV photolysis.....	90
<b>Figure 60:</b> Percent change in the UV absorption of PEN per wavelength due VUV photolysis.....	91
<b>Figure 61:</b> Percent change in the UV absorption of PET per wavelength due to remote oxygen atom exposure in the absence of photons.....	92
<b>Figure 62:</b> Percent change in the UV absorption of PEN per wavelength due to remote oxygen atom exposure in the absence of photons.....	93
<b>Figure 63:</b> The change in relative absorbance on IR spectra of PET due to the 300 nm broad spectrum UV photo-oxidation treatment.....	94
<b>Figure 64:</b> The change in relative absorbance on IR spectra of PET due to the 253.7 nm UV photo-oxidation.....	95
<b>Figure 65:</b> The change in relative absorbance on IR spectra of PET due to the 184.9/253.7 nm UV photo-ozonation treatment.....	97
<b>Figure 66:</b> The change in relative absorbance on IR spectra of PET due to the 300 nm broad spectrum UV photolysis in nitrogen.....	99
<b>Figure 67:</b> The change in relative absorbance on IR spectra of PET due to the 253.7 nm UV photolysis in nitrogen.....	100
<b>Figure 68:</b> The change in relative absorbance on IR spectra of PET due to the 184.9/253.7 nm UV photolysis in nitrogen.....	101



<b>Figure 69:</b> The change in relative absorbance on IR spectra of PET due to the VUV photo-oxidation.....	103
<b>Figure 70:</b> The change in relative absorbance on IR spectra of PEN due to the VUV photo-oxidation.....	104
<b>Figure 71:</b> The change in relative absorbance on IR spectra of PET due to the VUV photolysis.....	106
<b>Figure 72:</b> The change in relative absorbance on IR spectra of PEN due to the VUV photolysis.....	107
<b>Figure 73:</b> The change in relative absorbance on IR spectra of PET due to remote oxygen atom exposure in the absence of photons.....	109
<b>Figure 74:</b> The change in relative absorbance on IR spectra of PEN due to remote oxygen atom exposure in the absence of photons.....	110
<b>Figure 75:</b> Photon depth of penetration throughout the washed and untreated 0.01mm PET film.....	113
<b>Figure 76:</b> Photon depth of penetration throughout the washed and untreated 0.01mm PEN film.....	113
<b>Figure 77:</b> Photon population density as a function of depth within a 253.7 nm UV photoemission treated PET sample.....	115
<b>Figure 78:</b> The Norrish IA(bottom) and IB(top) mechanism applied on PET [30, 62]. Note: Same pathway can be applied for PEN by replacing the benzene (1,4 substitution) group with naphthalate (2,6 substitution).....	116
<b>Figure 79:</b> Norrish type I applied to PEN after delocalization of radical across C-O bond [19]. Note: Same pathway can be applied for PET by replacing the naphthalate (2,6 substitution) with. benzene (1,4 substitution).....	117

<b>Figure 80:</b> The Norrish II mechanism applied on PET [30]. Note: Same pathway can be applied for PEN by replacing the benzene (1,4 substitution) group with naphthalate (2,6 substitution).....	117
<b>Figure 81:</b> Formation and break down of hydroperoxide on PEN [19]. Note: Same pathway can be applied for PET by replacing the naphthalate (2,6 substitution) with. benzene (1,4 substitution).....	118
<b>Figure 82:</b> Propagation of the breakdown of the hydroperoxide on PEN [19]. Note: Same pathway can be applied for PET by replacing the naphthalate (2,6 substitution) with. benzene (1,4 substitution).....	119
<b>Figure 83:</b> Termination sequence via a cage reaction to produce an anhydride on PEN [19]. Note: Same pathway can be applied for PET by replacing the naphthalate (2,6 substitution) with. benzene (1,4 substitution).....	119
<b>Figure 84:</b> Carboxylic acid end group formation of PET via dehydrogenation [40]. Note: Same pathway can be applied for PEN by replacing the benzene (1,4 substitution) group with naphthalate (2,6 substitution).....	120
<b>Figure 85:</b> Propagation and evolution of CO gas from Norrish IA and IB initiated PET [30]. Note: Same pathway can be applied for PEN by replacing the benzene (1,4 substitution) group with naphthalate (2,6 substitution).....	121
<b>Figure 86:</b> Termination mechanism of Norrish type IB initiated PET to form aldehydes [30]. Note: Same pathway can be applied for PEN by replacing the benzene (1,4 substitution) group with naphthalate (2,6 substitution).....	121
<b>Figure 87:</b> Crosslinking termination sequence of aryl radical on PEN [19]. Note: Same pathway can be applied for PET by replacing the naphthalate (2,6 substitution) with. benzene (1,4 substitution).....	122
<b>Figure 88:</b> Photocrosslinking variation that can take place on PET and PEN [61].....	123
<b>Figure 89:</b> Photodegradation of Norrish II initiated PET to produce vinyl and carboxylic end groups. Note: Same pathway can be applied for PEN by replacing the benzene (1,4 substitution) group with naphthalate (2,6 substitution).....	126

**Figure 90:** A possible termination of radical Aryl and ether groups on a PET [30].

Note: The pathway can be applied for PEN by: 1)replacing the benzene (1,4 substitution) group with naphthalate (2,6 substitution 2) work through the empty available rearrangements at 1,3-8 substitution pattern possibilities while taking symmetry into account.....127

**Figure 91:** Propagation of the radical aryl group of PET with oxygen gas, followed by radical peroxide break down along with dehydrogenation to form a phenol end group

[40]. Note: Same pathway can be applied for PEN by replacing the benzene (1,4 substitution) group with naphthalate (2,6 substitution).....128

**Figure 92:** Photo-Claisen rearrangement of a PET aryl ether product [30]. Note: The pathway can be applied for PEN by: 1)replacing the benzene (1,4 substitution) group with naphthalate (2,6 substitution 2) work through the empty available rearrangements at 1,3-8 substitution pattern possibilities while taking symmetry into account.....129

**Figure 93:** Photo-Fries rearrangement of the aryl formate reaction product of PET [64].

Note: Same pathway can be applied for PEN by replacing the benzene (1,4 substitution) group with naphthalate (2,6 substitution).....129

**Figure 94:** Hydrogen elimination on PEN via radical oxygen atoms [19]. Note: Same pathway

can be applied for PET by replacing the naphthalate (2,6 substitution) with. benzene (1,4 substitution).....131

**Figure 95:** Formation and break down of peroxy radical to form radical esters [40].

Note: Same pathway can be applied for PEN by replacing the benzene (1,4 substitution) group with naphthalate (2,6 substitution).....132

**Figure 96:** Photocyclization of PET via the Norrish-Yang reaction [58]. Note: Same pathway can

be applied for PEN by replacing the benzene (1,4 substitution) group with the naphthalate (2,6 substitution).....134

## ABSTRACT

Polyethylene Terephthalate (PET) is a widely used polymer in the bottling, packaging, and clothing industry. In recent years an increasing global demand for PET has taken place due to the Solar Disinfection (SODIS) process. SODIS is a method of sterilizing fresh water into drinkable water. The PET bottles are used in the process to contain the water during solar irradiation due to its highly transparent optical property. Alongside PET, polyethylene 2,6-naphthalate (PEN) is used in bottling and flexible electronic applications. The surface of PEN would need to be modified to control the hydrophilicity and the interaction it exudes as a substrate. The UV light absorption properties of PET and PEN are of great importance for many applications, and thus needs to be studied along with its photochemical resistance.

The optical and chemical nature of PET was studied as it was treated by UV photo-oxidation, photo-ozonation, and photolysis under atmospheric pressure. Another investigation was also used to study PEN and PET as they are treated by vacuum UV (VUV) photo-oxidation, VUV photolysis, and remote oxygen reactions. The extent of the photoreactions' effect into the depth of the polymers is examined as treatment conditions are changed. The different experimental methods established the rate of several competing photoreactions on PET and PEN during irradiance, and their effect on the optical quality of the polymers.

# 1.....INTRODUCTION

## 1.1 Surface modification versus bulk region reactions

Surface modification is the general process of altering the surface of a material either through chemical or physical means. The definition of surface is the first few atomic layers of the materials [1, 2]; however, the extent may often be interpreted differently. Depending on the intensity and the properties of the material used, the alteration can be a lot deeper. The main intention of surface modification is changing the physical or chemical properties of the interacting atomic layer with the environment. This would include the change of hydrophilicity, surface roughness, chemical reactivity, etc [3-4]. There are many types of treatments that could fall under the category of surface modification, with an extremely wide variety of results [5-10]. The materials that are commonly modified at the surface are semiconductor wafers, thin films, and many types of polymers. Two methods that can be used in surface modification are gas phase photochemical reactions [4], and another is plasma phase radiation reactions [11]. In both cases a reaction occurs that varies with depth depending on the experimental parameters applied.

## 1.2 Poly(Ethylene Terephthalate) (PET)

There are six very commonly used polymers which are given a top priority in terms of recycling. These polymers are designated with recycle numbers from 1-6: polyethylene terephthalate, high density polyethylene, polyvinyl chloride, low density polyethylene, polypropylene, and polystyrene, respectively. One of the most commonly

occurring polymers in domestic settings is PET, shown in Fig. 1, which is used in most beverage bottles [12].

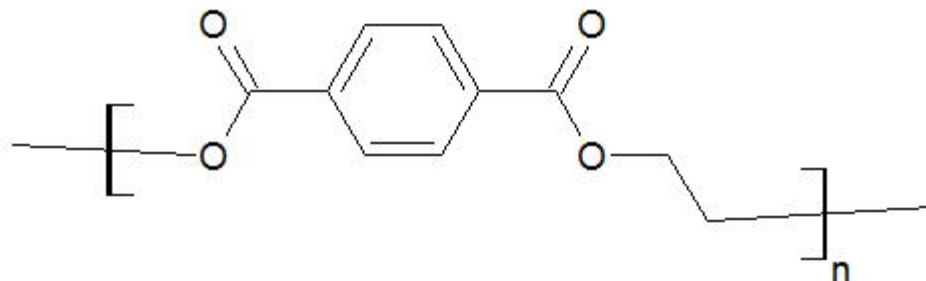


*Figure 1: Poly(Ethylene Terephthalate) (PET) structure.*

PET was discovered and patented in 1941 by the Calico printer's association's chemists, John Rex Whinnfield and James Tennant Dickson. PET is a linear thermoplastic copolymer formed from the condensation reaction between ethylene glycol and terephthalic acid. PET has a glass transition temperature ( $T_g$ ) of  $\sim 69^\circ\text{C}$  and a melting point (mp) of  $265^\circ\text{C}$ , thus giving it good thermal stability. The polymer is known to have a low elasticity along with a tensile strength of  $\sim 48.3$  to  $72.4$  MPa in its pure form which ensures a manageable structural soundness. The idea for PET bottles was then patented by a Dupont employee named Nathaniel Wyeth in 1973 [12, 13]. PET's inertness and physical/structural soundness under standard conditions causes the substance to be widely used in packaging and bottling. The polymer is very cheap to manufacture and mold due to its ideal thermal stability, and its low  $T_g$ . PET in its pure form degrades to experience discoloration along with crosslinking. PET is photosensitive, where several reactions may occur upon photo-irradiance [13, 14] as described in section 1.4-1.9 below.

### 1.3 Poly(Ethylene 2,6-Naphthalate) (PEN)

The number seven in the recycling table is denoted to special polymers that aren't very common and thus signifying most polymers that are not often recycled [12]. One of these polymers is polyethylene 2,6-naphthalate (PEN) shown in Fig. 2, which is commonly used in place of PET in certain applications.

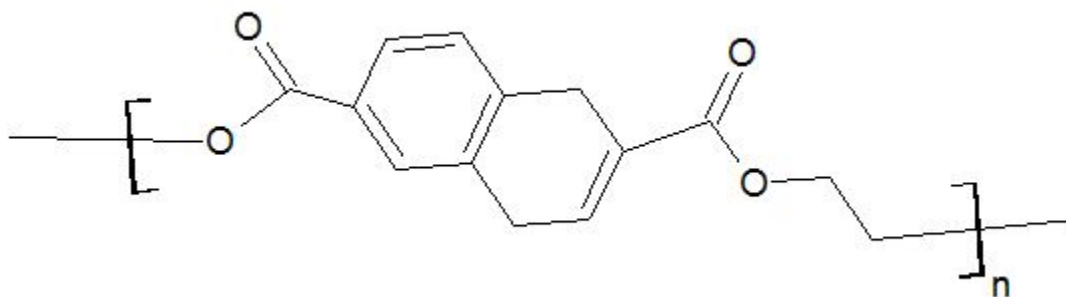


*Figure 2: Poly(Ethylene 2,6-Naphthalate) (PEN) structure.*

The naphthalene ring causes the polymer to have a more rigid structure which has a higher resistance to oxygen diffusion than that of PET. The larger conjugated structure causes the polymer to have higher fluorescence intensity which is helpful in plastic organization/separation recycling. Due to PEN's low oxygen permeability, it is used in bottling of oxidizable products such as alcoholic beverages. PEN was discovered by Dupont in 1953 and patented as a thermoplastic fiber for use primarily in carpets. PEN is a thermoplastic copolymer produced via a condensation reaction between naphthalene-2,6-dicarboxylate and ethylene glycol. PEN has a  $T_g$  of 123°C, a melting point of 265°C, and a tensile strength of 150-265MPa [15, 16]. Due to these properties, its use in plastic displays and flexible electronics has been investigated [17, 18]. Since PEN is a specialty polymer, it is harder to mass produce making it more expensive than PET. The  $O_2$

permeability of PET versus PEN is 4.9 and 1.7 ccm/m<sup>2</sup>-day-atm, respectively [19]. There haven't been a lot of studies on the degradation of PEN, however, most state that PEN is more chemically resistant than PET [15, 16, 19, 20].

#### 1.4 UV photo-oxidation reactions

There are several investigation approaches which have been attempted to observe the effects of exposure of ultraviolet light on PET in the presence of oxygen at atmospheric conditions, otherwise known as UV photo-oxidation [19, 21-27]. UV photo-oxidation is classically defined by the flow of O<sub>2</sub> gas over a certain material's surface in the presence of a certain UV light. Depending on the conditions applied the UV light maybe absorbed by the material and/or the oxygen causing a reaction to occur at the surface. PET and PEN mainly absorb in the UV region, from 3 to 22 eV as shown in Fig. 3 [28].

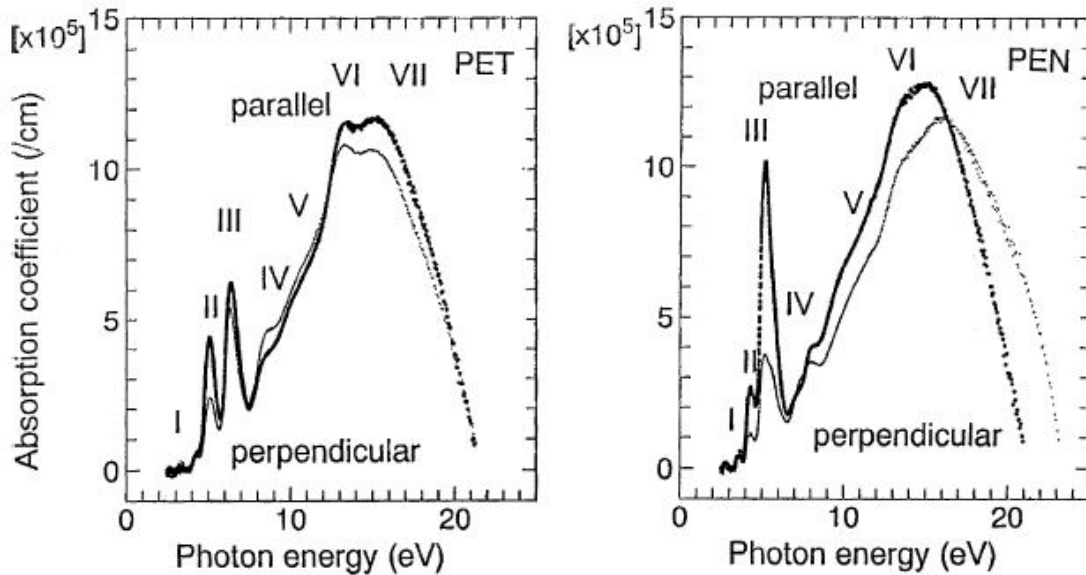


Figure 3: The UV photo-absorption spectrum of PET and PEN, where the identifiable peaks are labeled from I to VII [28].



The absorption spectrum of PET and PEN are very similar. The main difference between the two polymers is the length of the conjugation, which causes a decrease in the transitional energy gaps [1]. The peaks labeled as I-III originate from the allowed transitional band of  $^1A_g \rightarrow ^1B_u$  that are due to the  $\pi \rightarrow \pi^*$  excitation [28, 29]. The band at peak III was identified to consist of two peaks with different polarization at 6.33 and 6.44 eV [28]. On the other hand, the peaks labeled as IV-VII are mainly associated with  $\sigma$  electron excitation [28, 29].

The effects of photo-oxidation on PET was studied with low pressure mercury lamps, where  $\lambda=184.9$  &  $253.7$  nm UV light is emitted onto oxygen to produce ozone [3, 21, 25]. The highly reactive ozone along with the presence of light causes the formation of carboxylic end groups, vinyl end groups, phenols, and the evolution of CO and CO<sub>2</sub> [21, 25]. Another study examined photo-oxidation of PEN compared to PET was analyzed for treatments with wavelengths  $> 300$  nm. The treatment caused the polymers to undergo depolymerization via the Norrish mechanisms [19]. The Norrish I and II mechanisms are radical-based photoreactions that are dependent on the presence of carbonyl-containing functional groups [30]. The conclusion made was similar to the previous papers [22, 24] where photo-crosslinking and photo-degradation/chain scission was observed. Scheirs and Gardette studied the effect of long term photo-oxidation and noted that due to the formation of extended conjugation a higher extinction coefficient is observed in the visible region [19]. The effects of this treatment has been regarded for the most part as a surface treatment where only the top 10-15  $\mu\text{m}$  are effected [19]. Low-molecular-weight oxidized materials were also formed during photo-oxidation [3, 19, 21, 25]. Other than

Scheirs and Gardette's papers [19], the majority of studies however only analyzed the surface via X-ray Photoelectron Spectroscopy (XPS), contact angle, or some form of microscopy.

## **1.5 UV photolysis reactions**

UV photolysis is defined as the interaction of a material with UV photons in the absence of any interacting molecules. There is little data available on the investigation of the ultraviolet light exposure of PET in the absence of oxygen at atmospheric conditions. At atmospheric pressures, UV photolysis can be achieved by pumping in an inert gas to displace air, therefore, the UV light reacts only with the material. The type of gas to be chosen must be monitored by the analytical tool. For example, 2,6-dimethylnaphthalate (DMN), a unit structure of PEN, was studied by flash photolysis in a nitrogen atmosphere [24]. The study concluded that chain scission occurred by decarboxylation or the breakdown of the carbonyl linkage [19, 24]. This type of treatment is mainly to study the interaction of the UV light on the polymer, without the risk of interference from the major absorbing gases. This also is different from the vacuum photolysis due to the fact that there is no differential pressure that forces trapped gases/molecules to escape.

## **1.6 Vacuum UV (VUV) plasma phase photo-oxidation**

Vacuum UV (VUV) photo-oxidation is defined as the use of various plasma techniques in a vacuum to treat a polymer in the presence of oxygen gas. Previous studies of PET treated with VUV photo-oxidation via several types of plasmas are available [26, 27, 31-32]. The plasma can be created through many pathways, however they all involve

the excitation of a certain gas to the point of near ionization [33]. The classical method of achieving a plasma is through extreme heat, however other methods are available to achieve plasma at room temperature. A classical method is to use an RF frequency generator to ionize the gas particle. An electromagnetic field can then be applied to cause the near-ionization particle to resonate with the other gases to continually knock electrons and create plasma [26-27, 31-33]. The plasma begins to relax thus emitting a strong VUV light, which along with the nearly ionized plasma may react with the material and/or oxygen which is flowed into the chamber. The previous work indicates that the surface chemistry of the material changed as was analyzed by XPS and Atomic Force Microscopy (AFM) techniques. The results showed that the plasma causes the oxygen to form oxygen radicals that react with the PET to form hydroxyl, carbonyl, and carboxyl functional group containing products [26, 31-32]. The AFM showed a more significant increase in surface roughness due to the plasma photo-oxidation than UV photo-oxidation [32]. There are, however, little data available on the VUV plasma photo-oxidation of PEN.

## **1.7 Vacuum UV plasma phase photoreactions**

The terms VUV photolysis refers to the emission of plasma radiation onto a sample in a vacuum, where no foreign gases are introduced. This method is different from UV photolysis due to the low interaction of photons with other atmospheric gases, and also the availability of plasma particles. Several studies were conducted to study VUV photolysis on PEN and PET using several types of plasmas [31-32, 34-37]. The use of oxygen or nitrogen plasmas, may often lead to the addition of nitrogen or oxygen-based

bonds from the plasma particles [31-32, 34-35]. The use of argon and hydrogen plasmas was discovered to have a limited interaction between the plasma particles and the PET, therefore vacuum photolysis is the dominant treatment [36-37]. CO<sub>2</sub> was detected due to the breakdown of ester groups [36]. Photolysis using the Ar plasma caused scission to occur in the macromolecule chains, which increased the radical concentration leading to carbonification which caused degradation in the optical properties of PET [37].

### **1.8 Remote oxygen atom reactions**

The exposure of plasma onto oxygen gas to form radical oxygen atoms, while the photons are not directly emitted onto the sample is a technique known as remote oxygen atom exposure. This is usually achieved by placing the sample downstream of the plasma/O<sub>2</sub> mixture, while the end of the plasma source is placed at an angle to point the photons away from the sample. This is done to study the effects of the radical oxygen mechanism in the absence of the photoreactions that are involved in VUV photo-oxidation [38, 39]. The remote oxygen plasma reaction on PET and PEN was studied in atmospheric pressure, where the breakdown of oxygen takes a different path from that in a vacuum [40]. The authors concluded that there were dramatic changes that took place in terms of the surface properties of both PET and PEN. XPS revealed that the ester carbon peak increased by 11 and 24% for PET and PEN, respectively [40]. The C-O species increased by 5% for both polymers and a decrease of 18-29% decrease in the C 1s peak at 285eV which is recognized as the aromatic carbon atoms. The interpretation for these results is that the aromatic rings on the polymer chain are being oxidized [40].

## **1.9 Implications of bulk modifications of PET and PEN**

The use of UV light in filtration plants is a practice that has been used for a fair amount of time. The World Health Organization (WHO) stated that PET bottles can be used in water deprived locations to sterilize the available water by using the radiation from the sun [41]. Solar disinfection, SODIS, is the method of use the sun's radiation to sterilize the non-safe drinking water. The idea is that the UV and near UV light from the sun is able to denature some of the important enzymes of the harmful bacteria in the water. The heat produced from the sun's energy also contributes to the acceleration of the bacteria's death. The WHO calls for the use of PET bottles to be filled with water, then placed at an angle towards the sun for 6 hours [41]. Other things can be added to the water, such as certain plant leaves, to help oxygenate the water and bottle. This oxygenation of the water helps increase the amount of UV light transmitted to the bacteria through the water [41]. The integrity of PET's optical properties is thus of great importance. Some studies have been initiated to observe the degradation of PET's optical and chemical properties [42]. The group found several aldehyde, organic photoproduct, and phthalate additives in the water stored in the bottles [42]. The structural improvement that maybe the result of these photoreactions are of great importance in both PET and PEN. The change in the thermal stability and dielectric properties are two important factors that would need to be considered due to photo-degradation [20].

## **1.10 Implications of surface modification for PET and PEN**

The effects of the photoreactions will have a wide range of impact on the physical and chemical nature of the surface of the polymers. The most apparent change is the

wettability or hydrophilicity of the polymer. An example of the importance of the hydrophilicity is the adhesion of conductive semiconductor materials such as indium-tin-oxide [43, 44]. One of the biggest problems with PET bottles is the large quantity not being recycled, which remains in landfill sites, due to its low rate of degradation because of its hydrophobic nature and low adsorption. The photo-oxidation and other photoreactions may help improve the hydrophilicity and adsorption characteristics [45].

## **2.....RESEARCH OBJECTIVES**

This thesis aims to investigate and compare the effects of UV and plasma photoreactions between PET and PEN. The main objectives of this research are to:

- a) Illustrate the differences and similarities in terms of photo-stability of PET and PEN.
- b) Demonstrate that the photo-degradation effects of certain treatments may extend beyond the surface into the bulk region of the films.
- c) Show and compare the chemical changes resulting from each treatment and its result on the optical and physical properties of the films.
- d) Study the types of mechanisms involved in these photoreactions while noting the extent of each specific mechanism with light intensity and photon energy.

The treatments and analytical techniques were:

- a) UV photo-oxidation of PET with: i)  $\lambda = 253.7$  nm and ii) a broad spectrum 300 nm UV light. The resulting changes are observed at the surface with XPS, water contact angle goniometry, and Scanning Electron Microscopy (SEM). The bulk region was studied with a Fourier Transform Infrared Spectroscopy (FTIR) and UV absorption spectroscopy.
- b) UV photo-ozonation of PET using  $\lambda=253.7/184.9$  nm UV light to generate ozone from oxygen gas. The resulting changes are observed at the surface and bulk using the same techniques as UV photo-oxidation. Depth profile XPS was also used to scan the depth several nm at a time.

- c)** UV photolysis of PET is applied using three treatments in pure nitrogen gas: i)  $\lambda = 253.7$  nm, ii) a broad spectrum 300 nm, and iii) 253.7/184.9 nm. The changes are analyzed with the same techniques as UV photo-oxidation, with the exception of SEM.
- d)** VUV photo-oxidation of i) PET and ii) PEN using an Ar+O<sub>2</sub> plasma mixture. The changes are observed at the surface and bulk region with the same methods as UV photolysis.
- e)** VUV photolysis of i) PET and ii) PEN using an Ar plasma mixture. The results are obtained using the same analytical techniques as VUV photo-oxidation.
- f)** Remote oxygen atom study of i) PET and ii) PEN is applied using an Ar+O<sub>2</sub> plasma mixture placed parallel to the sample so no photons are effecting the polymers. The analytical instruments used are those used in VUV photo-oxidation. Finally a control remote argon atom study is conducted on i) PET and ii) PEN applied using Ar plasma placed parallel to the sample so that again no photons reach the polymers. The surface was studied with XPS to determine if there are any changes.



### **3.....EXPERIMENTAL**

#### **3.1 Materials**

##### **3.1.1 Poly(ethylene terephthalate)**

A roll of research grade poly(ethylene terephthalate) was purchased from the Goodfellow Corporation, Pennsylvania, USA. The polymer film is biaxially oriented with a thickness of 0.1mm. The biaxial orientation refers to the polymer chains being stretched into place by a process of machine stretching and heat crystallization [12,13,16]. Each sample was cut down to 1.5 cm by 2 cm rectangles. To mark the sides a small notch is cut in the upper left corner. The location of the notch indicates which side is up for treatment. Before treatment, each sample is washed and degreased in an ethanol ultra sonic bath at room temperature for 10 min. Several organic washing fluids such as methanol, acetone, ethanol, and isopropanol were used to experimentally wash the PET sample; of where ethanol showed the cleanest results by XPS, while preserving the chemical and structural integrity of the polymer surface. The samples are individually placed on clean 90 mm diameter filter papers in sterilized petri dishes. The petri dishes are placed in a ventilation hood to dry the samples on each side for 10 min. The samples are then analyzed before and after each treatment to analyze the changes that occurred to the particular film.

##### **3.1.2 Poly(ethylene 2,6-naphthalate)**

A roll of poly(ethylene 2,6-naphthalate) was donated by Dr. Jeremy Grace from Kodak. The roll was part of a footage marker of an inkjet printing, however the entire film was cleaned using CO<sub>2</sub> snow cleaning along with acetone and isopropanol

sonication. The films purity was confirmed with XPS measurements, which showed no contamination on the cleaned surface. Each sample, like PET, was cut down to a 1.5 cm by 2 cm rectangle. To mark the sides, a small notch is cut in the upper left corner to indicate the side that was treated. Each sample, before treatment, is washed and degreased in an ethanol ultrasonic bath at room temperature for 10 min to clean the sample directly before the treatment is performed. The samples are individually placed on clean 90 mm diameter filter papers in sterilized petri dishes. The samples are then dried in the hood on each side for 10 min. The samples are analyzed before and after each treatment to analyze the changes that occurred to the particular film.

## **3.2 UV photoreactions**

### **3.2.1 Atmospheric pressure UV photo-oxidation**

A Rayonet photo-reaction chamber; produced by the southern new England Ultraviolet Co., Inc., Branford, CT; is used. The photo-reactor contains 16 lamp slots, where two types of lamps can be installed depending on the type of treatment. A low pressure mercury that emits a 253.7 nm UV light is used for one treatment. Another treatment uses a medium pressure mercury lamp, RPR-3000, which emits a broad spectrum UV light with a maxima at 300 nm, as shown in Fig. 4.

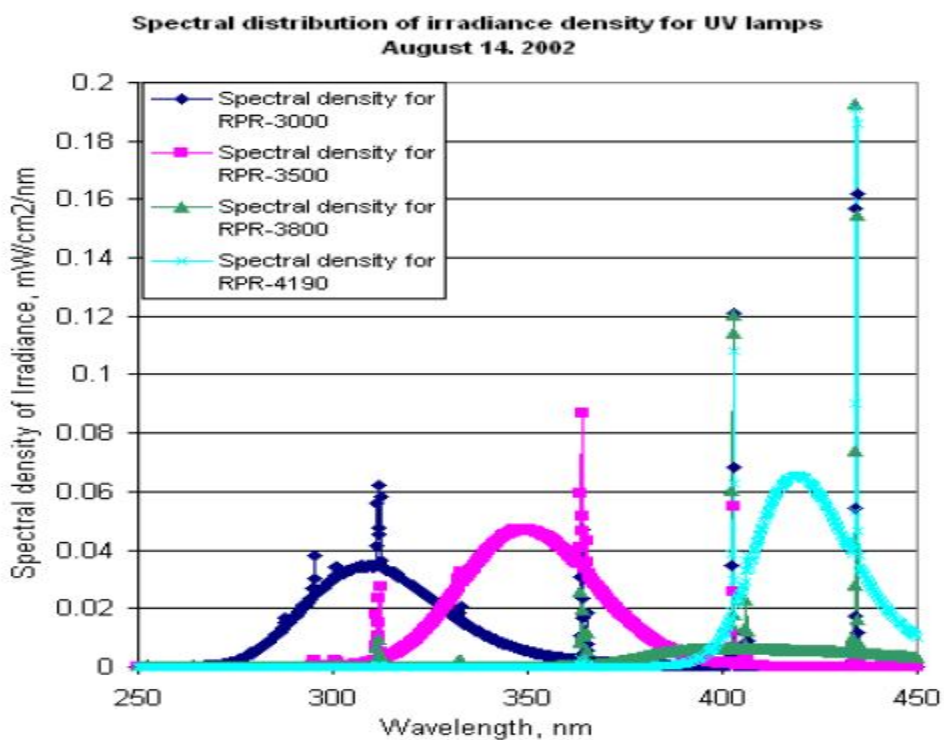
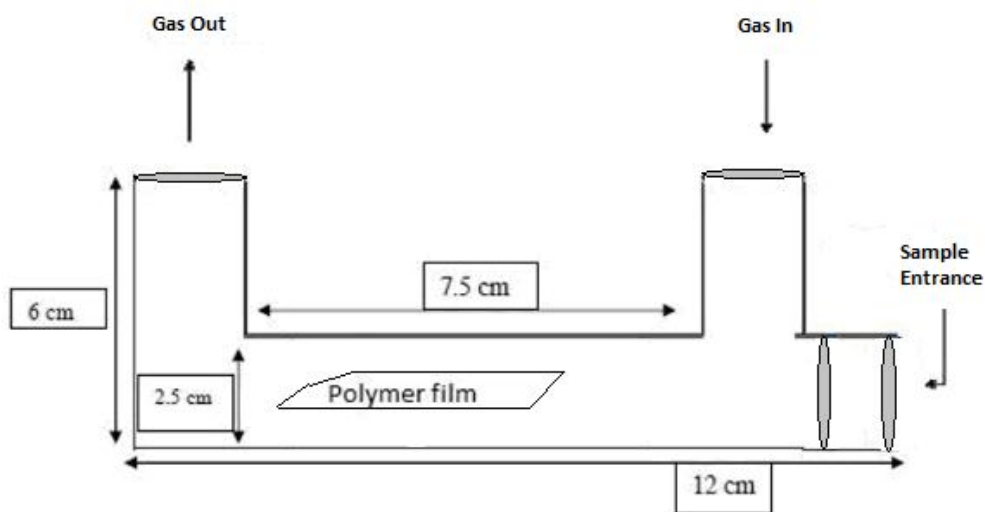
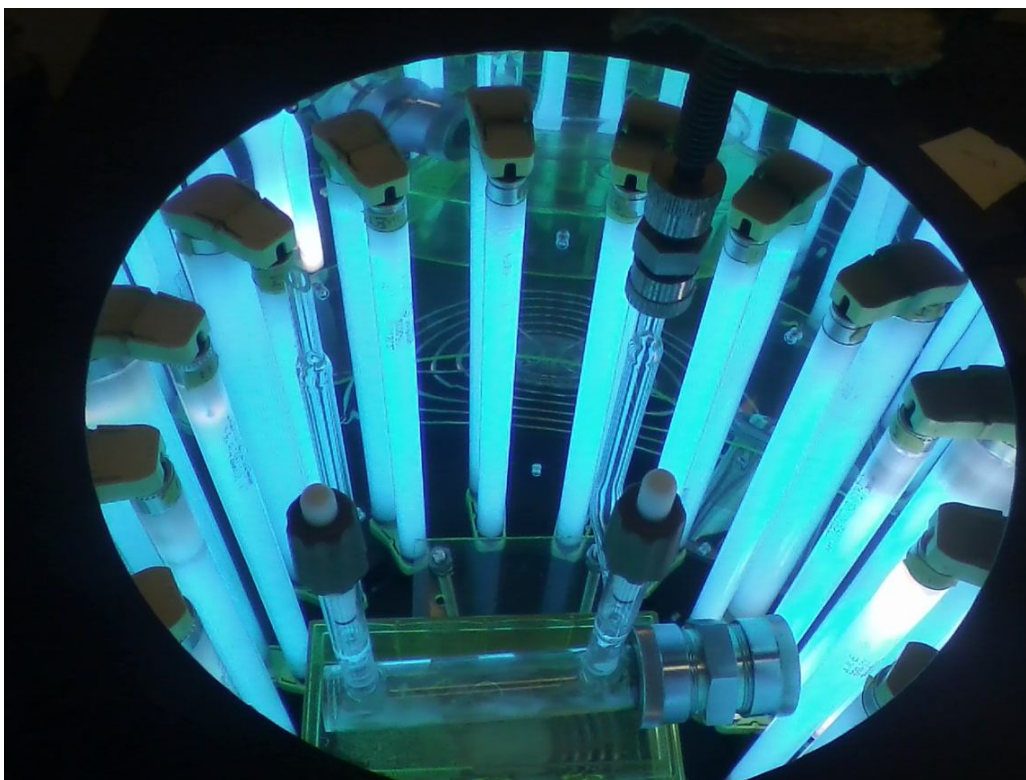


Figure 4: The emission spectrum of the medium pressure mercury lamp, labeled as RPR-3000 and is shown in blue [46].

After the sample is cleaned and analyzed before treatment, it is placed horizontally in a quartz glass cell, custom made by Suprasil® as shown in Figs. 5 and 6.



*Figure 5: Custom made quartz glass UV sample holder/chamber. The polymer film is placed horizontally with the notch in the upper left corner as shown in the figure.*



*Figure 6: The quartz chamber is placed in the middle of the photoreactor. The gas supply line is connected (shown on right) to one side and the other side (left) is an outlet.*

The sample is placed into the quartz cell horizontally where the marked side up (notch in the upper left corner) as shown in Fig. 5. The sample is placed horizontally so that the side that is studied receives the most amount of light exposure. The sample entrance is sealed with two viton® O-rings and a swagelok fitting. The two gas ports contain two shutoff valves that connect to a male-end of a swagelok fitting. The two shutoff valves are left open, where one side is connected to the gas inlet hose. An ultra-high purity oxygen gas cylinder is connected to a TA instruments gas flow controller. The flow controller is set so that the oxygen flows at a rate of 43 cm<sup>3</sup>/min. With the quartz cell in the photoreactor, oxygen gas is allowed to flow through the cell for 10 min with the lights off. This is done to displace the atmospheric gases in the cell with pure oxygen. The lamps are then powered up for the specific time required. The low pressure mercury lamps (253.7 nm) were used to treat the PET films for 15, 30, 60, 90, 120, and 150 min as shown in Fig. 6. When the medium pressure mercury lamps (300 nm spectrum) are installed, the treatment times on the PET films are 30, 60, 90, 120, 150, and 180min. Both treatments use the same setup, with the exception of the lamps.

### **3.2.2 Atmospheric pressure UV photo-ozonation**

The UV photo-ozonation treatment is similar to the UV photo-oxidation, however, low pressure mercury lamps, which emit both  $\lambda=253.7$  and 184.9 nm UV light, are used. Oxygen absorbs UV light of wavelength  $\leq 242.4$  nm as shown in Fig. 7 [47].

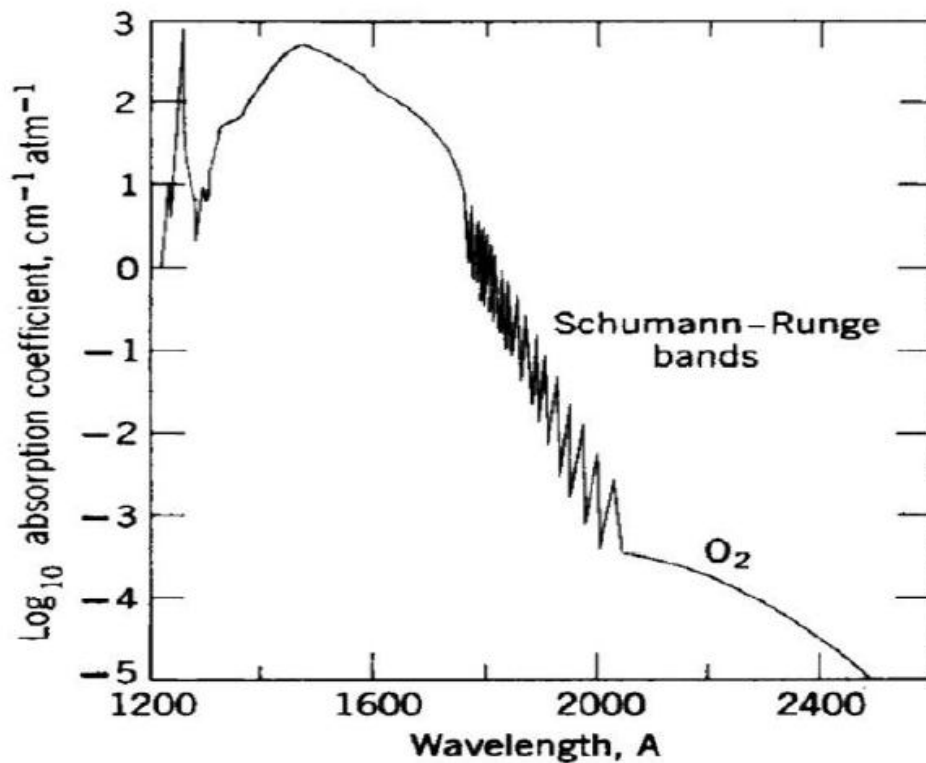
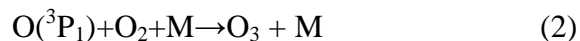
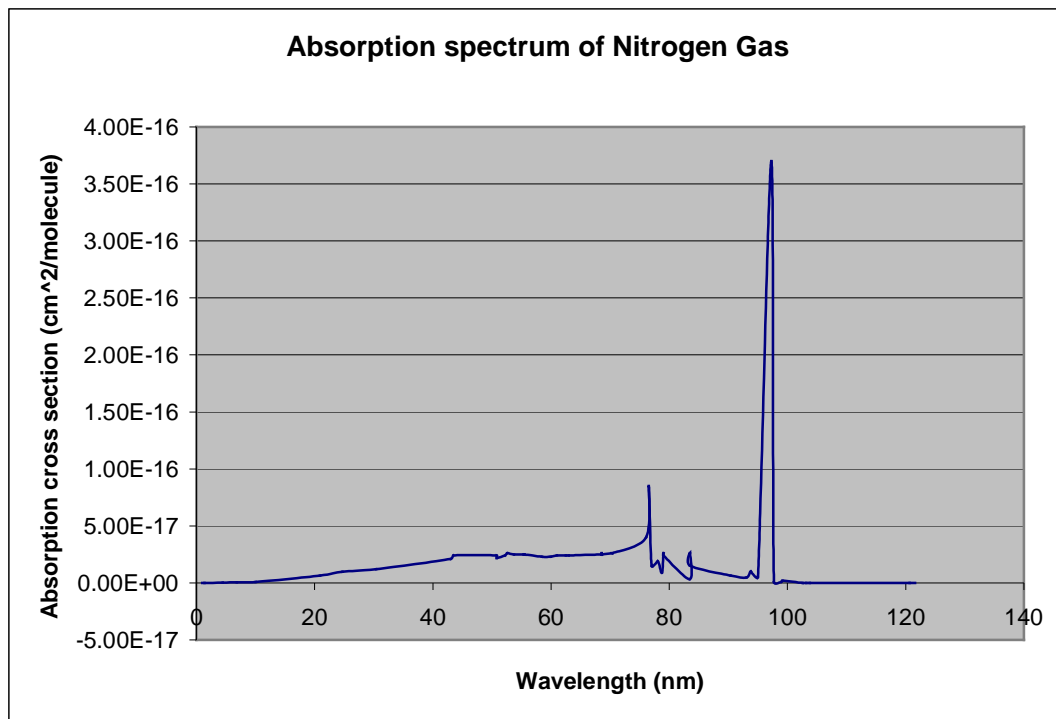


Figure 7: The UV absorption spectrum of oxygen ( $O_2$ ) gas [47].

The  $O_2$  tends to dissociate upon the absorption of the 184.9 nm photons to form triplet P oxygen atoms. These O atoms are unstable and tend to react with the  $O_2$  and a third body (M) that acts to absorb any excess energy from the dissociation of the  $O=O$   $\pi$  bond. With this reaction, ozone is formed as shown in reactions (1) and (2) [48].



Since the air outside the photochemical reactor consists of approximately 21% oxygen, then the oxygen in the air outside the cell would absorb the 184.9 nm photons. Nitrogen gas absorb light mainly at the VUV region as shown in Fig. 8, thus will be inert at the wavelengths used in these treatments [49].



*Figure 8: Nitrogen gas absorption spectrum is located mainly in VUV region [49].*

Therefore, pure nitrogen gas was pumped into the Rayonet photoreactor to displace the atmospheric gases. This particular photoreactor chamber contains an inlet valve that allows for a gas to be distributed throughout the photoreactor as shown in Fig. 9.



*Figure 9: A Rayonet photo-reactor chamber.*

The nitrogen gas is pumped in at 4.78 L/min for 10 min to displace all of the air in the photo-reactor. Like the UV photo-oxidation, the PET is placed horizontally with the marked side up in the quartz cell where oxygen is flown for 10 min at 43 cm<sup>3</sup>/min. The PET films were treated for 2, 4, 5, 6, 8, 10, 15, 20, 25, 30, 45, and 60 min.

### **3.2.3 Atmospheric pressure UV photolysis**

The UV photolysis treatment is used to study the interaction of light at atmospheric pressure in the absence of oxygen. The procedure for the UV photolysis is exactly like the UV photo-oxidation and photo-ozonation with the exception of the gas used. Ultra high purity nitrogen gas is used instead of oxygen gas because it does not absorb light



between  $\lambda=184.9$  to 360 nm and it was used in previous flash photolysis techniques with DMN to displace oxygen [24]. Therefore, the photo-reactions of PET were studied in the presence of nitrogen.

### 3.3 Plasma photoreactions

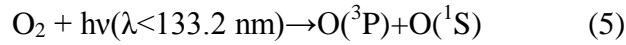
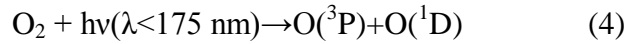
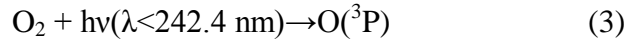
#### 3.3.1 VUV photo-oxidation

The vacuum ultraviolet light is achieved via an argon plasma which is powered by a microwave generator. A roughing pump is used to achieve a baseline pressure of 0.15-0.35 torr. Argon gas is flowed through a mass flow controller into a quartz glass plasma cavity, as shown in Fig. 10, at a rate of 50 standard cubic centimeters per minute (SCCM).



*Figure 10: Ar plasma pointing down towards the sample inside the vacuum chamber.*

The argon plasma is powered by a microwave plasma generator that operates at 18-30 Watts, with a frequency of 2.45 GHz. The samples are located downstream from the plasma cavity; oxygen gas is pumped into the vacuum chamber over the samples at a rate of 10 SCCM. The oxygen gas is pumped at a distance away from the cavity so that it would not affect the MW cavity and Ar plasma. The Ar plasma interaction with the O<sub>2</sub> causes the formation of O radical atoms as shown in reactions (3) - (5) [48].



The setup is shown in Fig. 11, where the plasma cavity is pointed towards the samples so that only the photons would be able to react with the oxygen and the sample.

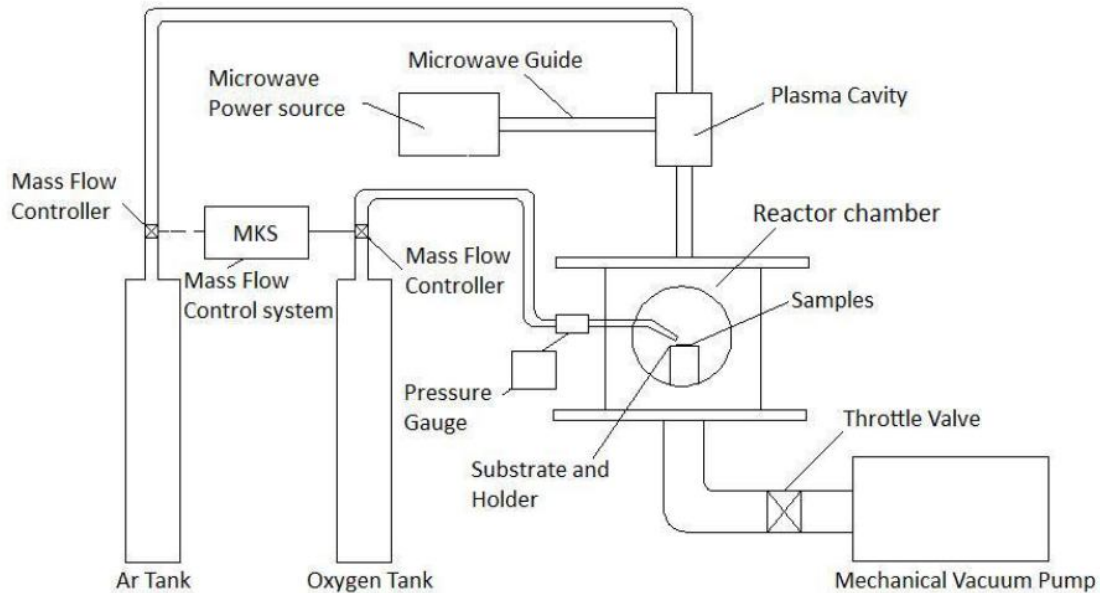


Figure 11: Schematic of the VUV photo-oxidation setup [50].

The Samples used in this treatment were both PET and PEN, which are placed with the notch in the upper left corner on a 2x2 cm microscope glass slide in a sample holder. The

films are treated for 5, 10, 15, 20, 25, 30, 60, 90, 120, and 150 min. The samples are also analyzed before and after they were treated.

### **3.3.2 VUV photolysis**

The idea of VUV photolysis is to study the effect of the plasma and its photons on the sample in the absence of any additional gases. Therefore the VUV photolysis treatments have a similar procedure to the VUV photo-oxidation with the exception of not pumping in oxygen gas. The treatment times used on PEN and PET are 5, 15, 30, 60, 90, 120, and 150 min.

## **3.4 Remote oxygen reaction**

### **3.4.1 MW discharge Ar and O<sub>2</sub> mixture**

This treatment is similar to the VUV photo-oxidation, however the oxygen is pumped within the plasma cavity. The oxygen is introduced in the cavity to insure that the charged and metastable argon plasma particles fully interact with the O<sub>2</sub> molecules. In this particular treatment the effect of O radical atoms are studied in the absence of the interaction of light radiation with the sample; thus the samples are placed indirectly from the light downstream of the cavity as shown in Figs. 12 and 13.

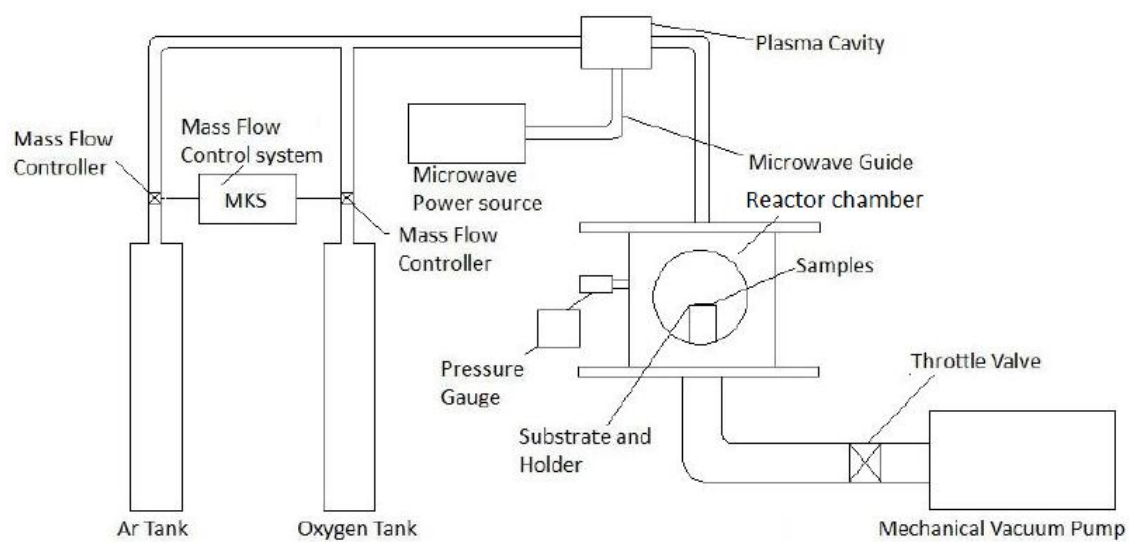


Figure 12: Schematic of the remote oxygen atom reaction setup [50].



Figure 13: Schematic of the parallel placement of the plasma source, to remove the interaction of photons with the sample while still being downstream.

The oxygen and argon gas are both pumped at the same rate as that which was used for VUV photo-oxidation. The plasma operates at the same 18-30 Watts power interval, and same frequency as the VUV photo-oxidation. The PET and PEN films were both treated for 5, 10, 15, 20, 25, 30, 60, 90, 120, 150, and 180 min. The samples were analyzed before and after the treatment.

### **3.4.2 MW discharge Ar**

The simple discharge of plasma where no photons are directed onto the sample is used as a control to confirm that no active plasma particles actually reach the sample. The setup is exactly like the MW discharge of Ar and O<sub>2</sub> shown in Fig. 11, with the exception of oxygen not being flown into the system. The control PET and PEN samples were treated for 10, 30, 60, and 90 min.

## **3.5 Analysis techniques**

### **3.5.1 X-Ray Photoelectron Spectroscopy (XPS)**

X-Ray Photoelectron Spectroscopy is a versatile and extremely sensitive surface analysis technique. The top 2-10 nm of a material can be analyzed for its elemental and functional group composition. This instrument utilizes soft x-rays to eject electrons to the vacuum level with certain kinetic energies. The kinetic energy of the electron is related to the binding energy as shown in equation (6) [51].

$$\text{Binding energy} = \text{X-Ray energy} - \text{Kinetic energy} \quad (6)$$

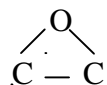
The kinetic energy of the electron is typically measured using a hemispherical capacitor, which is able to deflect electrons outside of certain energy level. The idea is a positive

charge is placed on one hemisphere, and parallel to it is another negatively charged hemisphere. The electrons that have a lower energy than that of the charged hemisphere will stick to the positive hemisphere and not reach the analyzer. On the same note, electrons that have energy that is too high compared to the capacitor will not be repelled by the negatively charge hemisphere. Therefore the electron's kinetic energy will be determined due to its relation with the charge on the hemispherical capacitor. Based on the current that reaches the transducer, the number of electrons can be determined to give the number of electrons with that specific binding energy [51].

The analysis was performed on a Physical Electronics model 5800 XPS by Dr. Tom Debies and Michael Mehan at Xerox Corporation's Webster NY lab. The samples were analyzed using a 45° take-off angle to observe the top 2-5 nm. A radius of 0.4 mm was analyzed on the specified treated side of the polymers. The 5800 XPS uses an Al K<sub>α</sub> X-ray beam with a 1486 eV power. The samples are charge neutralized with an irradiation of low energy electrons output by a BaO field emission neutralizer. This instrument is able to produce results with a 5% level of uncertainty for the major constituents and a 10% uncertainty for minor components.

The quantitative analysis of the XPS output is analyzed based on the binding energy and the current measured. The binding energy is specific to the atomic energy level, while the current is able to indicate the quantity of that atom available on the surface. The binding energies are influenced by the local chemical bonds and based on these small variations in energy, the functional groups can be determined. XPS was used to analyze the functional groups within the C 1s elemental curves. The location of the specific functional groups used within the XPS spectrum can be determined from the location of

epoxides, carbonyl, ester, anhydride, carbonate, sp<sup>3</sup> carbons, and sp<sup>2</sup> carbons are described in Table 1 [52].

Binding Energy (eV)	Assignment
284.7	C-C sp <sup>2</sup>
285.1	C-C sp <sup>3</sup>
286.0	C-O-C, 
287.0	C=O
288.6	O-C=O
289.8	O=C-O-C=O, O-(C=O)-O
292.0	Energy Loss

*Table 1: XPS literature assignment of various functional groups in a C1s peak [52].*

Curve fitting is applied after a high resolution spectrum is obtained. The curve fitting is performed by adding or removing peak values of a specific binding energy until a decent chi squared value is obtained. The idea is that a good curve with clear peaks of a certain height or width is to be obtained once a reasonable chi squared value is employed, in this case 2.0 was used.

Depth profile XPS is a technique that scans the surface of a material while it is being etched, so that the transitional/bulk region may be scanned in a layer by layer format. The etching is typically achieved by argon ion sputtering [51]. The sputtering energy was set to 2 kV, covering a 2x2 mm cross section at an etch rate of 2.86 nm/min. This particular

analysis was performed on 15 min UV photo-ozonation treatment sample, which showed a high increase in the oxygen composition on the surface. The UV photo-ozonation treatment sample was chosen because it represents the most extreme photo-oxidation due to the high photon energy used and concentration of highly reactive ozone. The technique is aimed to show the changes within the surface maybe very different from those taking place within the transitional/bulk region.

### **3.5.2 Scanning Electron Microscopy (SEM)**

Scanning Electron Microscopy is an imaging technique that studies the surface morphology of a conductive material. SEM is used to study the effects of certain treatments on the roughness and porosity. An electron gun uses a filament, typically tungsten, which is supplied with a high voltage to emit electrons. The electrons are condensed and focused onto the sample. The emitted primary electron beam causes the sample to scatter three main types of radiation. The first is that primary electron can be backscattered off of the surface in a somewhat inelastic manor. The primary electrons can also be absorbed by the sample as shown in Fig. 14, which causes the surface to be excited or ionized, resulting in high energy x-ray and/or secondary electron beams to be emitted during the relaxation phase. The secondary electrons are detected usually using a scintillator which would emit light with an intensity equivalent to that of the distance of the secondary electron from the surface to the detector [51].



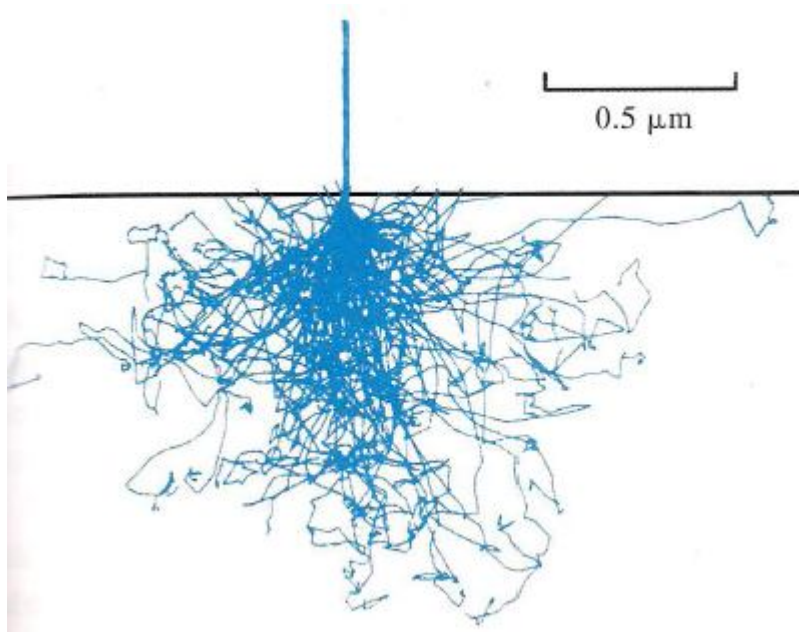


*Figure 14: Simulation of 50 primary electron scattering into a material [51].*

The SEM analysis was performed by Greg Thompson at Xerox using a Hitachi S-4800 FESEM to observe the UV photo-oxidized and photo-ozonated PET versus the control. Only the 253.7 & 300 nm broad spectrum UV photo-oxidation and photo-ozonation treatments are SEM analyzed. Since the PET films are not conductive they are most likely to build a charge due to the bombardment of the primary electrons [51]. The PET film is covered in a very thin gold film, approximately 10 nm in thickness, to be analyzed. The secondary electrons are analyzed at an accelerating voltage of 5000 V. The samples were analyzed at 10, 50, and 100 kX, which have a cross sectional length of 5.0  $\mu\text{m}$ , 1.00  $\mu\text{m}$ , and 500 nm, respectively.

### **3.5.3 UV Absorption Spectroscopy**

An ultraviolet-visible light absorption spectrometer is an instrument of major importance in the field of optics. The instrument is based on Beer-Lambert's law of

absorption, which is able to quantify the amount of light a material is able to absorb. The transmittance can be described as the intensity of light collected exiting the sample divided by the intensity of the incident light beam. The absorbance on the other hand is the negative logarithm of the transmittance, which describes the optical density of a material. Beer Lambert's law states that the absorbance is equal to the product of the concentration, path length, and the molar absorptivity. The Beer-Lambert law is typically used to describe the optical density of a material based on the specific concentration of a chemical in a mixture. The absorbance is also a function of the path length, which is the distance that the light has to travel through a material. The molar absorptivity is a value that is specific to a particular chemical or functional group, which is able to describe the absorbance at unit path length and molar concentration [1, 33, 51].

The particular instrument that was used is a Shimatzu UV 2401 model. This instrument is equipped with halogen and D2 lamps which, when combined with the detector, are able to study light from  $\lambda=190$  to 1000 nm. The film was initially observed with a standard film holder, however the absorption value was over the detectable limit. To accommodate this issue, an integrating spherical attachment is used. The integrating spherical attachment is designed to be able to collect light from an external optical source. The light collected undergoes several diffuse reflections; this disperses the light uniformly at the spherical wall as shown in Fig. 15. The radiation is integrated proportionally to the initial radiation and thus detected using a sphere detector. The attachment is thus able to cut down the amount of light produced by the instrument so that the absorption value is within the detectable range.

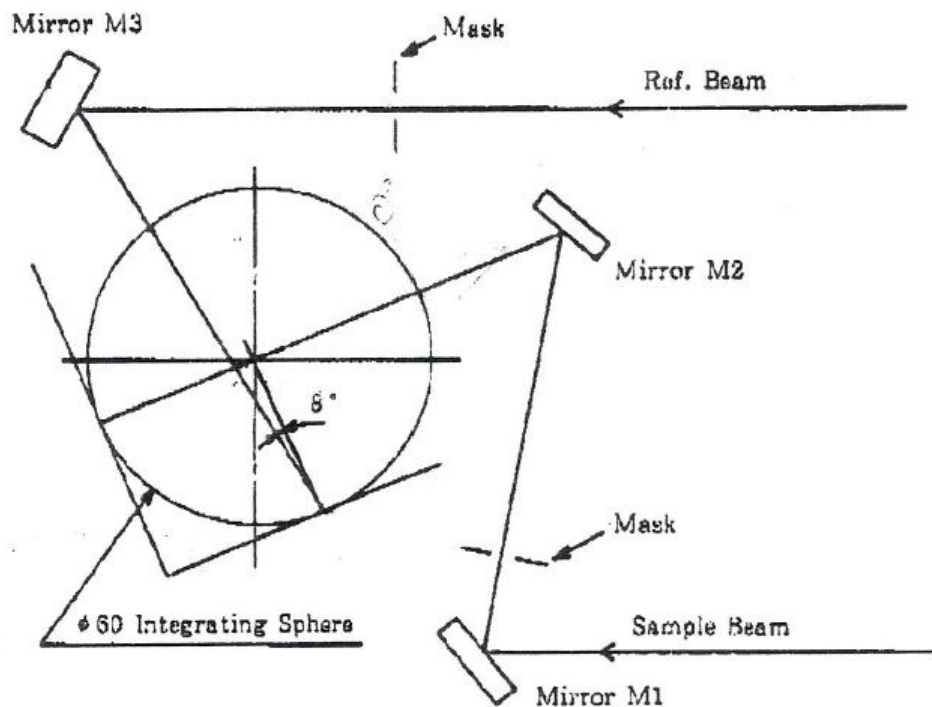


Figure 15: Schematics of the ISR-2200 Integrating Spherical attachment [53].

The samples were scanned at a slit width of 1.0 nm to allow for high resolution while providing enough light to accurately make the measurements. The PET film starts to have a significant absorption coefficient at the UV region starting at 320 nm, while PEN starts at 400 nm [28]. The Shimadzu UV 2401 model has a detector that is able to analyze light at a minimum wavelength of 190 nm. Therefore the PET is analyzed from 190 to 320 nm, while PEN is from 190 to 400 nm; both at a step of 1 nm. The data obtained is then analyzed by measuring the percent change in absorption per wavelength from before to after treatment, as well as the total change in absorbance in the particular analyzed range. An average measured error of 0.025 is obtained per wavelength.

### 3.5.4 FTIR

An infrared absorption spectrometer is an instrument that is similar to the UV-Vis with the exception of operating in the infrared region of the light spectrum. The instrument is based on the notion that infrared light would be absorbed by the material that results in a vibrational and rotational nuclear motion. The vibrational motion is a variable of the bond's tensile, compressional, and shear modulus of elasticity as guided by the simple harmonic motion principle. The vibration motion is simplified in the mass on a spring approximation, where the mass is the nucleus and the spring is the bond. There are many types of vibrational motion that can be described by different photon energies. The types of vibrations include stretching and bending of the bonds; there are also symmetrical and asymmetrical stretching patterns. The bending motion is more complicated which includes in-plane rocking and scissoring, along with out of plane wagging and twisting [51].

The functional groups on a material can be assessed by observing the intensities of the absorption of infrared light as a function of different photon energies. The increased population of a specific functional group would yield a higher absorption value. Therefore the major changes in the structure of the PET and PEN then can be monitored, per the different treatments to establish a plausible reaction mechanism and product. The IR spectroscopic mechanism used is a relative surface-transitional layer analysis technique, where the top 1-5  $\mu\text{m}$  are penetrated and analyzed. The exact depth of the analysis is calculated using the effective penetration depth ( $d_p$ ) formula shown in equation (7) and plotted in Figs. 16 and 17 using the literature values [51, 54]. The  $\lambda_c$  is

wavelength in the crystal,  $\theta$  is the angle of incidence which is  $90^\circ$ ,  $n_s$  and  $n_c$  are the refractive indexes of the sample and crystal, respectively [51].

$$d_p = \frac{\lambda_c}{2\pi \left[ \sin^2 \theta - (n_s/n_c)^2 \right]^{1/2}} \quad (7)$$

Therefore this analytical tool was used alongside the XPS to analyze the polymers deeper within the transitional layer and the bulk layer.

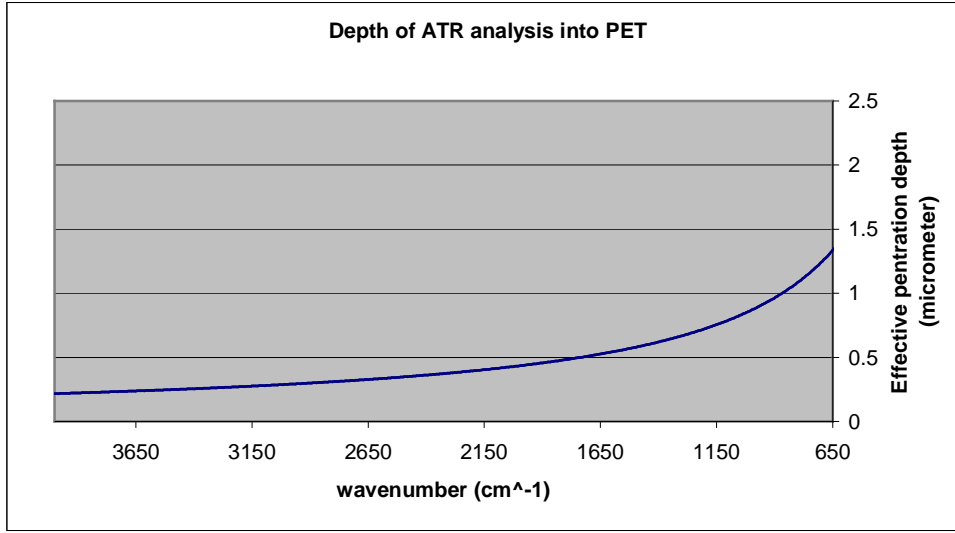


Figure 16: Depth of ATR analysis as a function of the wavenumber for PET [51, 54].

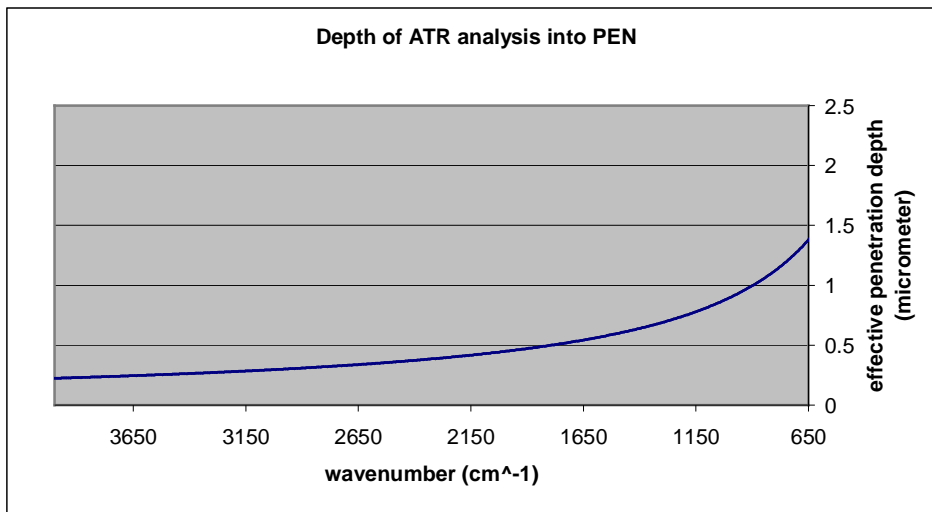


Figure 17: Depth of ATR analysis as function of the wavenumber for PEN [51, 54].

The IR spectrometer used is the Shimadzu IR Prestige-21 Model FTIR with an Attenuated Total Reflectance (ATR) crystal. The function of the ATR crystal is to be able to reflect the IR light between the source and polymeric material at least once. The reflections created between the sample and the ATR forms an evanescent standing wave, which is reflected to an IR detector to be analyzed [51]. In this research, a KBr window is used to scan the samples from 650- 4000  $\text{cm}^{-1}$ . The computer program, IR solution, is used to perform a Fourier transform function to be able to calculate the appropriate percent transmission from the wide spectral IR wave collected from the ATR crystal.

The data obtained is a percent transmittance versus the wavenumber, which is converted to the absorbance using the Beer-Lambert law. The overall intensity of the obtained spectrum varies based on the change of surface roughness, however the peaks' intensities relative to each other is accurate. The spectrum is then converted as a ratio of the aromatic skeletal stretching bands of the PEN and PET. The wavenumbers used were 1405 and 1374 $\text{cm}^{-1}$  for PET and PEN, respectively [55-58]. The change in the ratios at each wavenumber is calculated based on the data from before and after the treatments. The resulting change detected is a qualitative indication of which functional groups has increased or decreased. The functional groups that are analyzed can be described by the peaks at the wavenumbers shown in Table 2 [51, 55-59].

<b>PET Peak Wavenumber (cm<sup>-1</sup>)</b>	<b>PEN Peak Wavenumber (cm<sup>-1</sup>)</b>	<b>Functional group description</b>
1720 [55, 56]	1720 [57, 58]	C=O stretch: carbonyls
1270 [55, 56]	1270 [57, 58]	C-O stretch: Esters
1100 [55, 56]	1172 [57, 58]	C-O stretch: Ethers
1560 [56]	~1550 [51, 57, 59]	O-C & CCO groups stretch
~3700 [51, 59]	~3700 [51, 59]	-OH stretch: Phenol
~3500 [51, 59]	~3500 [51, 59]	-OH stretch: Carboxylic acid
727 [55, 56]	770 [58]	-C=O: Carbonyl out of plane deformation on aromatic ring
850 [55, 56]	830 [58]	C-H bending: Hydrogen deformation on aromatic ring
1020 [55, 56]	1126 & 1087 [57]	-C=O: carbonyl 1,4-substitution (PET) or 2,6-substitution (PEN)
1400 [55, 56]	1375 [57, 58]	C-C stretch: aromatic skeletal stretching bands (This can be represented by the ratio of the overall spectrum)
2960 [55, 56]	2990 [58]	-C-H stretch: Aliphatic alkanes
~1650 [51, 59]	~1650 [51, 59]	C=C stretch: Vinyl groups

*Table 2: IR spectra peak assignment for functional groups on PET and PEN [51, 55-59].*

### 3.5.5 Contact angle Goniometry

A contact angle goniometer was used to measure the surface wettability or hydrophilicity. A drop of water is placed on a material's surface, which may bead or spread out depending on the hydrophilicity of the surface (Fig. 18). The surface wettability is determined by the angle between a flat horizontal surface with the base of the water droplet, otherwise known as the contact angle. As the contact angle increases

the material is known to be more hydrophobic, which indicates a lower miscibility with the hydrophilic water.

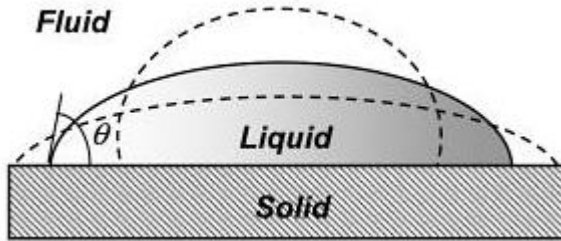


*Figure 18: The increase in contact angle from a hydrophilic to a more hydrophobic surface [60].*

There are several ways to measure the relative contact angle of materials. The method used in this research was the dynamic sessile drop method, specifically, advancing angle mode which is measuring the maximum contact angle obtained as the volume of the water droplet is increased to a certain amount, 10 $\mu$ L were used in this study [60].

A Rame Hart model 200 standard goniometer was used in this analysis to calculate the desired contact angle. The PET or PEN films are placed on a clean and pre-balanced stage, where a 10  $\mu$ L syringe is used to add water to the surface. The syringe is filled to the 10  $\mu$ L line, and the maximum angle is measured as the volume is increased to 10  $\mu$ L. The angle is measured using a high resolution camera with the Drop image advanced software, under the surface contact angle mode. The error in the contact angle is measured to be 0.4 $^{\circ}$ .



## **4.....RESULTS**

### **4.1 XPS**

The top 2-5 nm of each sample was analyzed versus an untreated and washed control using the XPS elemental survey from 0 to 1000eV. The C 1s spectra of the binding energy versus the normalized intensity is presented along with a tabulated curve fit functional groups analysis, based on the assignments shown in Table 1, for each treated sample compared to its control.

#### **4.1.1 Untreated controls**

##### **I PET control**

The atomic percent of the control sample was 71.59 %, 27.33 %, and 1.08 % for carbon, oxygen, and nitrogen, respectively. The observed composition falls within the instrumental error range of the recognized stoichiometric values, 71.4% carbon and 28.6% oxygen. The C1s spectrum of an untreated and washed PET film is displayed in Fig. 19.

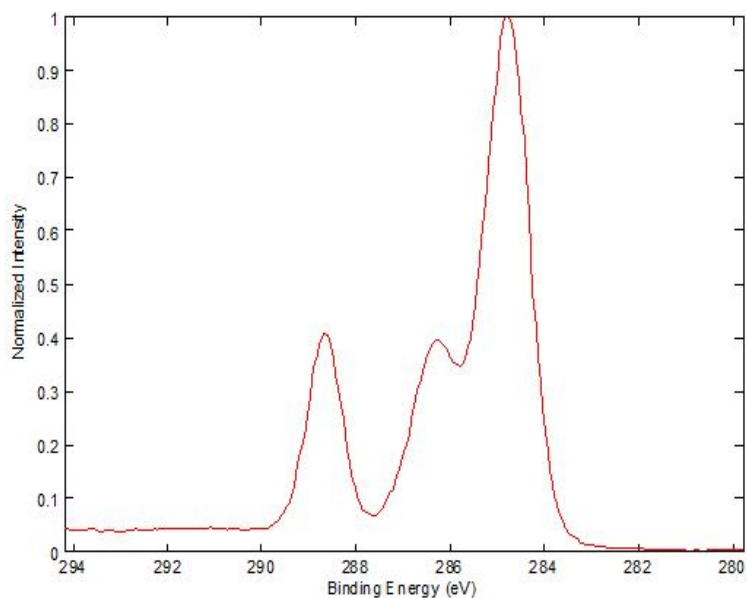


*Figure 19: The C 1s spectrum of an untreated and washed PET sample.*

## **II PEN control**

The atomic percent of the scanned PEN was 76.66 %, 23.15 %, 0.19% for carbon, oxygen, and nitrogen respectively. The experimental composition obtained falls within the stoichiometric values, 77.78 % for carbon and 22.22% for oxygen, as error is considered. The C 1s spectrum of an untreated and washed PEN sample is displayed in Fig. 20.

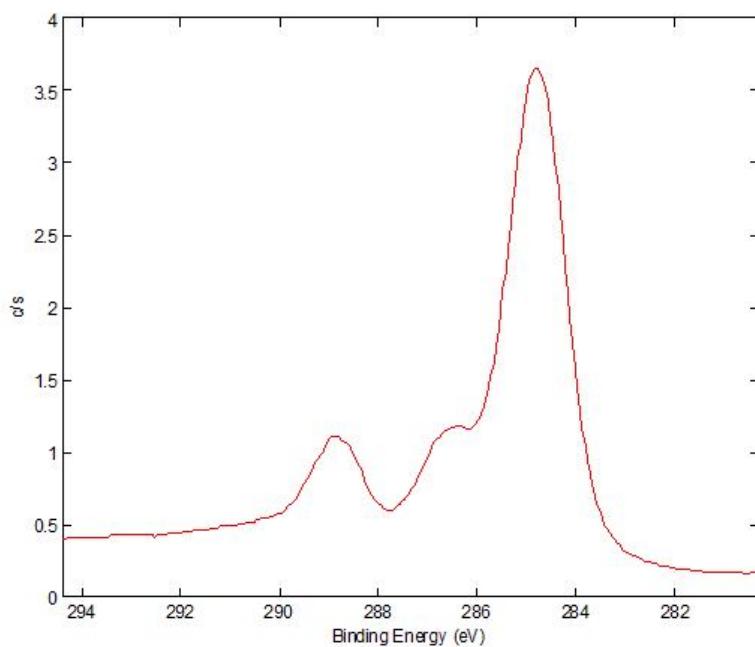


*Figure 20: The C 1s spectrum of an untreated and washed PEN sample.*

#### **4.1.2 UV photo-oxidation**

##### **I. Atmospheric pressure 300 nm broad spectrum UV photo-oxidation of PET**

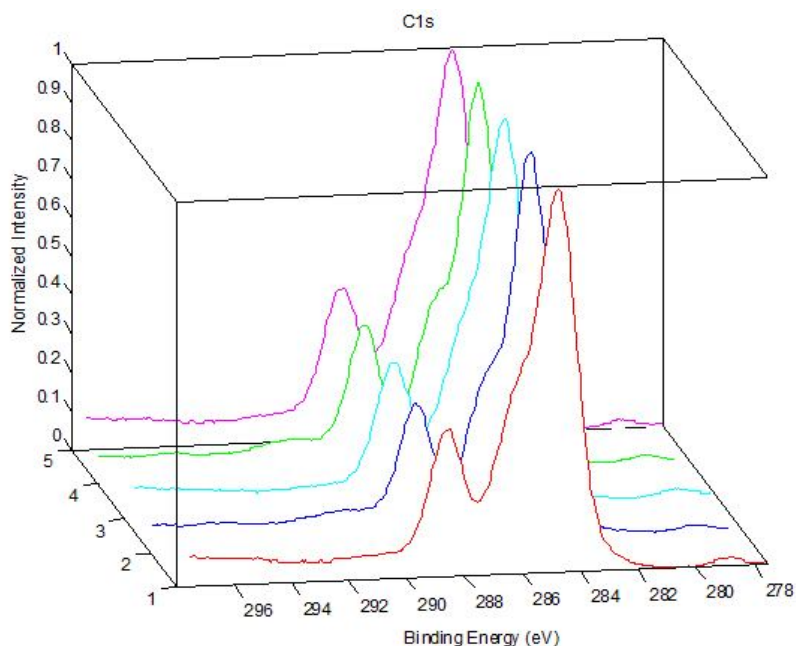
The oxygen composition slightly increased while carbon decreased as shown in Table

3. A slight nitrogen contamination comparable to the control was also detected on each sample.

Treatment time (min)	At% C	At% N	At% O
<b>Untreated and washed PET</b>	71.59	1.08	27.33
30	70.41	1.03	28.55
60	71.64	0.00	28.36
90	70.64	0.99	28.36
120	70.46	0.00	29.54
150	70.03	0.93	29.04
<b>PET Stoichiometric Composition</b>	71.40	0.00	28.60

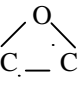
*Table 3: XPS elemental percent composition of PET exposed to the 300 nm broad spectrum UV photo-oxidation treatment.*

The overlapped C 1s spectrum of each treated PET sample is shown in Fig. 21.



*Figure 21: Overlapped C1s spectra of the 300 nm broad spectrum UV photo-oxidized PET per the exposure times; where 1-5 are 30, 60, 90, 120, and 150 min, respectively.*

The C 1s functional groups analysis for Fig. 21 is presented in Table 4.

Species	Control	30 min	60 min	90 min	120 min	150 min
C-C sp <sup>2</sup>	38.0	38.2	32.4	27.4	29.5	35.1
C-C sp <sup>3</sup>	20.8	20.1	25.8	29.6	28.7	21.2
C-O-C, 	21.7	17.4	18.0	18.5	18.1	18.1
C=O	1.4	8.4	4.9	6.6	4.3	7.6
O-C=O	17.5	14.0	12.8	15.4	13.5	15.1
O=C-O-C=O, O-(C=O)-O	0.3	1.7	4.0	2.3	3.7	2.6
Energy Loss	0.4	0.2	2.1	0.3	2.2	0.4

*Table 4: XPS C 1s functional group analysis for the 300 nm broad spectrum UV photo-oxidation of PET.*

## II. Atmospheric pressure 253.7 nm UV photo-oxidation of PET

The oxygen composition uniformly increased while the carbon decreased as a function of time as displayed in Table 5.

Treatment time (min)	At% C	At% N	At% O
Untreated and washed control	71.59	1.08	27.33
60	66.50	1.08	32.42
90	65.76	0.91	33.32
120	65.09	0.97	33.94
150	63.80	1.05	35.14
PET Stoichiometric Composition	71.40	0.00	28.6

Table 5: XPS elemental percent composition of PET exposed to the 253.7 nm UV photo-oxidation treatment.

The C 1s spectrum of each treated sample is displayed in Fig. 22.

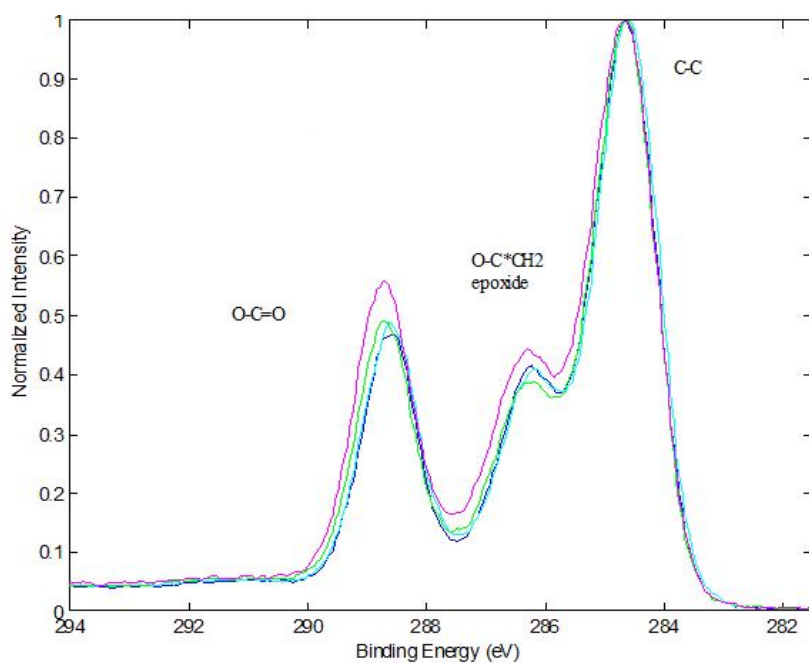
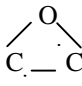


Figure 22: C 1s spectra of 253.7 nm UV photo-oxidized PET samples; where red, blue, cyan, green, and magenta are the 0, 60, 90, 120, and 150 min treated samples, respectively.

The functional group analysis for Fig. 22 is displayed in Table 6.

Species	Control	60 min	90 min	120 min	150 min
C-C sp <sup>2</sup>	38.0	33.3	32.3	28.6	32.6
C-C sp <sup>3</sup>	20.8	20.0	20.8	24.2	18.0
C-O-C, 	21.7	18.1	17.6	15.7	16.0
C=O	1.4	5.5	5.5	7.6	8.1
O-C=O	17.5	22.5	22.5	19.6	22.9
O=C-O-C=O, O-(C=O)-O	0.3	0.0	0.7	3.4	1.5
Energy Loss	0.4	0.6	0.7	1.0	0.9

*Table 6: XPS C 1s functional groups analysis for the 253.7 nm UV Photo-oxidation of PET.*

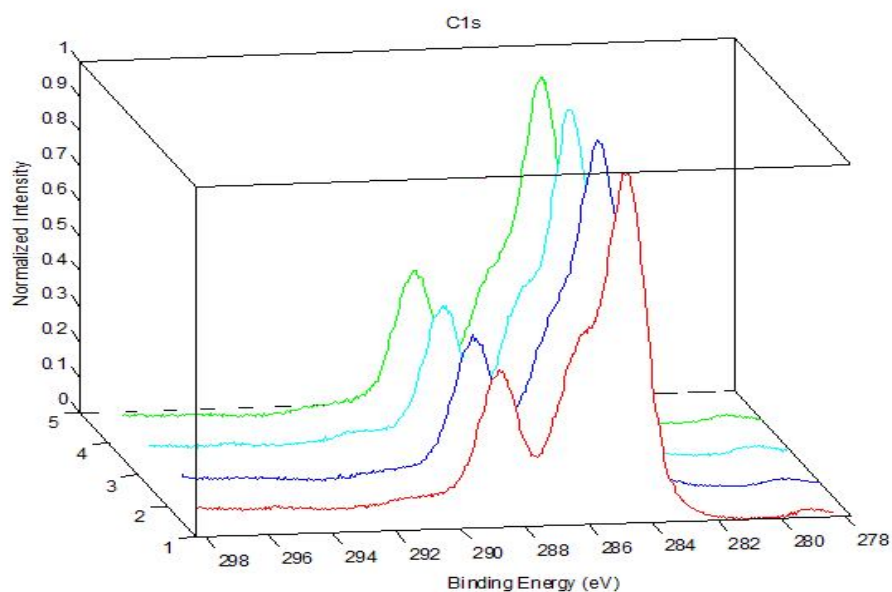
#### 4.1.3 Atmospheric pressure 184.9/253.7 nm UV photo-ozonation of PET

The treatment showed a similar trend to the 253.7nm UV photo-oxidation with the exception of a faster saturation point as shown in Table 7. Some nitrogen contaminants were found on each sample similar to the control.

Treatment time (min)	At% C	At% N	At% O
<b>Untreated and washed control</b>	71.59	1.08	27.33
4	66.60	0.34	33.05
8	66.38	1.28	32.34
15	66.12	0.44	33.44
30	65.55	1.11	33.34
<b>PET Stoichiometric Composition</b>	71.40	0.00	28.60

*Table 7: XPS elemental percent composition of PET exposed to the 184.9/253.7 nm UV photo-ozonation treatment.*

The C 1s spectrum of the photo-ozonated PET samples is displayed in Fig. 23.

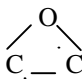


*Figure 23: C 1s spectra of 184.9/253.7 nm UV photo-ozonated PET samples; where 1-4 shown on z axis are the 4, 8, 15, and 30 min treated samples, respectively.*



The functional groups analysis of the C 1s spectrums of each sample shown in Fig.

23 is presented in Table 8.

Species	Control	4 min	8 min	15 min	30 min
C-C sp <sup>2</sup>	38.0	35.6	39.3	35.0	35.4
C-C sp <sup>3</sup>	20.8	17.9	15.6	18.6	18.6
C-O-C, 	21.7	15.8	15.7	16.2	16.3
C=O	1.4	10.1	8.5	8.9	6.5
O-C=O	17.5	15.1	16.5	14.1	16.7
O=C-O-C=O, O-(C=O)-O	0.3	3.8	3.6	5.4	5.1
Energy Loss	0.4	1.8	0.9	2.0	1.4

*Table 8: XPS C 1s functional groups analysis for the 184.9/253.7 nm UV photo-ozonation of PET.*

The 15 min 184.9/253.7 nm UV photo-ozonation treated PET sample was depth analyzed using XPS as displayed in Fig. 24. The polymer is etched several nm at time, where each indicated depth is scanned for the elemental composition at the 2-5 nm range.

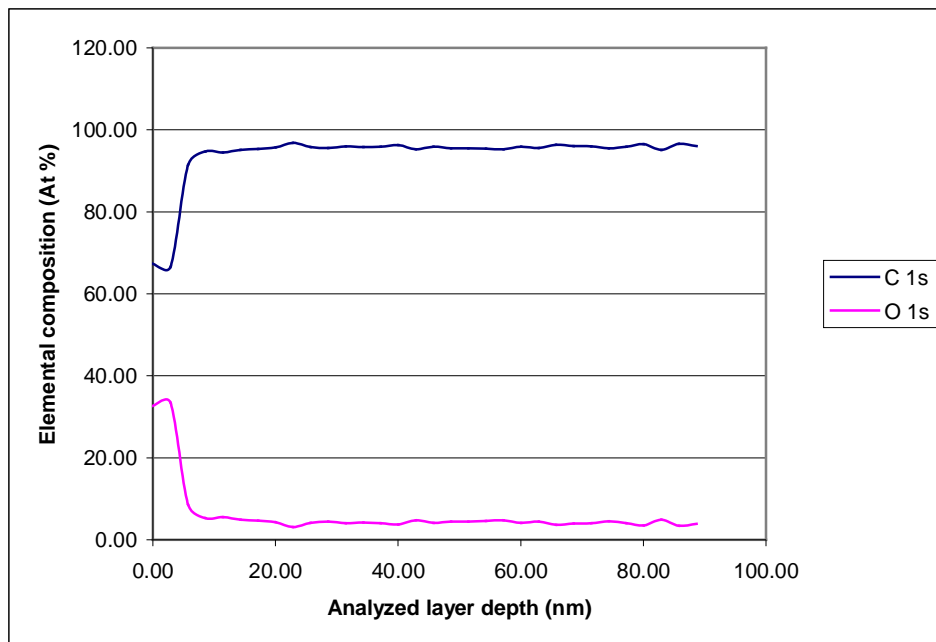


Figure 24: Depth profile XPS analysis of a 15 min 184.9/253.7 nm UV photo-ozonation treated PET sample.

#### 4.1.4 UV photolysis

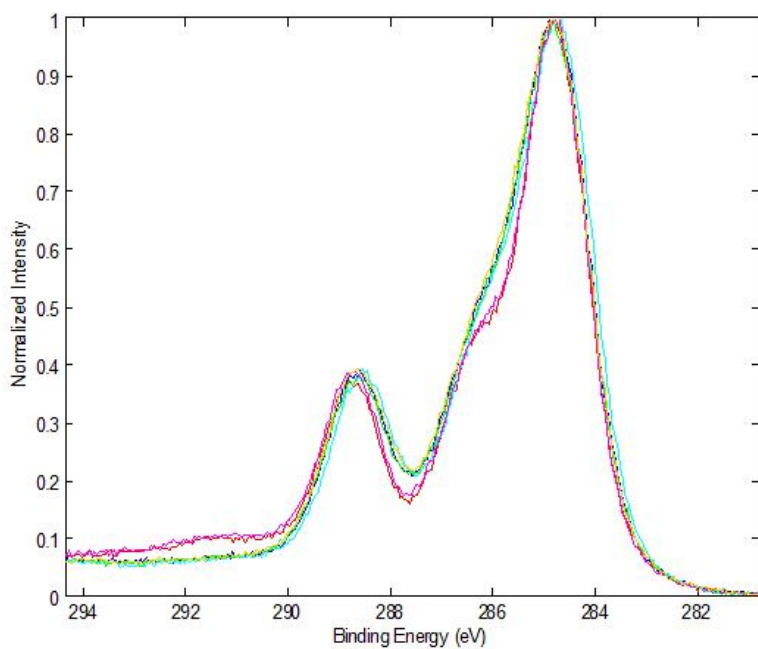
##### I. Atmospheric pressure 300 nm broad spectrum UV photolysis of PET in nitrogen

The oxygen and carbon composition did not change significantly beyond the error limits as shown in Table 9. A small nitrogen contamination was found similar to the UV photo-oxidation.

<b>Treatment time (min)</b>	<b>At% C</b>	<b>At% N</b>	<b>At% O</b>
30	70.70	0.07	29.23
60	70.47	0.76	28.77
90	70.30	0.84	28.86
120	70.54	0.76	28.69
150	70.12	0.08	29.80
180	70.11	0.90	28.98
<b>PET Stoichiometric Composition</b>	71.40	0.00	28.60

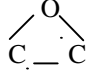
*Table 9: XPS elemental percent composition of PET exposed to a 300 nm broad spectrum UV photolysis in nitrogen.*

The overlapped C 1s spectrum of the 300 nm broad spectrum UV photolysis treated PET samples is displayed in Fig. 25.



*Figure 25: The overlapped C 1s spectrum of each of the 300 nm broad spectrum UV photolysis treated PET samples; where red, green, blue, cyan, magenta, and yellow are the 30, 60, 90, 120, 150, and 180 min treated samples, respectively.*

The functional groups analysis of each of the C 1s spectrums in Fig. 25 is shown in Table 10.

Species	Control	30 min	60 min	90 min	120 min	150 min	180 min
C-C sp <sup>2</sup>	38.0	42.8	35.5	41.6	36.3	37.3	40.9
C-C sp <sup>3</sup>	20.8	17.8	23.8	19.5	24.0	22.4	18.7
C-O-C, 	21.7	15.5	16.4	15.8	15.9	15.9	17.3
C=O	1.4	4.8	5.9	4.7	4.9	4.2	4.9
O-C=O	17.5	11.2	16.8	16.8	14.4	11.9	14.7
O=C-O-C=O, O-(C=O)-O	0.3	5.8	1.6	1.6	4.1	6.4	3.3
Energy Loss	0.4	2.3	0.1	0.1	0.4	2.0	0.2

*Table 10: XPS C 1s functional groups analysis for the 300 nm broad spectrum UV photolysis of PET in nitrogen.*

## **II. Atmospheric pressure 253.7 nm UV photolysis of PET in nitrogen**

The oxygen composition of the treated samples were found to have gradually increased while the carbon decreased as displayed in Table 11. A slight nitrogen contamination similar to the UV photo-oxidation and control samples was detected.

<b>Treatment times (min)</b>	<b>At% C</b>	<b>At% N</b>	<b>At% O</b>
15	69.01	0.98	30.01
33	70.12	0.07	29.80
45	68.12	0.13	31.75
60	67.52	0.20	32.29
90	66.31	0.28	33.40
120	65.94	0.30	33.75
<b>PET Stoichiometric Composition</b>	71.40	0.00	28.60

*Table 11: XPS elemental percent composition of PET exposed to a 253.7 nm UV photolysis in nitrogen.*

The overlapped C 1s spectrum of each of the 253.7 nm UV photolysis treated PET samples is displayed in Fig. 26.

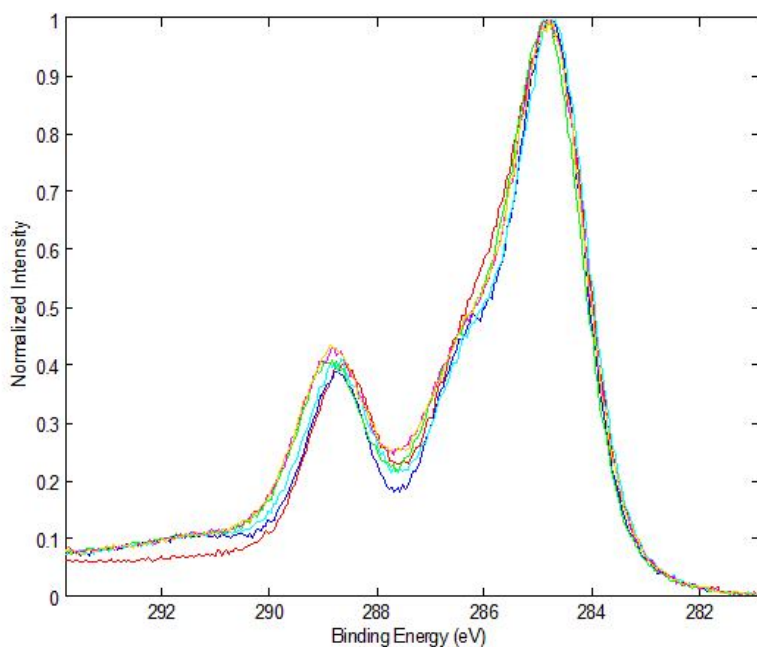


Figure 26: The C 1s spectrums of the 253.7 nm UV photolysis treated PET samples in nitrogen; where red, blue, green, cyan, magenta, and yellow are the 15, 33, 45, 60, 90, and 120 min treated samples, respectively.

The C 1s functional groups analysis for Fig. 26 is presented in Table 12.

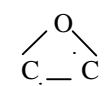
Species	Control	15 min	33 min	45 min	60 min	90 min	120 min
C-C sp <sup>2</sup>	38.0	34.1	35.7	38.1	30.5	33.1	32.8
C-C sp <sup>3</sup>	20.8	23.8	24.2	20.6	26.2	22.5	22.6
C-O-C, 	21.7	17.7	15.3	15.3	15.5	15.1	15.1
C=O	1.4	4.4	4.9	3.9	5.7	5.9	5.8
O-C=O	17.5	14.9	11.9	13.6	11.1	12.3	12.4
O=C-O-C=O, O-(C=O)-O	0.3	4.8	5.9	6.7	9.4	9.5	9.7
Energy Loss	0.4	0.4	2.2	1.8	1.7	1.6	1.7

Table 12: XPS C 1s functional groups analysis for the 253.7 nm UV photolysis of PET in nitrogen.

### III. Atmospheric pressure 184.9/253.7 nm UV photolysis of PET in nitrogen

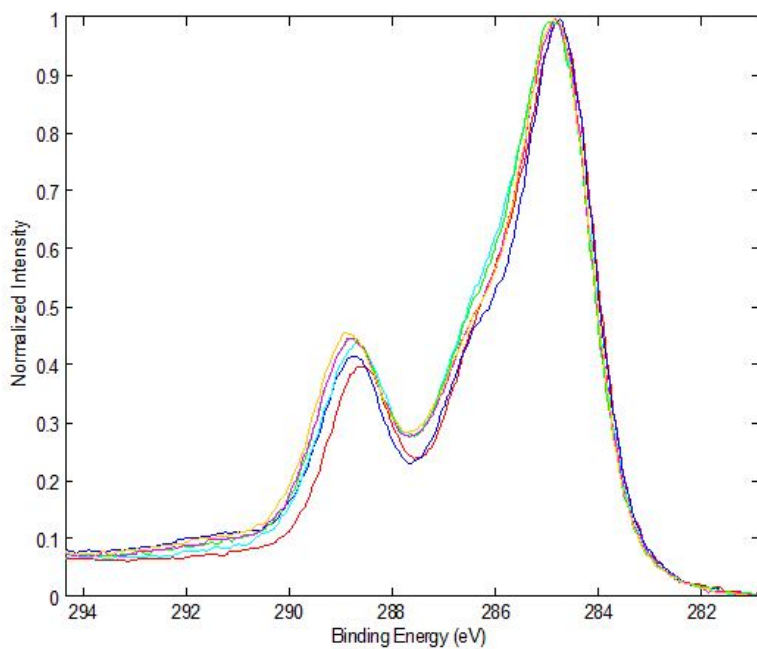
The oxygen composition has significantly increased at a gradual rate due to the treatment while the carbon content decreased as shown in Table 13. A slight nitrogen contamination of approximately 1% is also detected on each samples, including the control.

Treatment times (min)	At% C	At% N	At% O
5	69.30	0.98	29.71
10	67.33	0.43	32.24
15	67.18	1.01	31.81
25	66.66	1.03	32.31
45	65.73	1.14	33.14
60	64.89	1.38	33.73
<b>PET Stoichiometric Composition</b>	71.40	0.00	28.60

*Table 13: XPS elemental percent composition of PET exposed to a 184.9/253.7 nm UV photolysis in nitrogen.*

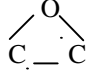
The overlapped C 1s spectrums of the 184.9/253.7 nm UV photolysis treated PET samples are presented in Fig. 27.





*Figure 27: The overlapped C 1s spectra of the 184.9/253.7 nm UV photolysis treated PET samples in nitrogen; where red, blue, yellow, green, magenta, and cyan are the 5, 10, 15, 25, 45, and 60 min treatment times, respectively.*

The functional groups assignments for the C 1s spectra shown in Fig. 27 is presented in Table 14.

Species	Control	5 min	10 min	15 min	25 min	45 min	60 min
C-C sp <sup>2</sup>	38.0	43.6	43.6	36.7	35.4	37.6	36.1
C-C sp <sup>3</sup>	20.8	15.3	14.2	18.1	19.1	17.5	17.9
C-O-C, 	21.7	16.0	15.1	16.7	15.8	14.9	14.4
C=O	1.4	6.7	5.3	7.0	7.1	7.2	7.6
O-C=O	17.5	14.3	12.4	13.1	12.8	12.6	12.0
O=C-O-C=O, O-(C=O)-O	0.3	3.9	7.6	7.8	8.6	9.2	10.4
Energy Loss	0.4	0.4	1.9	0.6	1.2	1.0	1.6

*Table 14: XPS C 1s functional groups analysis for the 184.9/253.7 nm UV photolysis of PET in nitrogen.*

#### 4.1.5 VUV photo-oxidation

##### I. VUV photo-oxidation of PET using Ar plasma

The oxygen composition was observed to initially increase while the carbon declined, then both values reached a plateau where they fluctuates as presented in Table 15. A slight nitrogen contamination of approximately 1% is also detected on each sample, including the control.

Treatment time (min)	At% C	At% N	At% O
<b>Washed and untreated control</b>	71.59	1.08	27.33
30	67.64	0.45	31.91
60	67.12	1.58	31.30
90	67.31	0.62	32.07
120	67.36	1.78	30.86
150	66.95	1.93	31.12
<b>PET Stoichiometric Composition</b>	71.40	0.00	28.60

Table 15: XPS elemental percent composition of PET exposed to VUV photo-oxidation.

The overlapped C 1s spectrum of the VUV photo-oxidized PET samples is shown in Fig. 28.

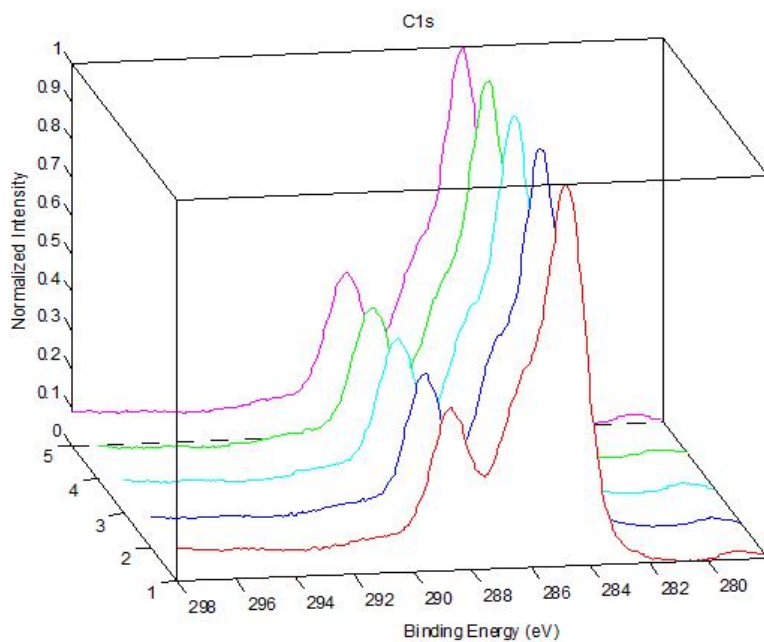


Figure 28: The overlapped C 1s spectrum of the VUV photo-oxidized PET samples; where 1-5 in the z-axis are the 30, 60, 90, 120, and 150 min treatment times, respectively.

The curve fitting for the C 1s spectrum shown in Fig. 28 is presented in Table 16.

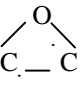
Species	Control	5 min	10 min	15 min	20 min	25 min
C-C sp <sup>2</sup>	38.0	35.0	32.9	35.3	33.2	34.7
C-C sp <sup>3</sup>	20.8	19.9	20.7	18.5	20.7	19.4
C-O-C, 	21.7	17.3	16.2	16.1	16.1	15.7
C=O	1.4	7.2	9.4	8.6	8.6	8.6
O-C=O	17.5	14.4	14.4	13.7	14.2	14.5
O=C-O-C=O, O-(C=O)-O	0.3	4.9	4.9	6.3	5.7	5.6
Energy Loss	0.4	1.3	1.6	1.6	1.5	1.5

Table 16: XPS C 1s functional groups analysis for the VUV photo-oxidation of PET.

## II. VUV photo-oxidation of PEN using Ar plasma

The oxygen composition of PEN increased to a saturation point while the carbon content followed the opposite trend as shown in Table 17. A slight nitrogen contamination similar to the control is detected.

<b>Treatment times (min)</b>	<b>At% C</b>	<b>At% N</b>	<b>At% O</b>
<b>Washed and untreated control</b>	76.66	0.19	23.15
5	74.15	0.39	25.46
10	72.47	0.46	27.06
15	70.44	0.64	28.92
20	70.52	0.88	28.60
25	67.38	0.78	31.84
30	70.39	0.58	29.03
60	70.48	0.55	28.96
90	70.16	0.48	29.35
120	70.09	0.66	29.24
150	69.70	0.71	29.59
<b>PEN Stoichiometric Composition</b>	77.78	0.00	22.22

*Table 17: XPS elemental percent composition of PEN exposed to VUV photo-oxidation.*

The C 1s spectra of the 5-25 min treated PEN sample is presented in Fig. 29, while the longer treatment times of 30-150 min is displayed in Fig. 30. The C 1s spectrum plots are separated into two figures for the sake of clarity.

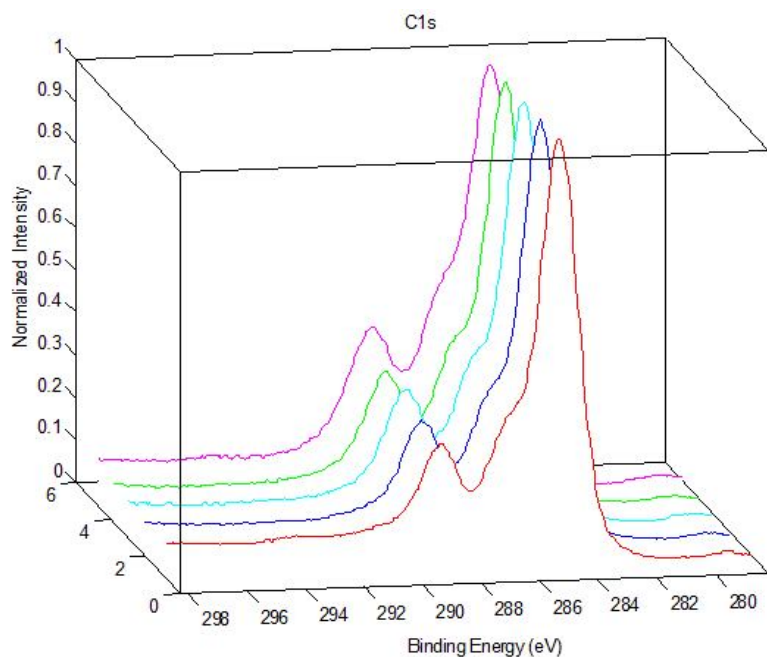


Figure 29: The overlapped C 1s spectrum of the VUV photo-oxidized PEN samples; where 1-5 are the 5, 10, 15, 20, and 25 min treatment times, respectively.

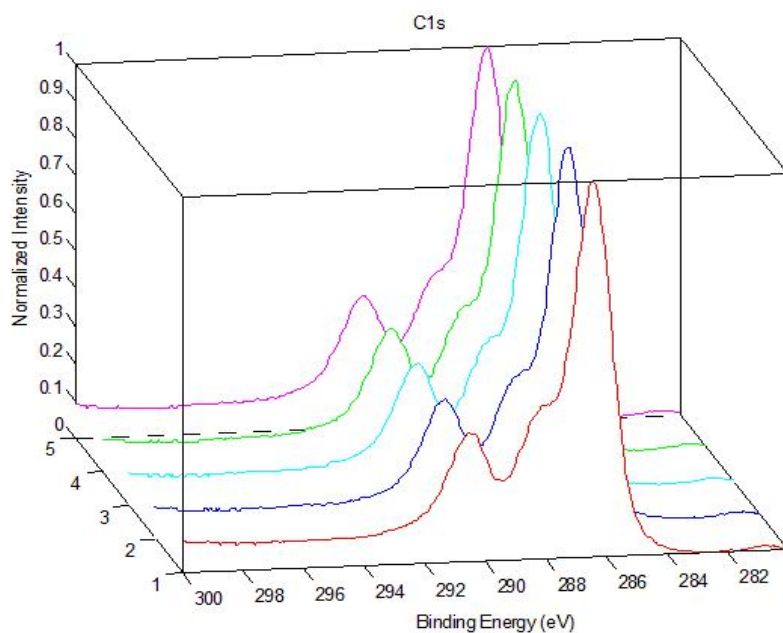


Figure 30: The C 1s spectrums of the VUV photo-oxidized PEN samples; where 1-5 are the 30, 60, 90, 120, and 150 min treatment times, respectively.

The C 1s functional group analysis for each of the VUV photo-oxidized PEN samples are presented in Table 18.

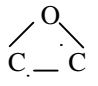
Species	Control	5 min	10 min	15 min	20 min	25 min	30 min	60 min	90 min	120 min	150 min
C-C sp <sup>2</sup>	47.7	52.0	44.0	46.2	38.9	46.4	40.2	45.2	39.5	39.2	45.0
C-C sp <sup>3</sup>	19.1	11.0	15.2	10.7	17.5	4.1	15.9	11.8	16.7	16.9	11.0
C-O-C, 	2.1	5.0	4.5	4.9	2.7	6.9	2.7	3.4	1.9	2.2	3.9
C=O	15.2	17.0	20.0	21.2	23.1	24.7	22.6	21.3	22.8	22.6	21.5
O-C=O	10.0	10.4	10.2	10.7	10.3	10.5	11.5	11.9	11.3	11.6	11.5
O=C-O-C=O, O-(C=O)-O	4.7	4.3	5.6	5.8	6.7	7.1	6.7	6.1	7.0	6.7	6.6
Energy Loss	1.2	0.4	0.6	0.5	0.8	0.3	0.4	0.3	0.8	0.6	0.5

Table 18: XPS C 1s functional groups analysis for the VUV photo-oxidation of PEN.

#### 4.1.6 VUV photolysis

##### I. VUV photolysis of PET using Ar plasma

The oxygen composition is found to have slightly decreased, while the carbon content increased as shown in Table 19. A slight nitrogen contamination is detected on each sample, including the control.

Treatment times (min)	At% C	At% N	At% O
15	69.89	1.44	28.67
30	69.93	1.37	28.70
60	70.51	1.66	27.83
90	70.42	2.29	27.29
120	70.43	2.36	27.21
150	70.52	2.60	26.88
<b>PET Stoichiometric Composition</b>	71.40	0.00	28.60

Table 19: XPS elemental percent composition of PET exposed to VUV photolysis.

The overlapped C 1s spectra of the VUV photolysis treated PET samples is shown in Fig. 31.

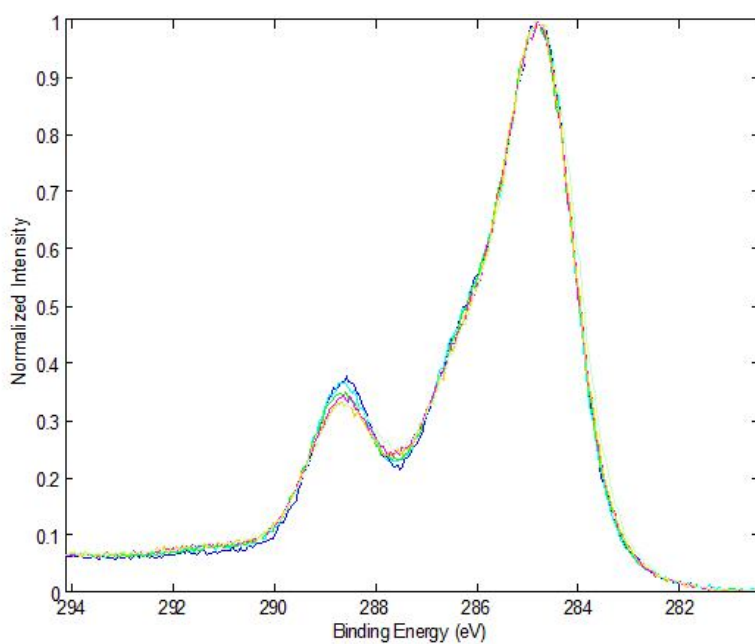


Figure 31: The C 1s spectrums of the VUV photolysis treated PET samples; where yellow, magenta, green, pale green, cyan, and blue are the 15, 30, 60, 90, 120, and 150 min treatment times, respectively.



The functional groups analysis of the C 1s spectra in Fig. 31 is shown in Table 20.

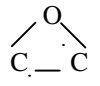
Species	Control	15 min	30 min	60 min	90 min	120 min	150 min
C-C sp <sup>2</sup>	38.0	44.2	42.4	43.7	44.0	45.2	48.0
C-C sp <sup>3</sup>	20.8	16.5	17.7	17.5	16.7	16.8	13.0
C-O-C, 	21.7	15.9	15.8	15.3	14.6	14.2	15.8
C=O	1.4	6.4	6.8	7.2	8.0	7.8	5.7
O-C=O	17.5	13.6	12.8	12.0	11.3	11.0	11.3
O=C-O-C=O, O-(C=O)-O	0.3	3.2	4.0	4.1	4.7	4.6	5.2
Energy Loss	0.4	0.3	0.5	0.4	0.8	0.5	1.0

Table 20: XPS C 1s functional groups analysis for the VUV photolysis of PET.

## II. VUV photolysis of PEN using Ar plasma

The oxygen composition increased to a saturation point immediately, the opposite trend is seen for carbon as presented in Table 21. A slight fluctuating nitrogen contamination is observed on each PEN sample.

<b>Treatment time (min)</b>	<b>At% C</b>	<b>At% N</b>	<b>At% O</b>
<b>Washed and untreated Control</b>	76.66	0.19	23.15
5	74.08	0.46	25.47
15	74.22	0.29	25.49
30	73.75	0.56	25.69
60	74.18	0.73	25.09
90	72.25	1.46	26.30
120	73.12	1.43	25.46
150	72.46	1.84	25.71
<b>PEN Stoichiometric Composition</b>	77.78	0.00	22.22

*Table 21: XPS elemental percent composition of PEN exposed to VUV photolysis.*

The C 1s spectra of the VUV photolysis treated PEN samples are displayed in Fig.

32.

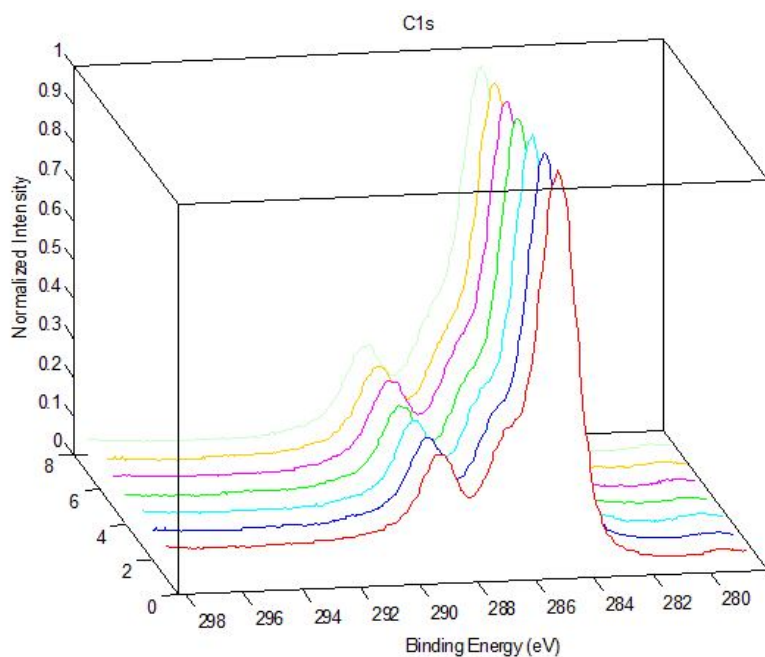


*Figure 32: The overlapped C 1s spectra of the VUV photolysis treated PEN samples; where 1-7 on the z axis are the 5, 15, 30, 60, 90, 120, and 150 min treated samples, respectively.*

The functional groups analysis of the C 1s spectrums shown in Fig. 32 is displayed in Table 22.

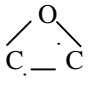
Species	Control	5 min	15 min	30 min	60 min	90 min	120 min	150 min
C-C sp <sup>2</sup>	47.7	41.8	43.4	41.7	39.9	44.2	46.4	43.3
C-C sp <sup>3</sup>	19.1	22.5	21.3	22.8	24.7	19.5	18.4	19.8
C-O-C, 	2.1	13.4	13.5	13.8	13.4	14.0	13.5	14.0
C=O	15.2	5.2	4.8	5.3	5.5	5.3	5.3	6.0
O-C=O	10.0	7.4	7.7	7.9	7.3	8.8	8.9	8.9
O=C-O-C=O, O-(C=O)-O	4.7	8.8	8.4	7.9	8.5	7.8	7.1	7.4
Energy Loss	1.2	0.9	0.8	0.7	0.8	0.5	0.5	0.6

Table 22: XPS C 1s functional groups analysis for the VUV photolysis of PEN.

#### 4.1.7 Remote exposure in the absence of photons

##### I. MW discharge of Ar/O<sub>2</sub> and Ar plasma on PET

The oxygen composition is observed to have increased to a saturation point while the carbon decreased as presented in Table 23. No significant change is observed for the remote argon treated samples beyond the error limits. A slight nitrogen contamination is detected on each samples similar to the VUV photo-oxidation samples.

<b>Treatment time (min)</b>	<b>At% C</b>	<b>At% N</b>	<b>At% O</b>
30 (Ar)	70.49	0.98	28.53
60 (Ar)	70.25	0.92	28.83
90 (Ar)	71.25	0.00	28.75
30 (Ar/O <sub>2</sub> )	66.10	0.70	33.20
60 (Ar/O <sub>2</sub> )	65.69	0.47	33.84
90 (Ar/O <sub>2</sub> )	67.77	1.06	31.17
120 (Ar/O <sub>2</sub> )	64.53	0.61	34.85
150 (Ar/O <sub>2</sub> )	66.06	1.44	32.50
<b>PET Stoichiometric Composition</b>	71.40	0.00	28.60

*Table 23: XPS elemental percent composition of PET exposed to remote oxygen atoms in the absence of photons.*

The C 1s spectrum of the remote argon treated PET samples is shown in Fig. 33, while the remote oxygen treated samples are displayed in Fig. 34.

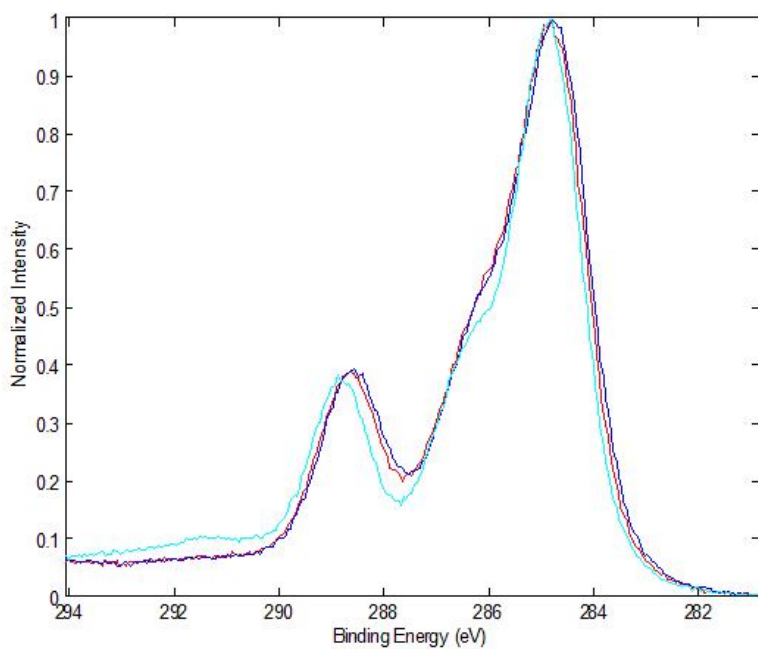


*Figure 33: The overlapped C 1s spectrum of the remote argon treated PET samples; where red, blue, and cyan are the 30, 60, and 90 min treated samples, respectively.*

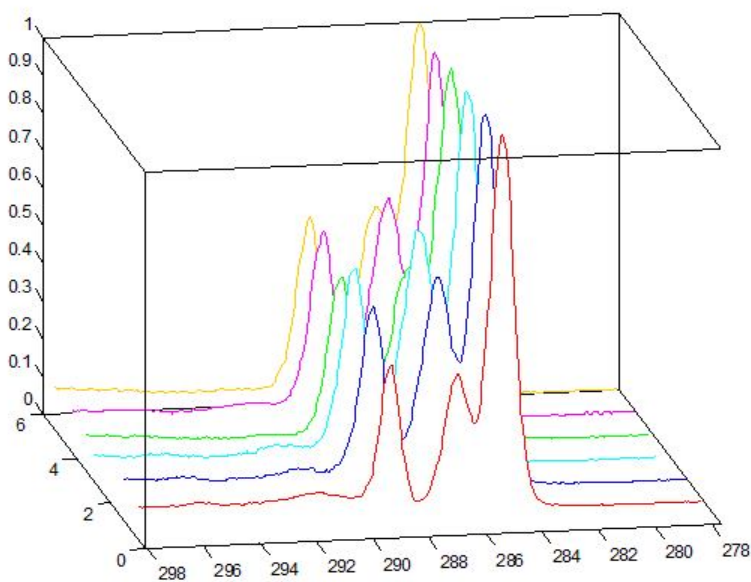


*Figure 34: The C 1s spectrums of the remote oxygen treated PET samples; where 2-6 on the z-axis are the 30, 60, 90, 120, and 150 min treated samples, respectively. Plot #1 is the 60 min remote argon treated sample as a comparison.*

The functional groups analysis of the C 1s spectrums in Fig. 33 and 34 are presented in Table 24.

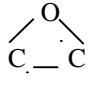
Species	Control	30 min (Ar)	60 min (Ar)	90 min (Ar)	30 min (Ar/O <sub>2</sub> )	60 min (Ar/O <sub>2</sub> )	90 min (Ar/O <sub>2</sub> )	120 min (Ar/O <sub>2</sub> )	150 min (Ar/O <sub>2</sub> )
C-C sp <sup>2</sup>	38.0	32.9	38.7	35.8	26.8	24.1	23.5	25.6	40.7
C-C sp <sup>3</sup>	20.8	23.8	20.0	22.6	22.1	21.9	29.8	21.1	11.6
C-O-C, 	21.7	18.4	18.3	17.8	22.3	22.4	22.1	22.3	22.5
C=O	1.4	6.2	5.6	4.8	7.8	9.4	4.5	8.7	5.5
O-C=O	17.5	17.5	15.0	11.1	16.9	18.0	19.2	18.8	17.7
O=C-O-C=O, O-(C=O)-O	0.3	0.8	2.2	5.8	3.0	2.7	0.5	2.2	2.0
Energy Loss	0.4	0.3	0.3	2.2	1.1	1.5	0.2	1.3	0.0

Table 24: XPS C 1s functional groups analysis for PET exposed to remote oxygen atoms in the absence of photons.

## II. MW discharge of Ar/O<sub>2</sub> and Ar plasma on PEN

The oxygen composition is found to have increased significantly while the carbon content decreased as shown in Table 25. An insignificant change is detected from the Ar only plasma discharge, where the changes fall within the error limits. A small nitrogen contamination is found on each PEN sample.

<b>Treatment time (min)</b>	<b>At% C</b>	<b>At% N</b>	<b>At% O</b>
<b>Washed and untreated control</b>	76.66	0.19	23.15
10 (Ar MW discharge)	76.88	0.14	22.97
60 (Ar MW discharge)	76.91	0.13	22.96
5 (O <sub>2</sub> /Ar MW discharge)	72.60	0.16	27.24
10 (O <sub>2</sub> /Ar MW discharge)	70.91	0.33	28.76
15 (O <sub>2</sub> /Ar MW discharge)	70.00	0.36	29.64
20 (O <sub>2</sub> /Ar MW discharge)	69.28	0.40	30.32
25 (O <sub>2</sub> /Ar MW discharge)	68.99	0.29	30.71
30 (O <sub>2</sub> /Ar MW discharge)	68.88	0.33	30.79
60 (O <sub>2</sub> /Ar MW discharge)	67.44	0.36	32.20
90 (O <sub>2</sub> /Ar MW discharge)	65.74	0.68	33.58
120 (O <sub>2</sub> /Ar MW discharge)	66.22	0.46	33.32
150 (O <sub>2</sub> /Ar MW discharge)	64.91	0.67	34.42
<b>PEN Stoichiometric Composition</b>	77.78	0.00	22.22

*Table 25: XPS elemental percent composition of PEN exposed to remote oxygen or argon atoms in the absence of photons.*

The overlapped C 1s spectrum of the treated PEN is displayed in Fig. 35.



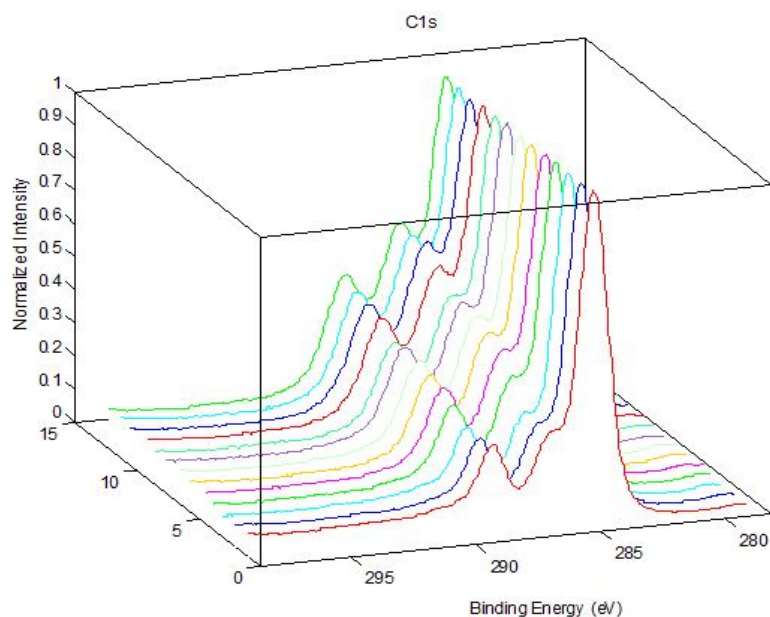


*Figure 35: The overlapped C 1s spectrum of the remote oxygen and remote argon treated stabled; where 1-3 are the 0, 10, and 60 min remote argon treated samples while the 4-14 are the 5, 10, 15, 20, 25, 30, 60, 90, 120, and 150 min remote oxygen treated samples, respectively.*

The C 1s functional groups analysis of Fig. 35 is shown in Table 26.

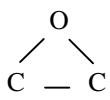
Species	C-C sp <sup>2</sup>	C-C sp <sup>3</sup>	C-O-C, 	C=O	O-C=O	O=C-O-C=O, O-(C=O)-O	Energy Loss
<b>Control</b>	47.7	19.1	2.1	15.2	10	4.7	1.2
<b>10 min (Ar)</b>	47.5	19.9	2.8	15.1	9.2	4.9	0.6
<b>60 min (Ar)</b>	43.3	24.2	1	16.2	9.2	5.2	0.9
<b>5 min (Ar /O<sub>2</sub>)</b>	37.2	23	0.3	22.6	9.9	6.1	0.9
<b>10 min (Ar /O<sub>2</sub>)</b>	45.6	12.2	2	23.2	11.2	5.3	0.5
<b>15 min (Ar /O<sub>2</sub>)</b>	37.6	17.4	0	27.5	11.1	5.7	0.7
<b>20 min (Ar /O<sub>2</sub>)</b>	42.4	11.5	0	27.8	11.3	6.4	0.6
<b>25 min (Ar /O<sub>2</sub>)</b>	36	15.8	0	29.3	11	7.3	0.8
<b>30 min (Ar /O<sub>2</sub>)</b>	41.9	12.2	0.9	28.4	11.4	4.9	0.3
<b>60 min (Ar /O<sub>2</sub>)</b>	39.8	8.9	0	33.1	11.1	6.6	0.5
<b>90 min (Ar /O<sub>2</sub>)</b>	35.2	9.9	0	35.7	10.9	7.7	0.6
<b>120 min (Ar /O<sub>2</sub>)</b>	39.5	6	0	36.2	11.3	6.6	0.4
<b>150 min (Ar /O<sub>2</sub>)</b>	39.8	4.3	0	36.3	11.7	7.5	0.4

Table 26: XPS C 1s functional groups analysis for PEN exposed to remote oxygen or argon atoms in the absence of photons.

## 4.2 Contact Angle

The average contact angle of all of the samples before each treatment is presented, followed by the percent change due to the treatment.

### 4.2.1 UV photo-oxidation

#### I. Atmospheric pressure 300 nm broad spectrum UV photo-oxidation of PET

The contact angle slightly decreased as shown in Fig. 36. The average measured advancing contact angle for each of the PET samples before treatment was 82.8 degrees.

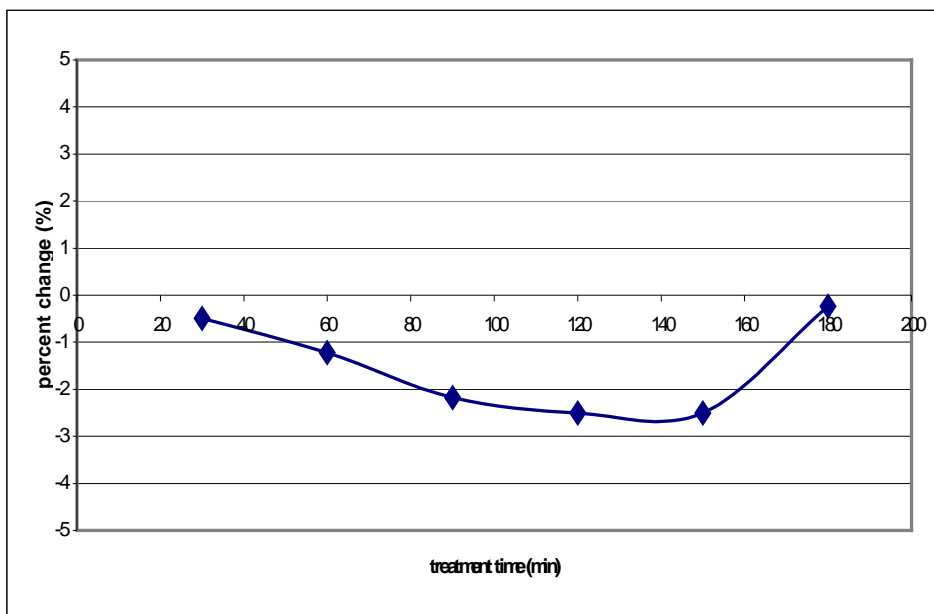


*Figure 36: Percent change in the advancing contact angle on PET due to the 300 nm broad spectrum UV photo-oxidation treatment.*

#### II. Atmospheric pressure 253.7 nm UV photo-oxidation of PET

The advancing contact angle is observed to gradually decrease due to the treatment as presented in Fig. 37. The average measured advancing contact angle for the pre-treated

samples of PET was 82.2 degrees.

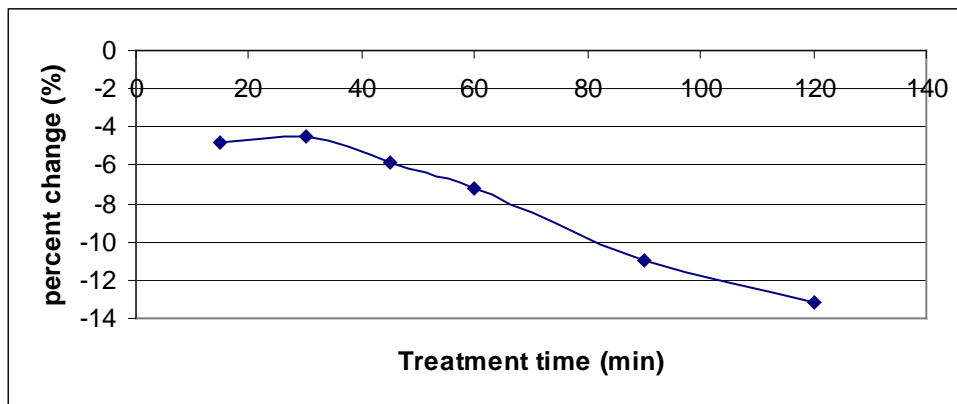


Figure 37: Percent change in the advancing contact angle on PET due to 253.7 nm UV photo-oxidation.

#### 4.2.2 Atmospheric pressure 184.9/253.7 nm UV photo-ozonation of PET

The percent change in the contact angle shows an overall decreasing trend as shown in Fig. 38. The average advancing contact angle of the PET samples before treatment was 82.8 degrees.

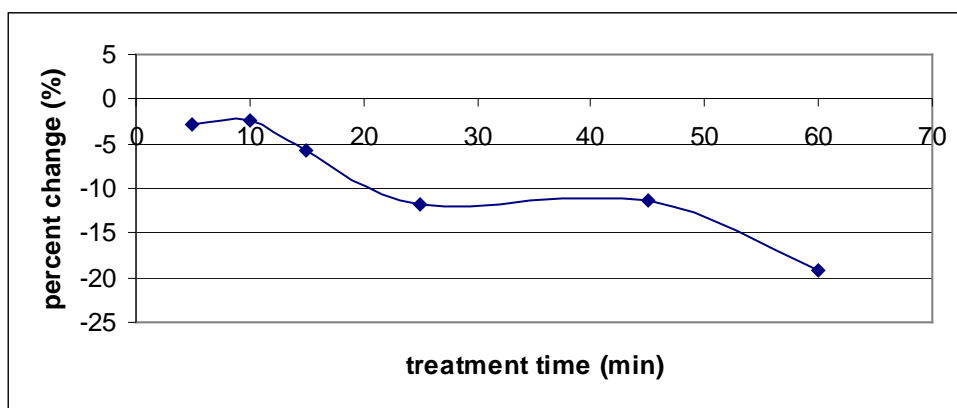
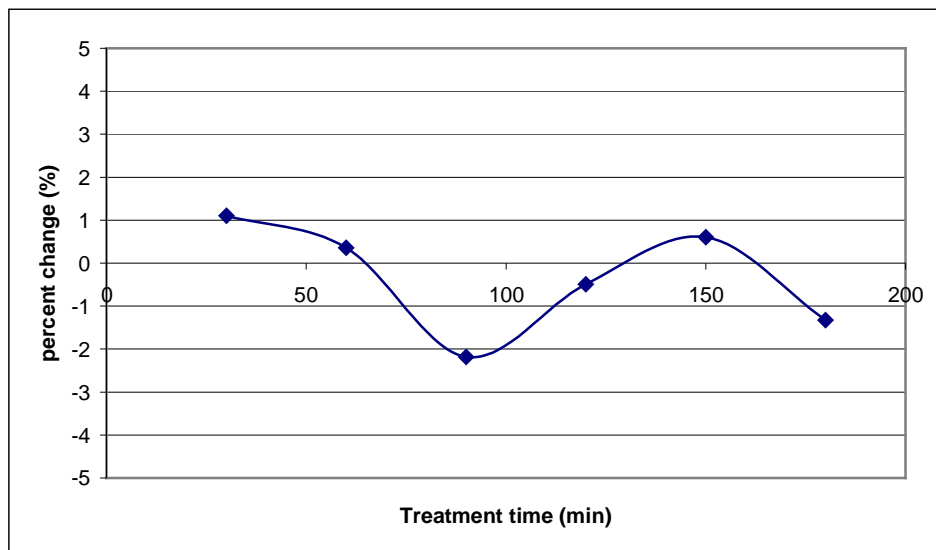


Figure 38: Percent change in the advancing contact angle on PET due to the 184.9/253.7 nm UV photo-ozonation treatment.

### 4.2.3 UV photolysis

#### I. Atmospheric pressure 300 nm broad spectrum UV photolysis of PET in nitrogen

The contact angle is found to have insignificantly changed as shown in Fig. 39. The average measured advancing contact angle for the untreated PET samples was 82.4 degrees.



*Figure 39: Percent change in the advancing contact angle on PET due to the 300 nm broad spectrum UV photolysis in nitrogen.*

#### II. Atmospheric pressure 253.7 nm UV photolysis of PET in nitrogen

The contact angle is found to slowly decrease due to the treatment as presented in Fig. 40. The average measured advancing contact angle for the PET samples before treatment was 82.4 degrees.

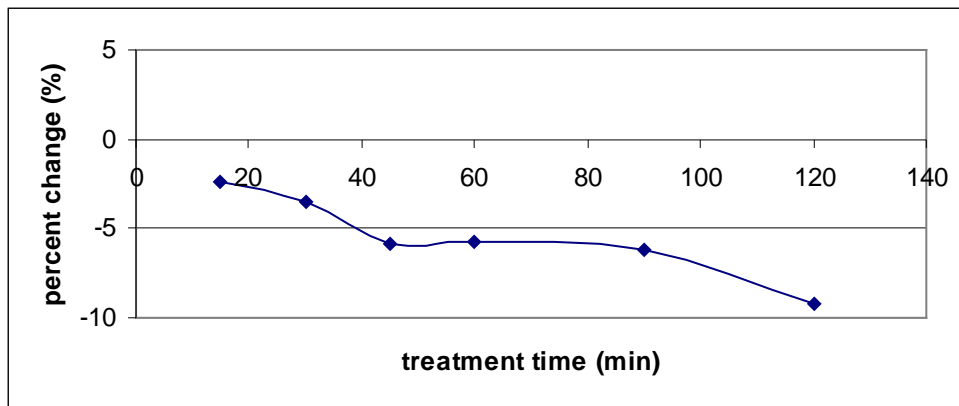


Figure 40: Percent change in the advancing contact angle on PET due to the 253.7 nm UV photolysis in nitrogen.

### III. Atmospheric pressure 184.9/253.7 nm UV photolysis of PET in nitrogen

The percent change in the contact angle was observed to decrease to minimum as shown in Fig. 41. The advancing contact angle of the untreated PET samples was 82.3 degrees.

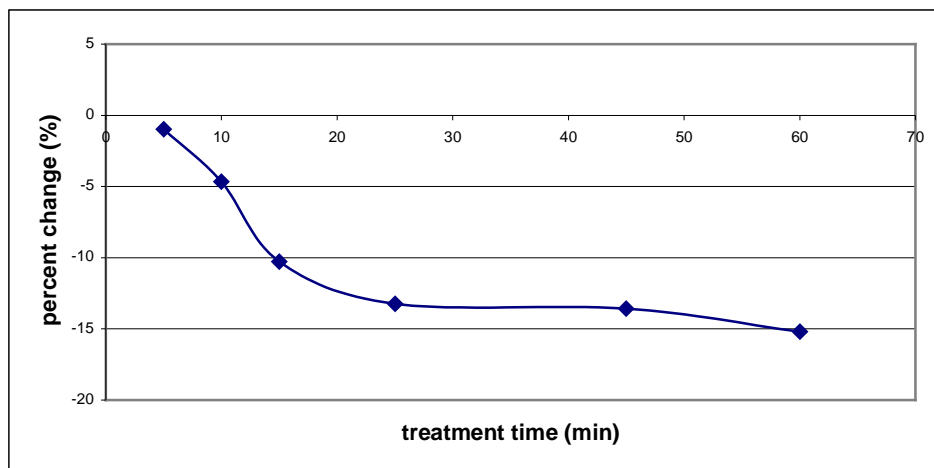


Figure 41: Percent change in the advancing contact angle on PET due to the 184.9/253.7 nm UV photolysis in nitrogen.

#### 4.2.4 VUV photo-oxidation

##### I. VUV photo-oxidation of PET using Ar plasma

The contact angle was measured to have decreased to a plateau as presented in Fig.

42. The average advancing contact angle for the untreated PET samples was 82.6 degrees.

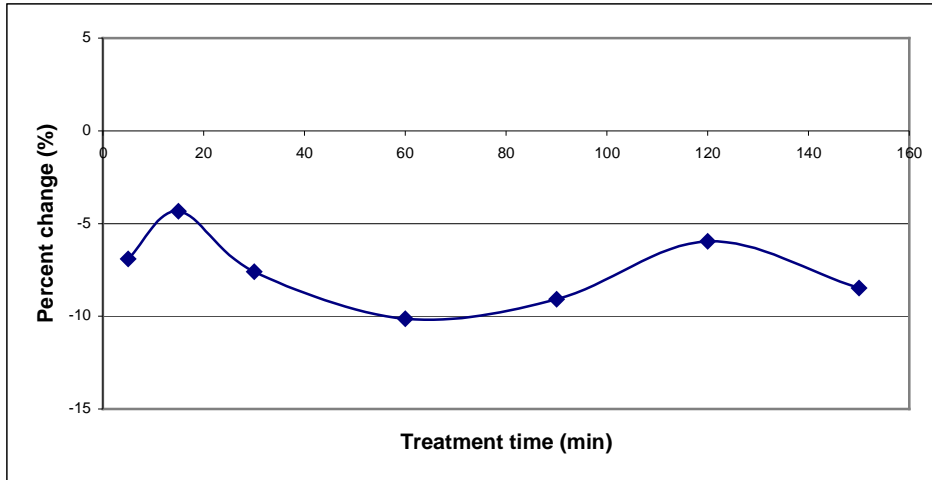


Figure 42: Percent change in the advancing contact angle on PET due to VUV photo-oxidation.

##### II. VUV photo-oxidation of PEN using Ar plasma

The contact angle like the 184.9/253.7 nm UV photolysis decreased to minima as shown in Fig. 43. The average measured advancing contact angle for all of the PEN samples before treatment was 83.2 degrees.

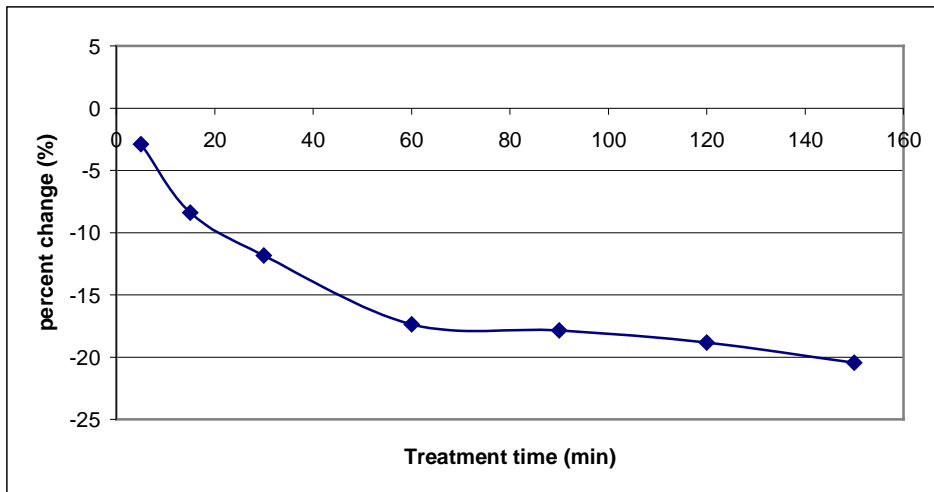


Figure 43: Percent change in the advancing contact angle on PEN due to VUV photo-oxidation.

#### 4.2.5 VUV photolysis

##### I. VUV photolysis of PET using Ar plasma

The percent change in the contact angle was observed to slowly decreased as shown in Fig. 44. The average measured advancing contact angle for the pre-treated PET samples was 82.4 degrees.



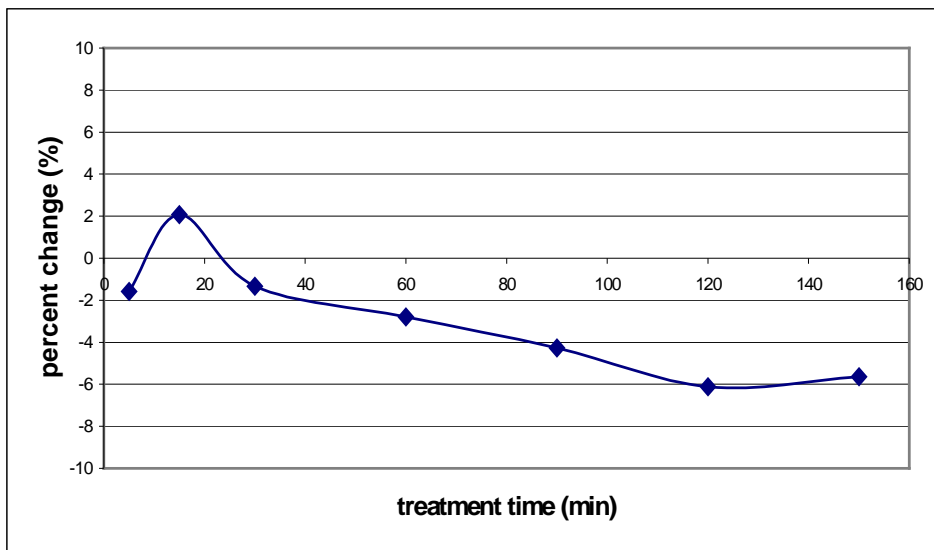


Figure 44: Percent change in the advancing contact angle on PET due to VUV photolysis.

## II. VUV photolysis of PEN using Ar plasma

The measured advancing contact angle was found to have decreased to minima as shown in Fig. 45. The average advancing contact angle for all of the pre-treated PET samples was 82.2 degrees.

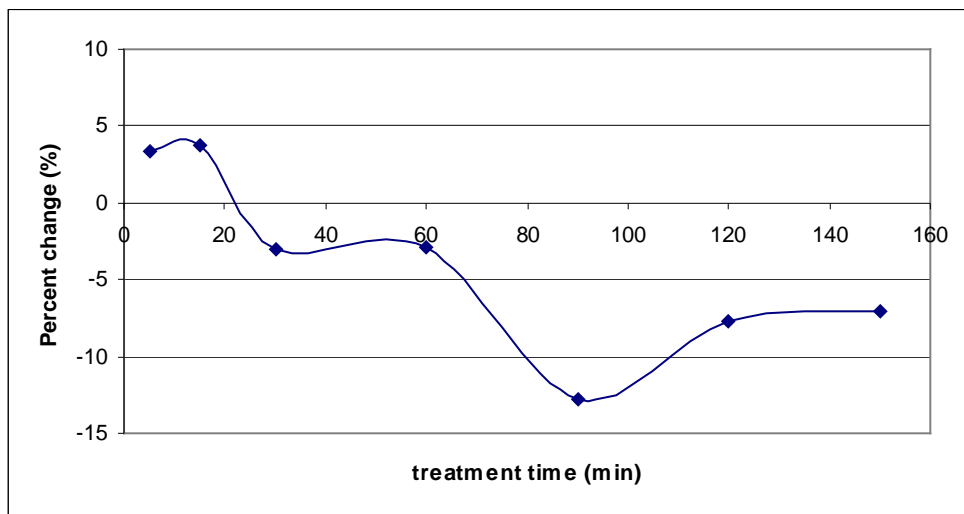
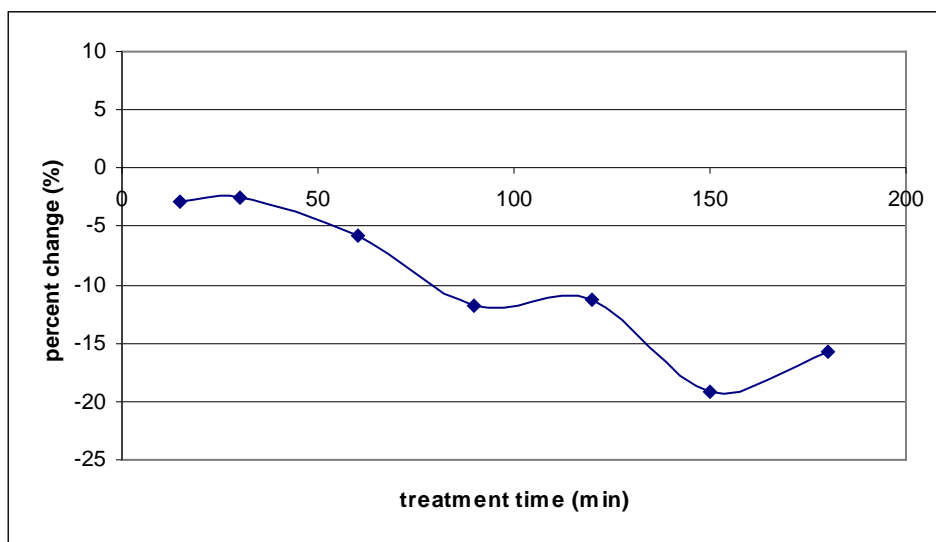


Figure 45: Percent change in the advancing contact angle on PEN due to VUV photolysis.

#### 4.2.6 Remote exposure in the absence of photons

##### I. Remote MW discharge of Ar/O<sub>2</sub> plasma on PET

The percent change in the advancing contact angle showed a significant overall gradual decrease as presented in Fig. 46. The contact angle of the PET samples before treatment was 82.5 degrees.



*Figure 46: Percent change in the advancing contact angle on PET due to remote oxygen atom exposure in the absence of photons.*

##### II. MW discharge of Ar/O<sub>2</sub> plasma on PEN

The contact angle was found to have significantly decreased as shown in Fig. 47. The average measured contact angle of the PEN samples before treatment was 83.3 degrees.

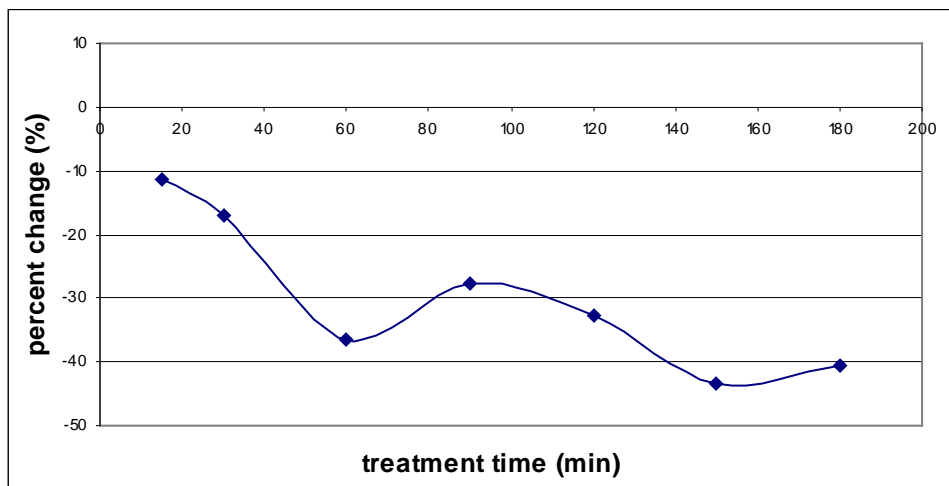


*Figure 47: Percent change in the advancing contact angle on PEN due to remote oxygen atom exposure in the absence of photons.*

### 4.3 SEM

#### 4.3.1 UV photo-oxidation

##### I. Atmospheric pressure 300 nm broad spectrum UV photo-oxidation of PET

The SEM scans of the untreated and the 90 min 300 nm broad spectrum UV photo-oxidized PET samples are displayed at 10, 50, and 100 kX magnification in Fig. 48.

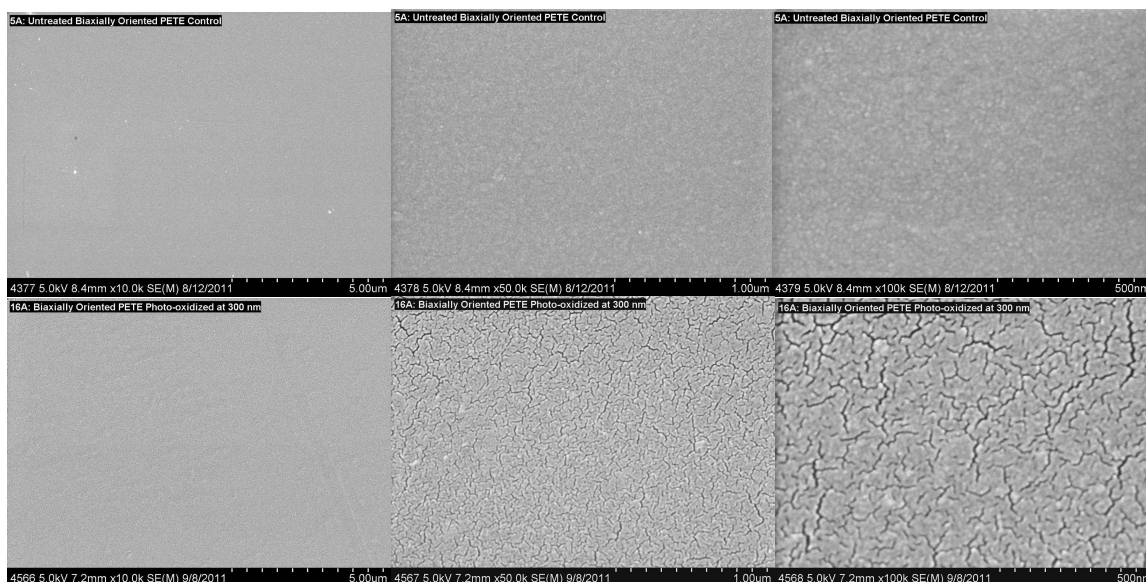


Figure 48: SEM scans of 10, 50, and 100kX (left to right) magnification of untreated (top) and 90 min 300 nm broad spectrum UV photo-oxidation treated (bottom) PET films.

## II. Atmospheric pressure 253.7 nm UV photo-oxidation of PET

The SEM scans of the untreated and 90 min 253.7 nm UV photo-oxidized PET samples are displayed at 10, 50, and 100 kX magnification in Fig. 49.

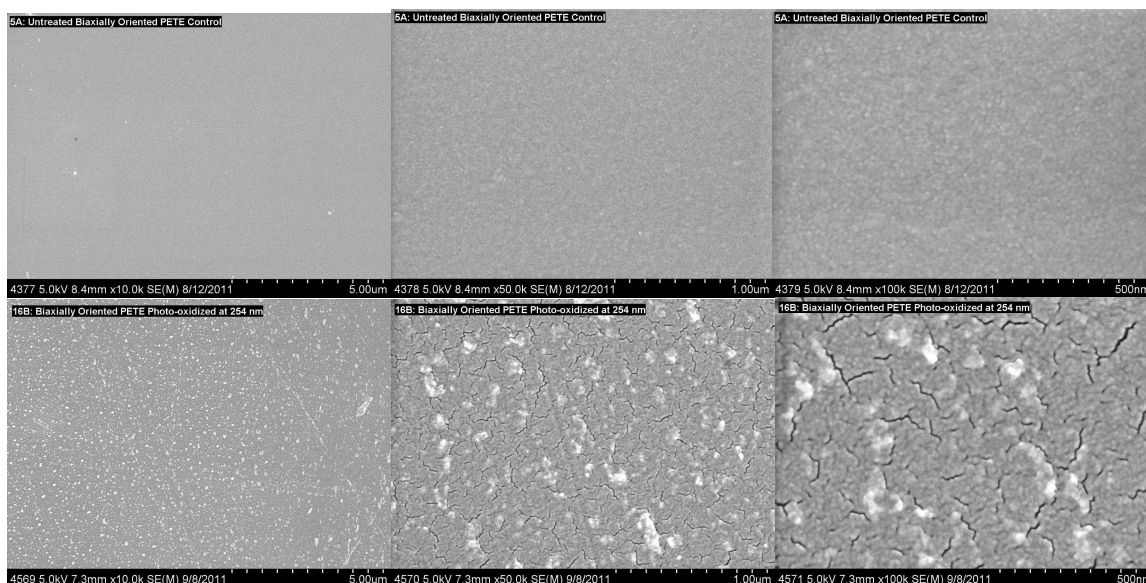
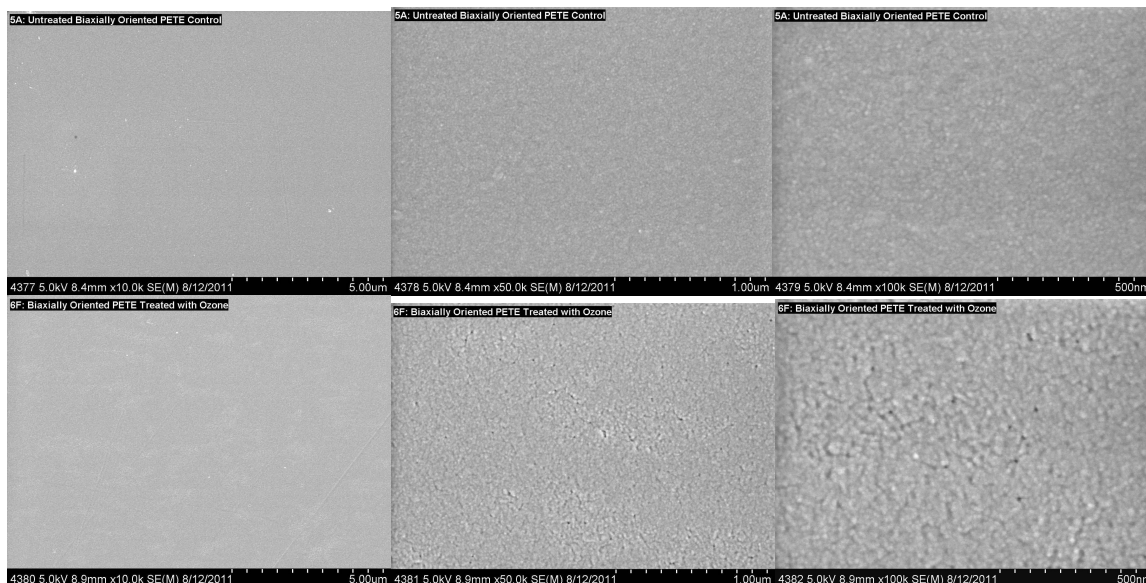


Figure 49: SEM scans of 10, 50, and 100kX (left to right) magnification of untreated (top) and 90 min 253.7 nm UV photo-oxidation treated (bottom) PET films.

### 4.3.2 Atmospheric pressure 184.9/253.7 nm UV photo-ozonation of PET

The SEM scans of the untreated and the 15min 184.9/253.7 nm UV photo-ozonated PET samples are displayed at 10, 50, and 100 kX magnification in Fig. 50.



*Figure 50: SEM scans of 10, 50, and 100kX (left to right) magnification of untreated (top) and 15 min 184.9/253.7 nm UV photo-ozonation treated (bottom) PET films.*

## 4.4 UV absorption spectroscopy

The total UV absorption is calculated by integrating all the absorption values from 190 to 320 nm for PET and 190 to 400 nm for PEN. The percent change in the total absorption is calculated and tabulated for each sample. The percent change per the wavelength is plotted to show which areas in the spectrum are changing and at what rate.

#### 4.4.1 UV photo-oxidation

##### I. Atmospheric pressure 300 nm broad spectrum UV photo-oxidation of PET

The integrated UV absorption of PET is observed to gradually decrease as revealed in Table 27.

Sample treatment time (min)	Percent change (%)
30	-6.31
60	-11.28
90	-17.36
120	-19.25
150	-17.65
180	-21.05

Table 27: Percent change in the total UV absorption of PET due to the 300 nm broad spectrum UV photo-oxidation treatment.

The specific change in absorption per  $\lambda$  is displayed in Fig. 51.

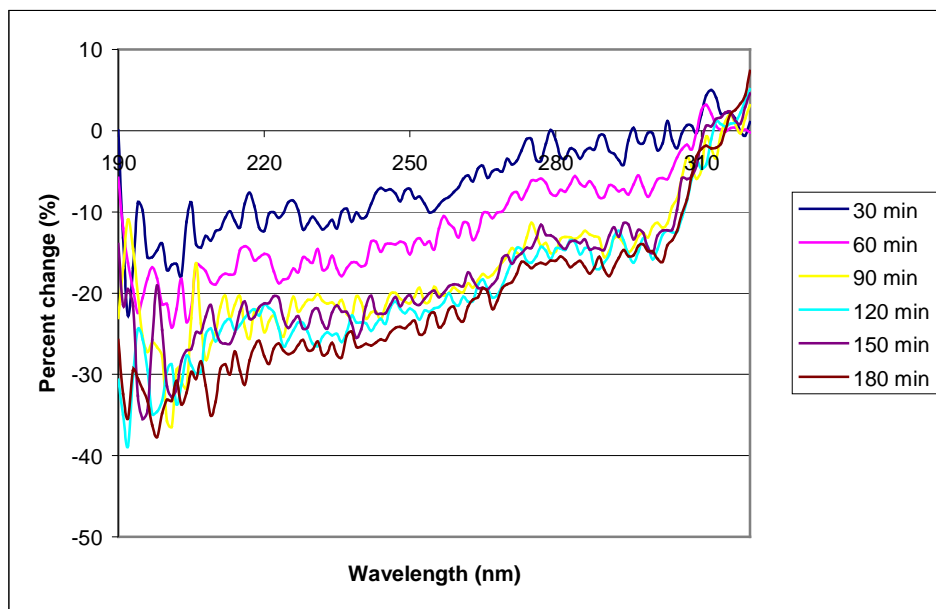


Figure 51: Percent change in the UV absorption of PET per wavelength due the 300 nm broad spectrum UV photo-oxidation treatment.

## II. Atmospheric pressure 253.7 nm UV photo-oxidation of PET

The total absorption due the treatment is found to have decreased then increased as shown in Table 28.

Sample treatment time (min)	Percent change (%)
15	-20.18
30	-19.53
45	-18.39
60	-19.28
90	-17.48
120	-15.57

Table 28: Percent change in the total UV absorption of PET due to the 253.7 nm UV photo-oxidation treatment.

The percent change is plotted per  $\lambda$  as presented in Fig. 52.

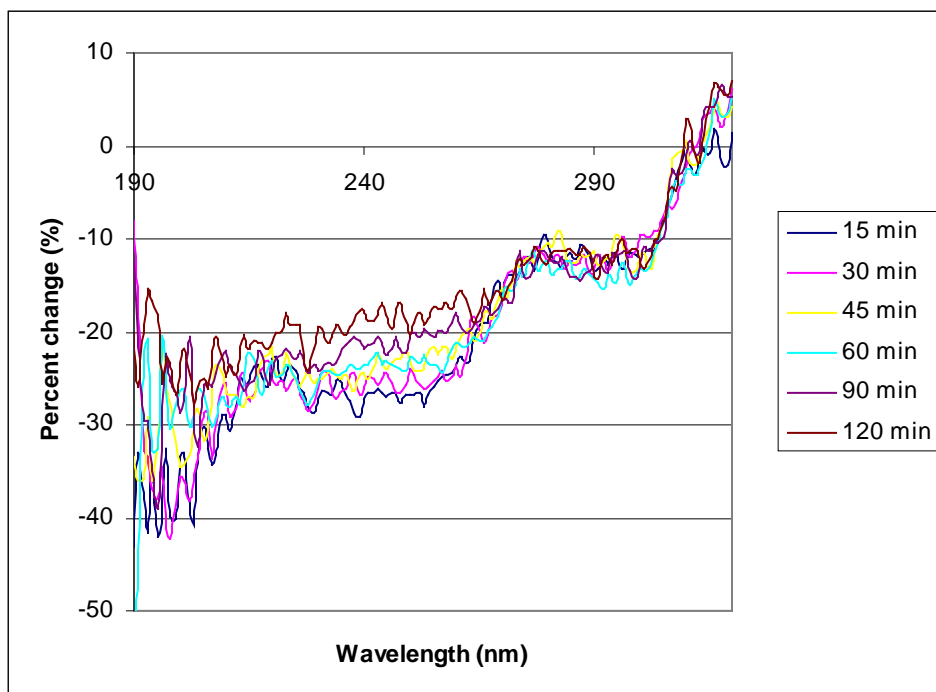


Figure 52: Percent change in the UV absorption of PET per wavelength due 253.7 nm UV photo-oxidation.

#### 4.4.2 Atmospheric pressure 184.9/253.7 nm UV photo-ozonation of PET

The change in the UV absorption sum (Table 29) initially decreases then increases in a similar fashion to the 253.7 nm UV photo-oxidation.

Sample treatment time (min)	Percent change (%)
5	-23.01
10	-21.39
15	-21.25
25	-20.13
45	-18.39
60	-18.30

Table 29: Percent change in the total UV absorption of PET due to the 184.9/253.7 nm UV photo-ozonation.

The detailed percent change absorption spectrum is shown in Fig. 53.

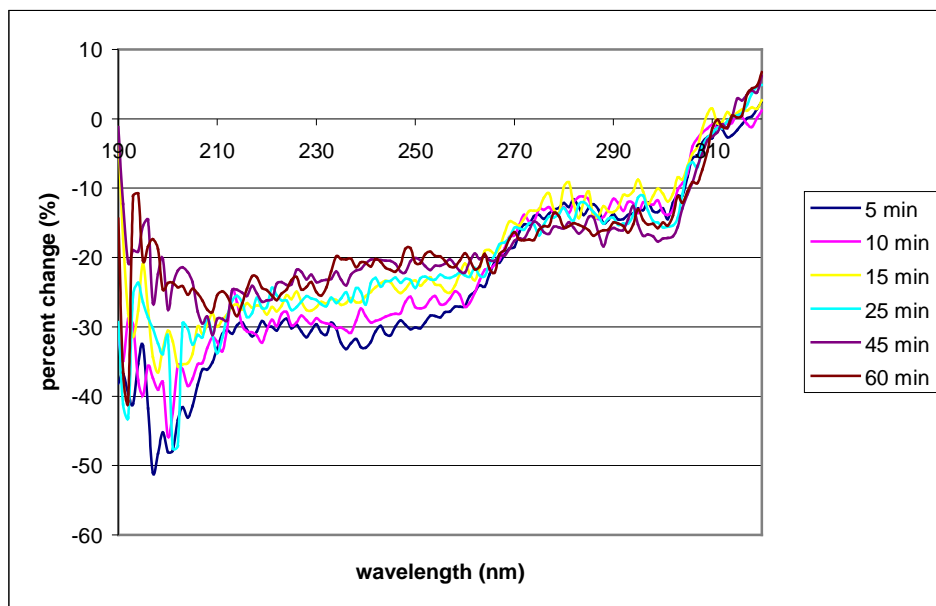


Figure 53: Percent change in the UV absorption of PET per wavelength due the 184.9/253.7 nm UV photo-ozonation treatment.



#### 4.4.3 UV Photolysis

##### I. Atmospheric pressure 300 nm broad spectrum UV photolysis of PET in nitrogen

The integrated UV absorption spectrum showed very little change but starts to show a slight decrease at higher times as shown in Table 30.

Sample treatment time (min)	Percent change (%)
30	1.21
60	1.39
90	1.42
120	0.86
150	0.54
180	-2.21

Table 30: Percent change in the total UV absorption of PET due to the 300 nm broad spectrum UV photolysis in nitrogen.

The percentage change per wavelength due to the treatment is displayed in Fig. 54.

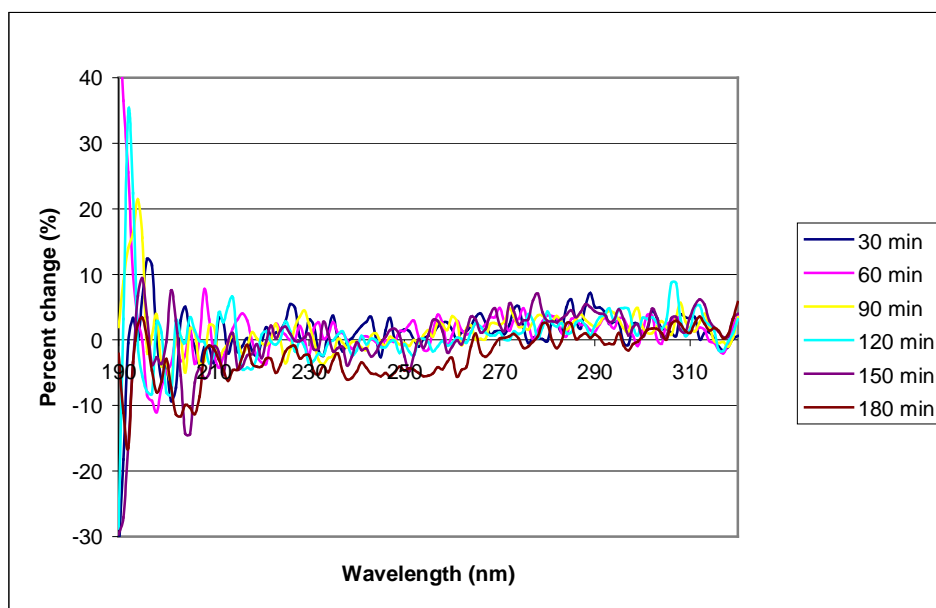


Figure 54: Percent change in the UV absorption of PET per wavelength due the 300 nm broad spectrum UV photolysis in nitrogen.

## II. Atmospheric pressure 253.7 nm UV photolysis of PET in nitrogen

The total UV absorption (Table 31) is shown to have increased as the treatment time is increased.

Sample treatment time (min)	Percent change (%)
15	1.31
30	-0.68
45	-0.24
60	1.69
90	5.14
120	6.38

*Table 31: Percent change in the total UV absorption of PET due to the 253.7 nm UV photolysis in nitrogen.*

The change detected per the wavelength is displayed in Fig. 55.

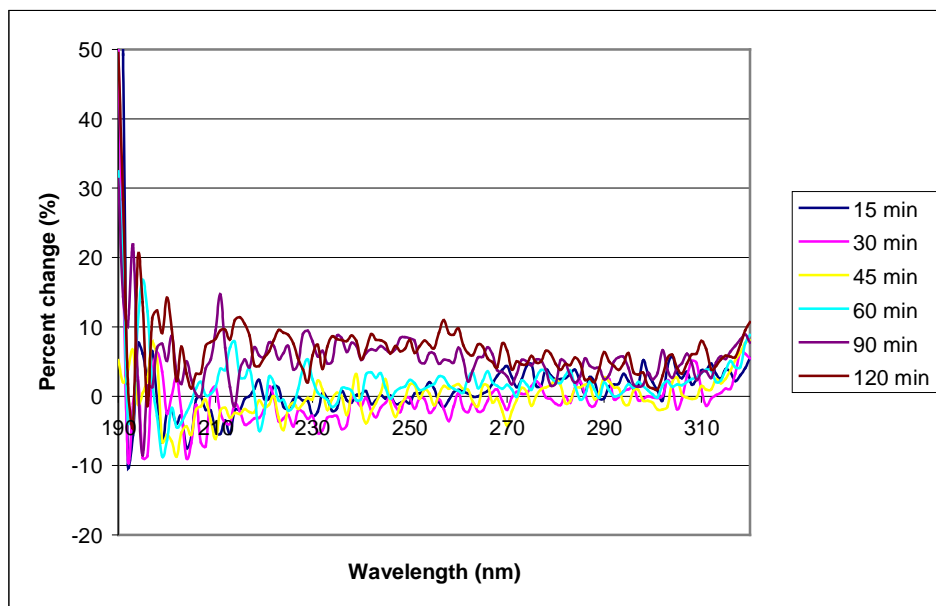


*Figure 55: Percent change in the UV absorption of PET per wavelength due the 253.7 nm UV photolysis in nitrogen.*

### III. Atmospheric pressure 184.9/253.7 nm UV photolysis of PET in nitrogen

The total absorption was found to initially decrease then increase beyond the original value at higher treatment times as shown in Table 32.

Sample treatment time (min)	Percent change (%)
5	-3.24
10	-6.36
15	1.76
25	2.21
45	6.84
60	8.01

Table 32: Percent change in the total UV absorption of PET due to the 184.9/253.7 nm UV photolysis in nitrogen.

The detailed percent change in the absorption spectrum per  $\lambda$  is displayed in Fig. 56.

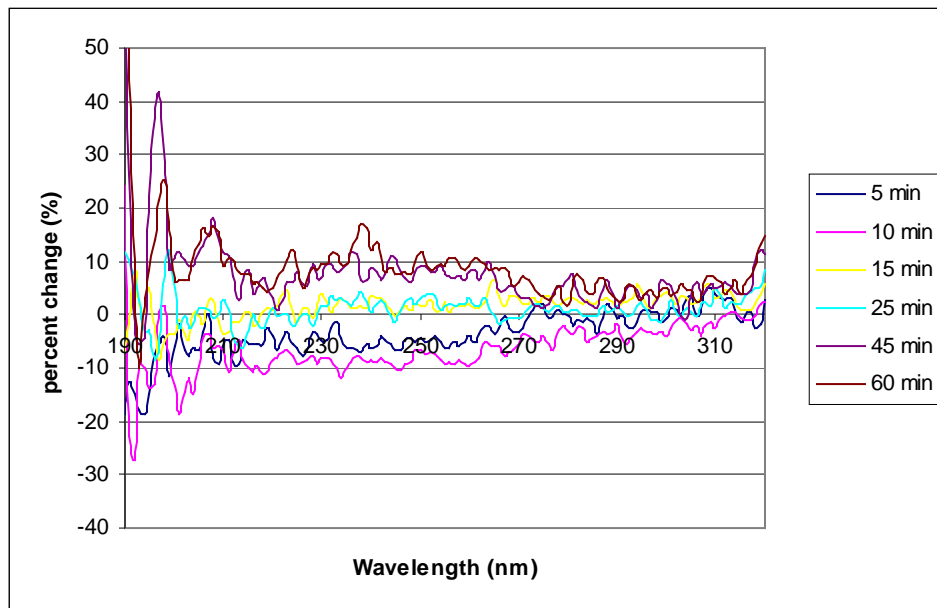


Figure 56: Percent change in the UV absorption of PET per wavelength due the 184.9/253.7 nm UV photolysis in nitrogen.

#### 4.4.4 VUV photo-oxidation

##### I. VUV photo-oxidation of PET using Ar plasma

The total UV absorption was found to have slightly decreased as shown in Table 33.

Sample treatment time (min)	Percent change (%)
5	-4.02
15	-5.30
30	-5.53
60	-4.69
90	-4.40
120	-3.77
150	-3.51

Table 33: Percent change in the total UV absorption of PET due to VUV photo-oxidation.

The percent change of the UV spectrum per the wavelength is displayed in Fig. 57.

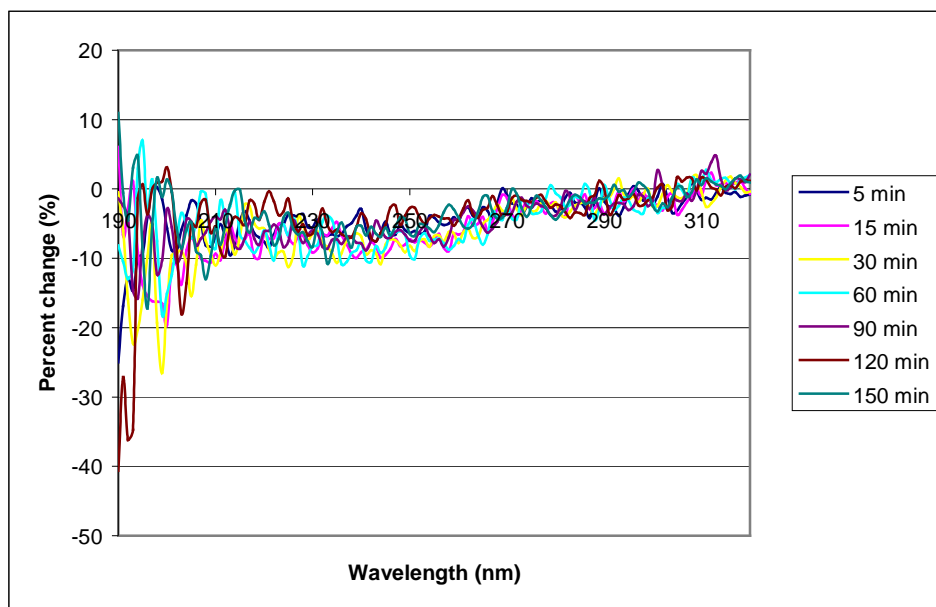


Figure 57: Percent change in the UV absorption of PET per wavelength due to VUV photo-oxidation.

## II. VUV photo-oxidation of PEN using Ar plasma

The UV absorption spectrum sum is found to have increased as shown in Table 34.

Sample treatment time (min)	Percent change (%)
5	0.33
15	1.05
30	2.26
60	4.51
90	6.10
120	8.78
150	9.55

Table 34: Percent change in the total UV absorption of PEN due to VUV photo-oxidation.

The specific percentage change in the spectrum due to the treatment is presented in

Fig. 58.

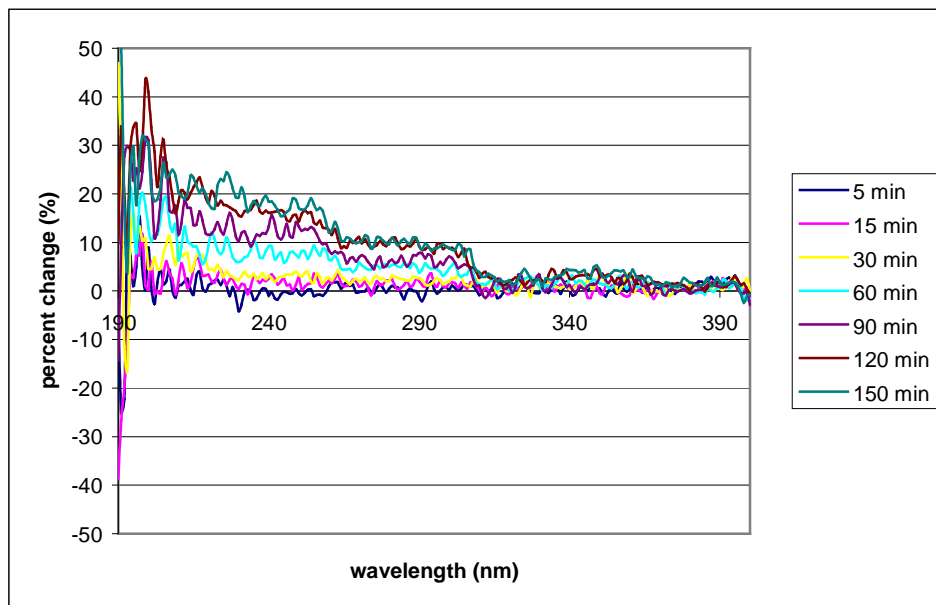


Figure 58: Percent change in the UV absorption of PEN per wavelength due VUV photo-oxidation.

#### 4.4.5 VUV photolysis

##### I. VUV photolysis of PET using Ar plasma

The integrated absorption spectrum is found to have decreased slightly similar to the UV photo-oxidation as observed in Table 35.

Sample treatment time	Percent change
5 min	-3.92%
15 min	-4.08%
30 min	-5.29%
60 min	-5.12%
90 min	-3.93%
120 min	-4.63%
150 min	-4.99%

Table 35: Percent change in the total UV absorption of PET due to VUV photolysis.

The detailed change in the UV spectrum per the wavelength is revealed in Fig. 59.

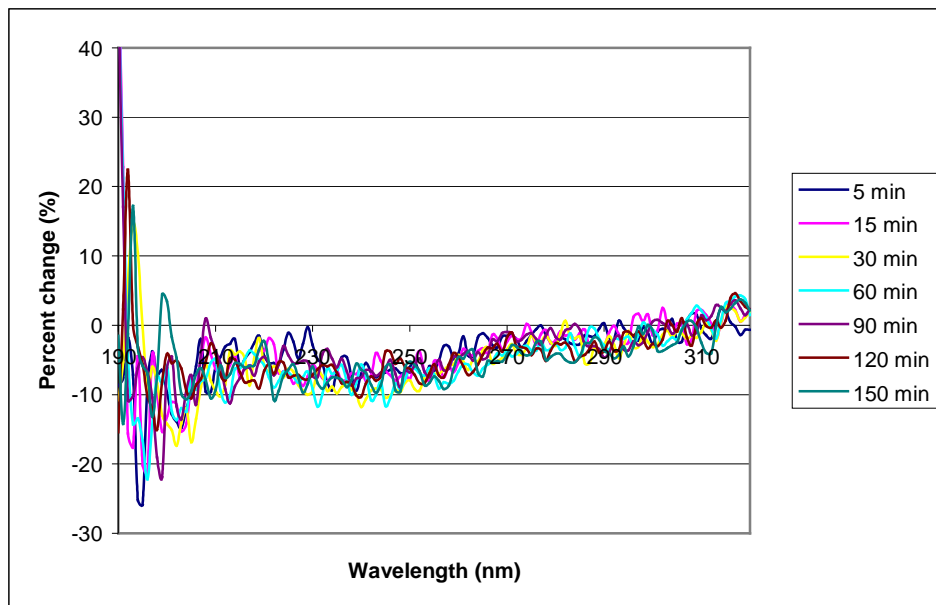


Figure 59: Percent change in the UV absorption of PET per wavelength due VUV photolysis.

## II. VUV photolysis of PEN using Ar plasma

The UV absorption summation is observed to have increased as revealed in Table 36.

Sample treatment time (min)	Percent change (%)
5	1.40
15	3.07
30	3.99
60	5.65
90	8.38
120	8.93
150	9.28

Table 36: Percent change in the total UV absorption of PEN due to VUV photolysis.

The percent change is plotted per  $\lambda$  as displayed in Fig. 60.

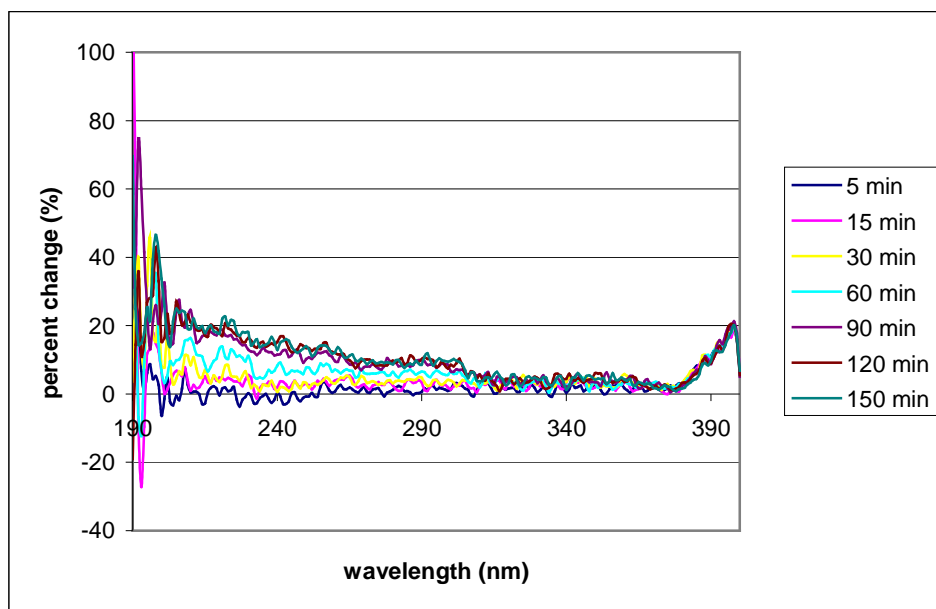


Figure 60: Percent change in the UV absorption of PEN per wavelength due VUV photolysis.

#### 4.4.6 Remote exposure in the absence of photons

##### I. MW discharge of Ar/O<sub>2</sub> plasma on PET in vacuum

The absorption spectrum sum was found to have slightly decreased as revealed in Table 37.

Sample treatment time	Percent change
15 min	-1.32%
30 min	-1.85%
60 min	-2.04%
90 min	-4.43%
120 min	-1.24%
150 min	-5.87%
180 min	-3.47%

*Table 37: Percent change in the total UV absorption of PET due to remote oxygen atom exposure in the absence of photons.*

The detailed change in the UV absorption per the wavelength is presented in Fig. 61.

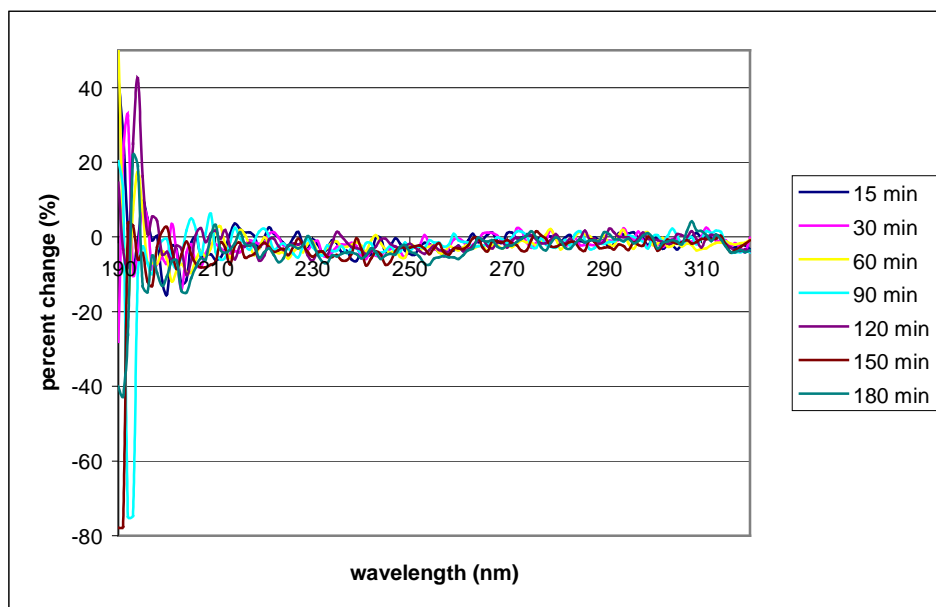


*Figure 61: Percent change in the UV absorption of PET per wavelength due to remote oxygen atom exposure in the absence of photons.*



## II. MW discharge of Ar/O<sub>2</sub> plasma on PEN in vacuum

The total UV absorption is found to have slightly increased as shown in Table 38.

Sample treatment time	Percent change
15 min	3.97%
30 min	5.97%
60 min	5.83%
90 min	4.17%
120 min	4.21%
150 min	4.07%
180 min	3.27%

Table 38: Percent change in the total UV absorption of PEN due to remote oxygen atom exposure in the absence of photons.

The slight change in the absorption spectrum is displayed in Fig. 62.

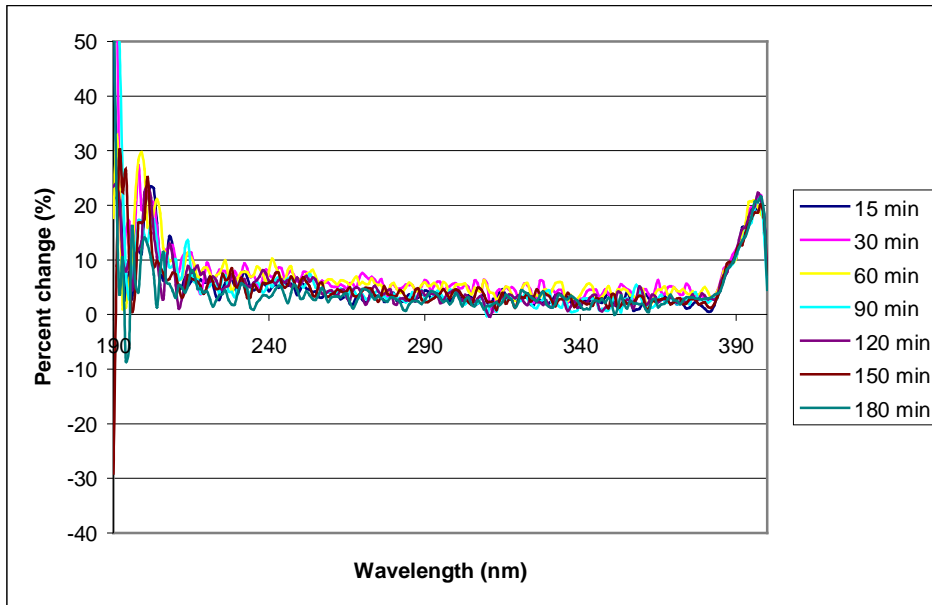


Figure 62: Percent change in the UV absorption of PEN per wavelength due to remote oxygen atom exposure in the absence of photons.

## 4.5 FTIR

The percent change in the IR absorption per wavenumber ( $\text{cm}^{-1}$ ) is plotted for each treatment from before and after treatment. A tabulated functional group analysis is also displayed based on Table 2. Since FTIR is an analytical tool that provides a qualitative analysis, therefore, the changes are only to roughly identify increases and decreases in concentration of functional groups.

### 4.5.1 UV photo-oxidation

#### I. Atmospheric pressure 300 nm broad spectrum UV photo-oxidation of PET

The PET samples' change in the relative absorbance due to the 300 nm broad spectrum photo-oxidation treatment is shown in Fig. 63.

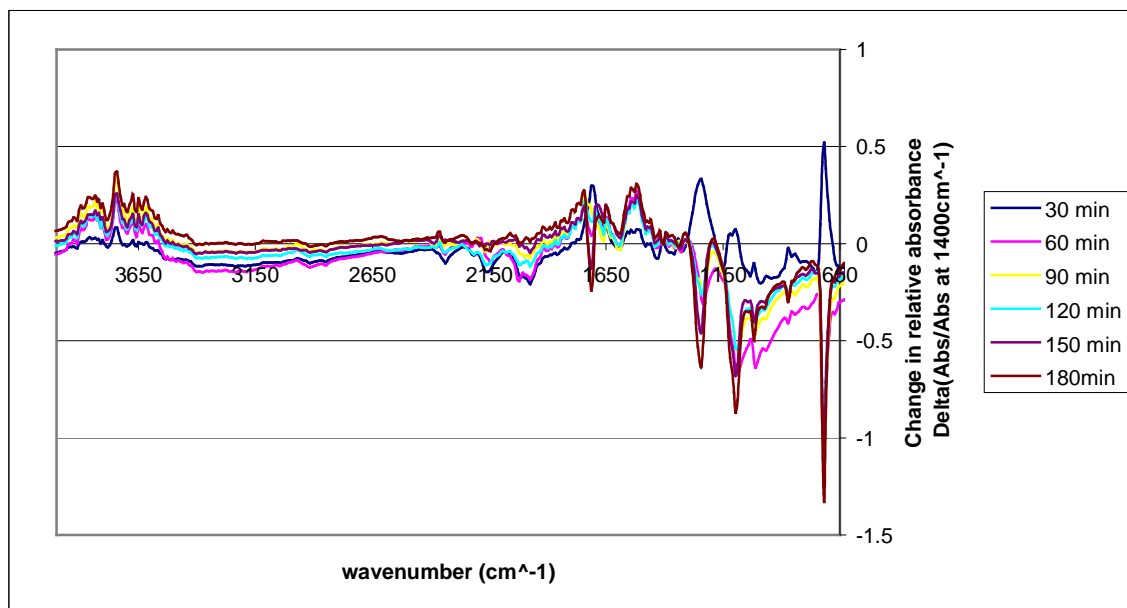


*Figure 63: The change in relative absorbance on IR spectra of PET due to the 300 nm broad spectrum UV photo-oxidation treatment.*

The qualitative observations of the functional group analysis for Fig. 63 is displayed at the section below in Table 39.

## II. Atmospheric pressure 253.7 nm UV photo-oxidation of PET

The difference in the relative absorbance before and after the 253.7 nm photo-oxidation treatment is displayed in Fig. 64.

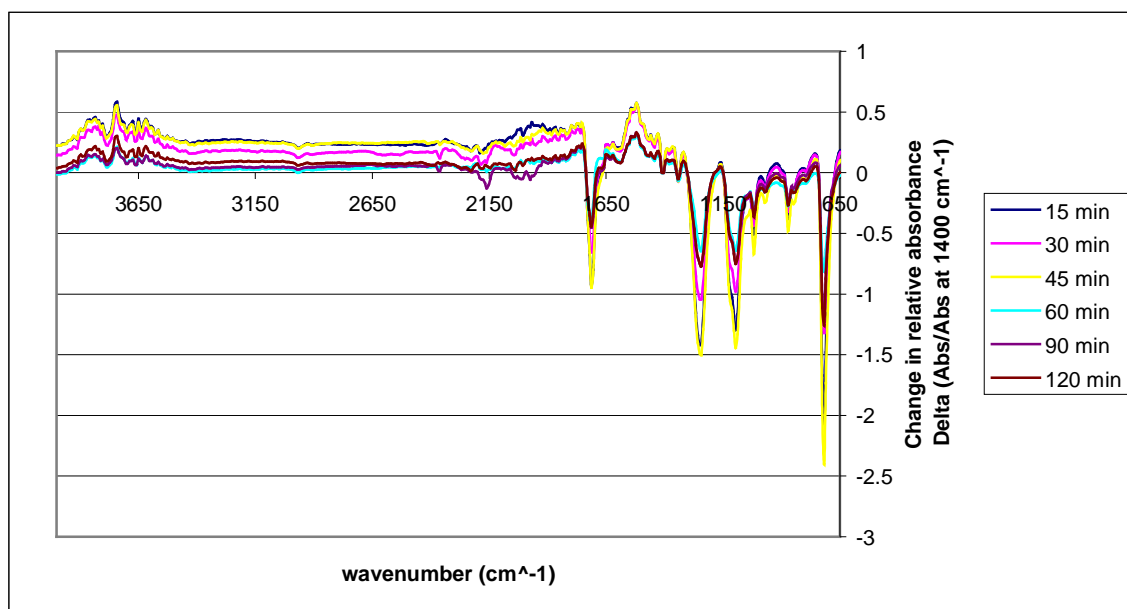


Figure 64: The change in relative absorbance on IR spectra of PET due to the 253.7 nm UV photo-oxidation.

The quantitative chemical analysis of the IR spectrums of the 300 nm broad spectrum and 253.7 nm UV photo-oxidation is shown in Table 39.

<b>Functional group description</b>	<b>Observed changes for the 300 nm broad spectrum UV photo-oxidation</b>	<b>Observed changes for the 253.7 nm UV photo-oxidation</b>
C=O stretch: carbonyls	Initial increase followed by decrease	Decrease
C-O stretch: Esters	Decrease	Decrease
C-O stretch: Ethers	Decrease	Decrease
O-C & CCO groups stretch	Increase	Increase
-OH stretch: Phenol	Increase	Increase
-OH stretch: Carboxylic acid	Increase	Increase
-C=O: Carbonyl out of plane deformation on aromatic ring.	Initial increase followed by decrease	Decrease
C-H bending: Hydrogen deformation on aromatic ring	Decreased	Decrease
-C=O: carbonyl 1,4-substitution (PET)	Decrease and broadened	Decrease
C-C stretch: aromatic skeletal stretching bands (This can be represented by the ratio of the overall spectrum) .	Increase	Decrease
-C-H stretch: Aliphatic alkanes	Slight decrease	Slight decrease
C=C stretch: Vinyl groups	Increase	Increase

*Table 39: IR functional group analysis of the 300 nm broad spectrum and 253.7 nm UV photo-oxidized PET film.*

#### 4.5.2 Atmospheric pressure 184.9/253.7 nm UV photo-ozonation of PET

The change in the relative absorbance due to the 184.9/253.7 nm photo-ozonation treatment is revealed in Fig. 65.

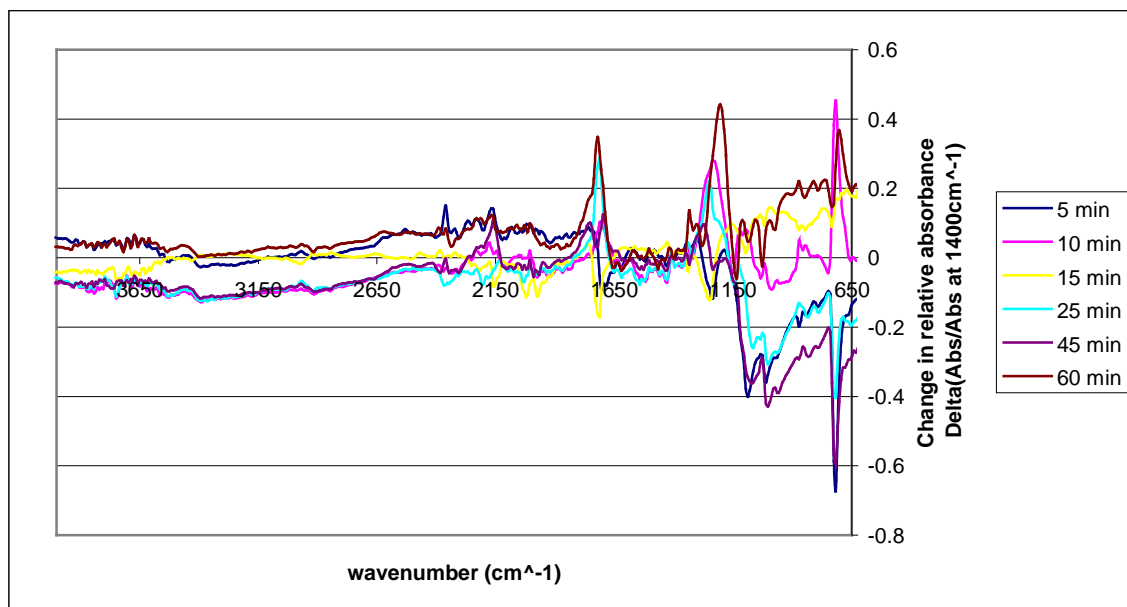


Figure 65: The change in relative absorbance on IR spectra of PET due to the 184.9/253.7 nm UV photo-ozonation treatment.

The changes in the functional groups observed in Fig. 65 is displayed in Table 40.

Functional group description	Observed changes
C=O stretch: carbonyls	Fluctuating
C-O stretch: Esters	Fluctuating
C-O stretch: Ethers	Fluctuating
O-C & CCO groups stretch	Increase
-OH stretch: Phenol	Increase
-OH stretch: Carboxylic acid	Increase
-C=O: Carbonyl out of plane deformation on aromatic ring.	Fluctuating
C-H bending: Hydrogen deformation on aromatic ring	Fluctuating and broadening
-C=O: carbonyl 1,4-substitution (PET)	Decrease
C-C stretch: aromatic skeletal stretching bands (This can be represented by the ratio of the overall spectrum) .	Increase
-C-H stretch: Aliphatic alkanes	Slight decrease
C=C stretch: Vinyl groups	Increase

*Table 40: FTIR functional group analysis of the 184.9/253.7 nm UV photo-ozonated PET.*

### 4.5.3 UV photolysis

#### I. Atmospheric pressure 300 nm broad spectrum UV photolysis of PET in nitrogen

The change in the samples' relative absorbance before and after the 300 nm broad spectrum UV photolysis treatment is shown in Fig. 66.

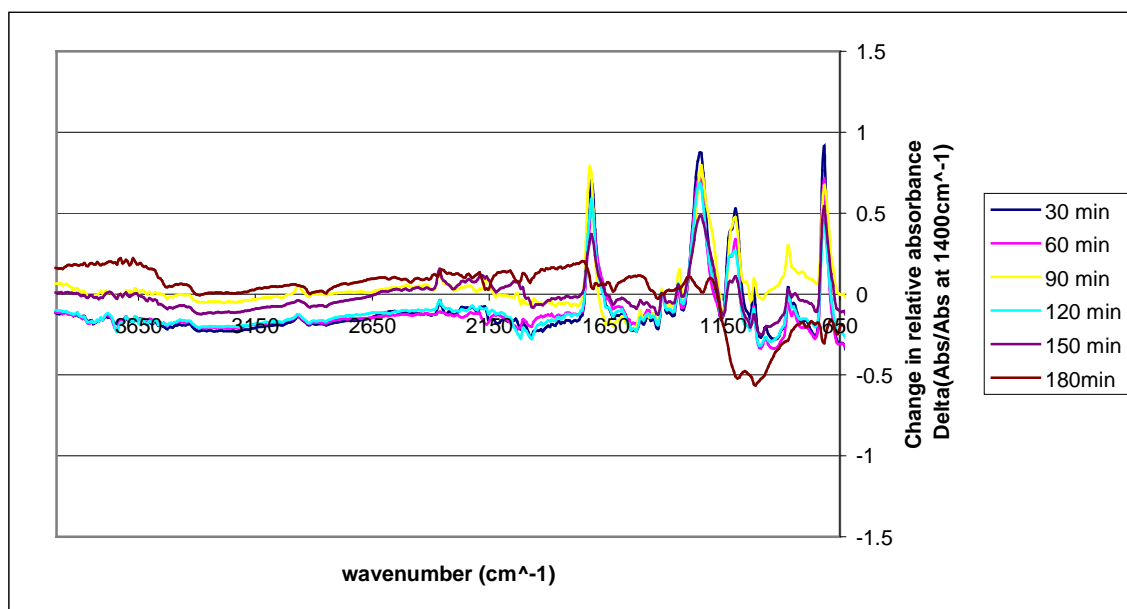


Figure 66: The change in relative absorbance on IR spectra of PET due to the 300 nm broad spectrum UV photolysis in nitrogen.

A detailed functional group analysis of Fig. 66 is displayed at section 4.5.3 III in Table 41.

#### II. Atmospheric pressure 253.7 nm UV photolysis of PET in nitrogen

The change in the relative absorbance from the 253.7 nm UV photolysis is presented in Fig. 67.

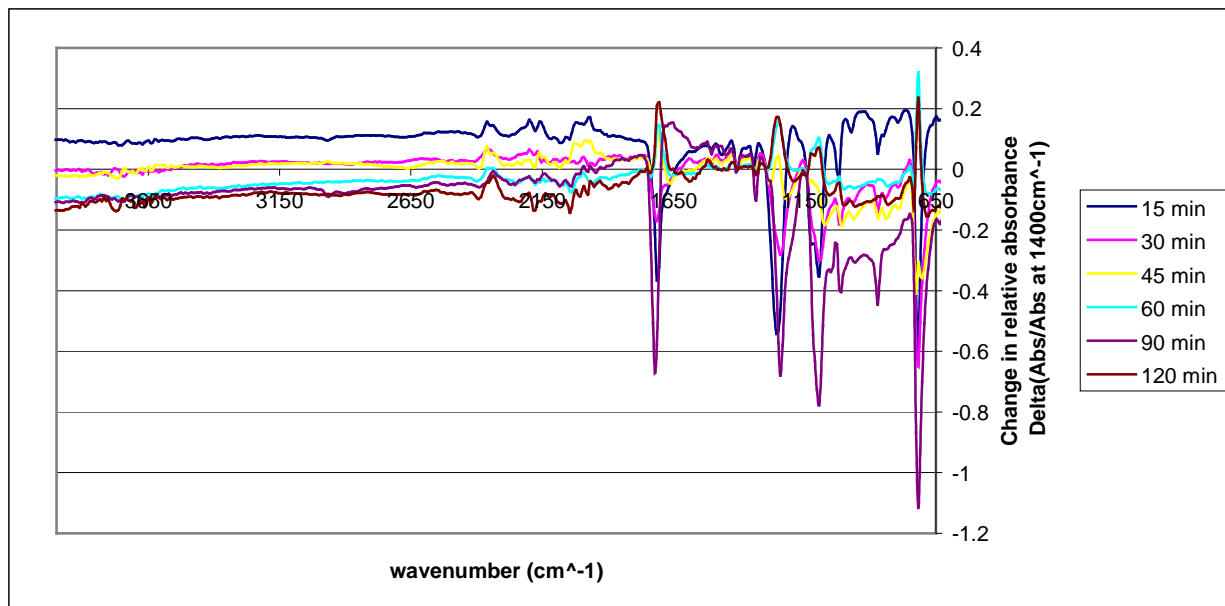


Figure 67: The change in relative absorbance on IR spectra of PET due to the 253.7 nm UV photolysis in nitrogen.

The functional group description of the IR spectrum in Fig. 67 is displayed at the section below in Table 41.

### III. Atmospheric pressure 184.9/253.7 nm UV photolysis of PET in nitrogen

The change in the IR relative absorbance due to the 184.9/253.7 nm UV photolysis treatment is presented in Fig. 68.



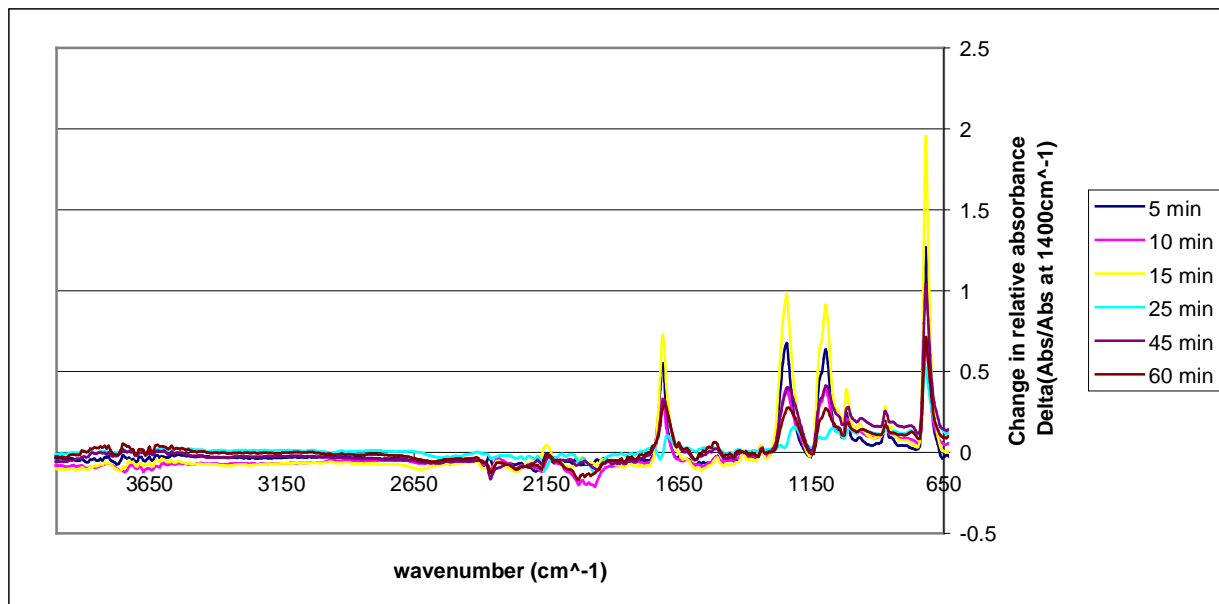


*Figure 68: The change in relative absorbance on IR spectra of PET due to the 184.9/253.7 nm UV photolysis in nitrogen.*

The functional group description of the IR spectrums of the 300 nm broad spectrum, 253.7 nm, and 184.9/253.7 nm UV photolysis treated PET is displayed in Table 41.

<b>Functional group description</b>	<b>Observed changes due to the 300 nm broad spectrum UV photolysis</b>	<b>Observed changes due to the 253.7 nm UV photolysis</b>	<b>Observed changes due to the 184.9/253.7 nm UV photolysis</b>
C=O stretch: carbonyls	Increase then decrease at 180 min	Fluctuating	Increase
C-O stretch: Esters	Increase then decrease at 180 min	Fluctuating	Increase
C-O stretch: Ethers	Increase then decrease at 180 min	Fluctuating	Increase
O-C & CCO groups stretch	Decrease then increase at 180 min	Increase	Increase
-OH stretch: Phenol	Increase	No significant change	very slight increase
-OH stretch: Carboxylic acid	Increase	No significant change	very slight increase
-C=O: Carbonyl out of plane deformation on aromatic ring.	Increase then decrease at 180 min	Fluctuating	Increase
C-H bending: Hydrogen deformation on aromatic ring	Increase then decrease slightly at 180 min with a broadening effect	Decrease along with broadening	Increase
-C=O: carbonyl 1,4-substitution (PET)	Increase then decrease at 180 min with a broadening effect	Decrease along with broadening	Increase
C-C stretch: aromatic skeletal stretching bands (This can be represented by the ratio of the overall spectrum) .	Slightly increase then decrease slightly at 180 min	Initial decrease followed by increase at high treatment times	Slight increase
-C-H stretch: Aliphatic alkanes	Slight increase	Slight decrease	No significant change
C=C stretch: Vinyl groups	Increase	No significant change	Slight increase

*Table 41: IR functional group analysis of the 300 nm broad spectrum, 253.7 nm, and 184.9/253.7nm UV photolysis of PET.*

#### 4.5.4 VUV photo-oxidation

##### I. VUV photo-oxidation of PET using Ar plasma

The relative absorbance difference due to VUV photo-oxidation treatment is shown in Fig. 69.

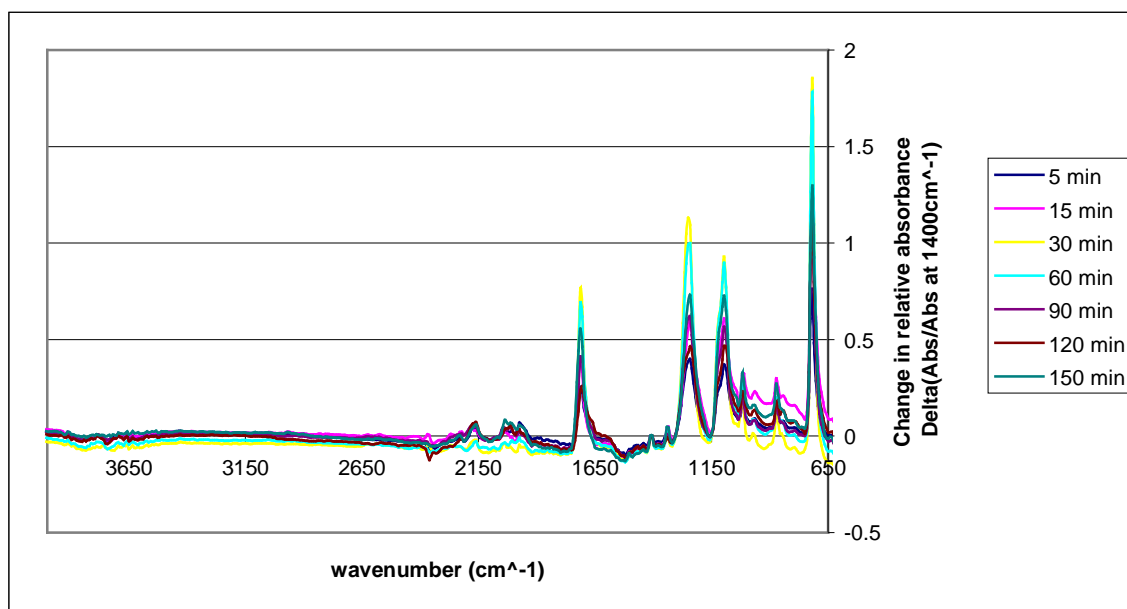


Figure 69: The change in relative absorbance on IR spectra of PET due to the VUV photo-oxidation.

The observed changes in the functional groups are described at the section below in Table 42.

##### II. VUV photo-oxidation of PEN using Ar plasma

The PEN samples' change in the relative absorbance due to the VUV photo-oxidation treatment is displayed in Fig. 70.

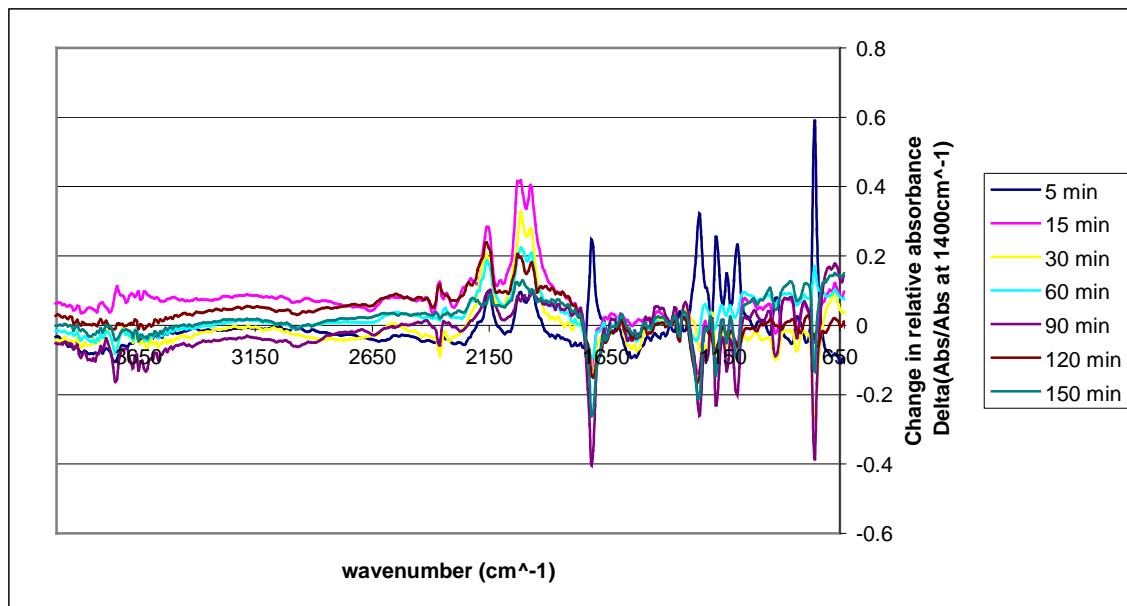


Figure 70: The change in relative absorbance on IR spectra of PEN due to the VUV photo-oxidation.

The detailed functional group analysis of the VUV photo-oxidation of PET versus the PEN is displayed in Table 42.

<b>Functional group description</b>	<b>Observed changes for PET</b>	<b>Observed changes for PEN</b>
C=O stretch: carbonyls	Increase	Initial increase then decrease at high treatment times
C-O stretch: Esters	Increase	Initial increase then decrease at high treatment times
C-O stretch: Ethers	Increase	Initial increase then decrease at high treatment times
O-C & CCO groups stretch	Decrease	Decrease
-OH stretch: Phenol	No significant change	Increase
-OH stretch: Carboxylic acid	No significant change	Increase
-C=O: Carbonyl out of plane deformation on aromatic ring.	Increase	Fluctuating
C-H bending: Hydrogen deformation on aromatic ring	Increase	Initial increase then decrease at high treatment times
-C=O: carbonyl 2,6-substitution (PEN)	Increase	Initial increase then decrease at high treatment times
C-C stretch: aromatic skeletal stretching bands (This can be represented by the ratio of the overall spectrum) .	No significant change	Fluctuating
-C-H stretch: Aliphatic alkanes	No significant change	Slight decrease
C=C stretch: Vinyl groups	Slight increase	Slight increase

*Table 42: IR functional group analysis of the VUV photo-oxidation treated PET and PEN.*

#### 4.5.5 VUV photolysis

##### I. VUV photolysis of PET using Ar plasma

The change in the relative IR absorbance before and after the VUV photolysis treatment is plotted as shown in Fig. 71.

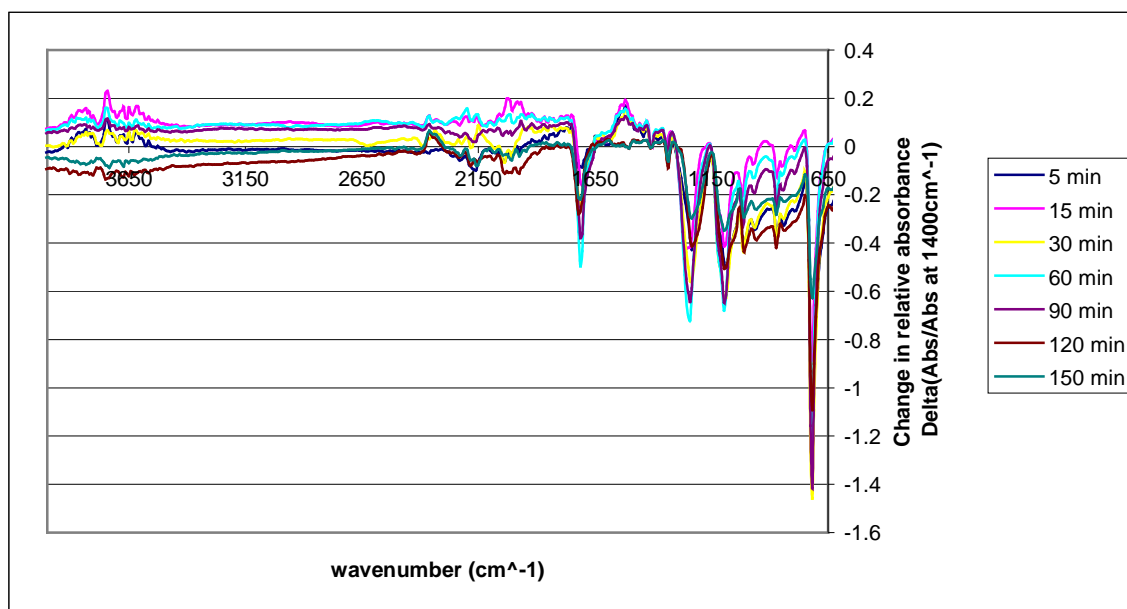


*Figure 71: The change in relative absorbance on IR spectra of PET due to the VUV photolysis.*

The change in the functional groups of Fig. 71 is described at the section below in Table 43.

## II. VUV photolysis of PEN using Ar plasma

The change in the PEN IR spectrum due to VUV photolysis is shown in Fig. 72.

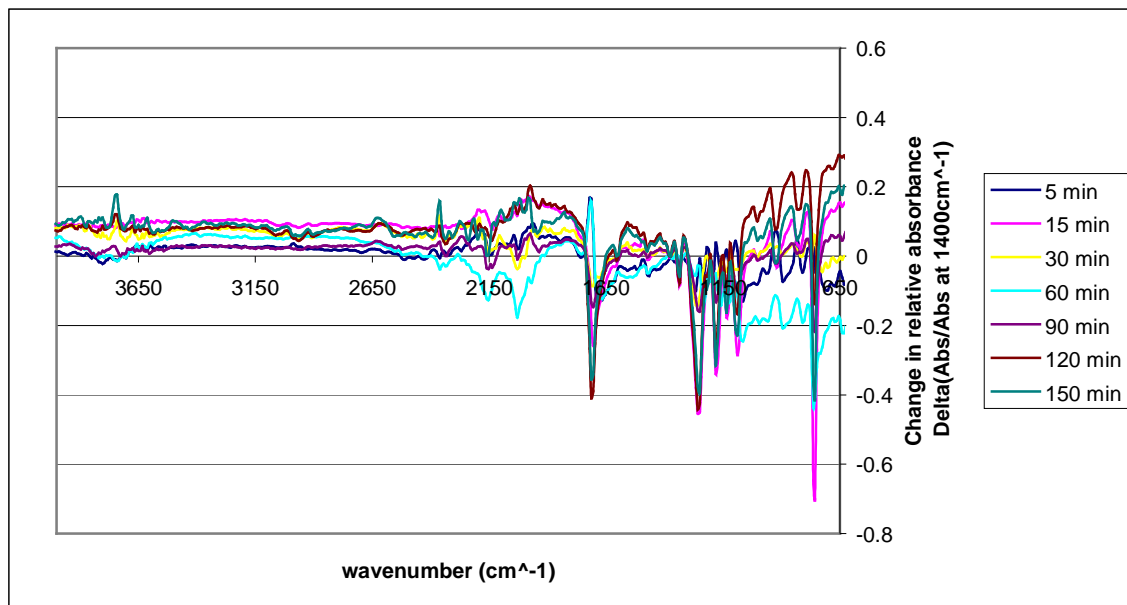


Figure 72: The change in relative absorbance on IR spectra of PEN due to the VUV photolysis.

The change in the functional groups of the VUV photolysis for PET and PEN is described in Table 43.

<b>Functional group description</b>	<b>Observed changes for PET</b>	<b>Observed changes for PEN</b>
C=O stretch: carbonyls	Decrease	Fluctuating
C-O stretch: Esters	Decrease	Fluctuating
C-O stretch: Ethers	Decrease	Initially increase then decrease at high treatment time
O-C & CCO groups stretch	Increase	Increase
-OH stretch: Phenol	Slight increase	Increase
-OH stretch: Carboxylic acid	Slight increase	Increase
-C=O: Carbonyl out of plane deformation on aromatic ring.	Decrease	Fluctuating
C-H bending: Hydrogen deformation on aromatic ring	Decrease	Fluctuating
-C=O: carbonyl 2,6-substitution (PEN)	Decrease	Initial increase then decrease at high treatment times
C-C stretch: aromatic skeletal stretching bands (This can be represented by the ratio of the overall spectrum) .	Initial increase followed by decrease at higher treatment times	Decrease
-C-H stretch: Aliphatic alkanes	No significant change	Decrease
C=C stretch: Vinyl groups	Slight increase	Increase

*Table 43: IR functional group analysis of the VUV photolysis treated PET and PEN.*



#### 4.5.6 Remote oxygen exposure in the absence of photons

##### I. MW discharge of Ar/O<sub>2</sub> plasma on PET in Vacuum

The change in the relative IR absorbance due to the remote oxygen atom exposure of PET is displayed in Fig. 73.

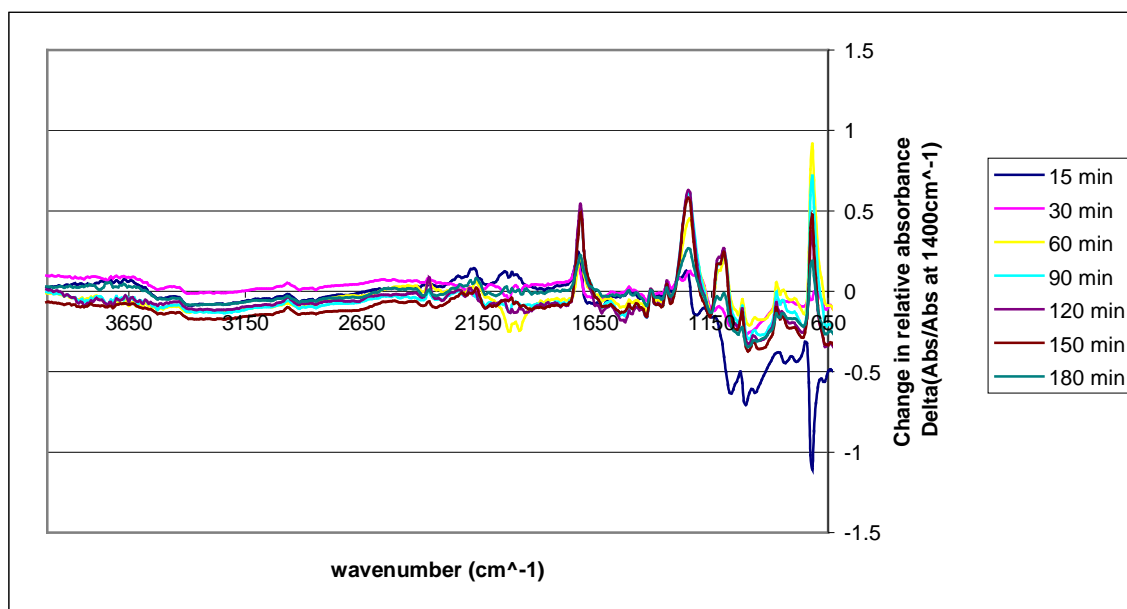


Figure 73: The change in relative absorbance on IR spectra of PET due to remote oxygen atom exposure in the absence of photons.

The detailed functional group description due to the treatment is shown in the section below in Table 44.

##### II. MW discharge of Ar/O<sub>2</sub> plasma on PEN in vacuum

The PEN samples' change in the relative absorbance before and after the remote oxygen atom exposure treatment is revealed in Fig. 74.

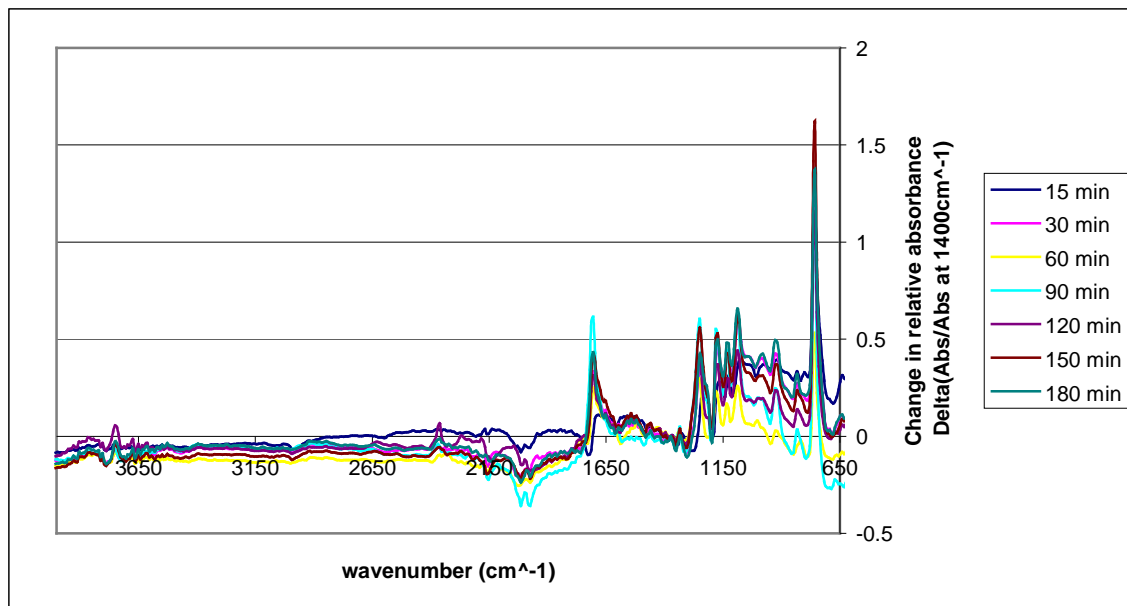


Figure 74: The change in relative absorbance on IR spectra of PEN due to remote oxygen atom exposure in the absence of photons.

The IR qualitative peak analysis for PET and PEN due to the remote oxygen atom exposure is displayed in Table 44.

<b>Functional group description</b>	<b>Observed changes for PET</b>	<b>Observed changes for PEN</b>
C=O stretch: carbonyls	Decrease	Increase
C-O stretch: Esters	Decrease	Increase
C-O stretch: Ethers	Decrease	Increase
O-C & CCO groups stretch	Increase	Increase
-OH stretch: Phenol	Slight increase	Slight increase
-OH stretch: Carboxylic acid	Slight increase	Slight Decrease
-C=O: Carbonyl out of plane deformation on aromatic ring.	Decrease	Increase
C-H bending: Hydrogen deformation on aromatic ring	Decrease	Increase
-C=O: carbonyl 2,6-substitution (PEN)	Decrease	Increase
C-C stretch: aromatic skeletal stretching bands (This can be represented by the ratio of the overall spectrum) .	Initial increase followed by decrease at higher treatment times	Increase
-C-H stretch: Aliphatic alkanes	No significant change	Decrease
C=C stretch: Vinyl groups	Slight increase	Slight increase

*Table 44: IR functional group analysis of the remote oxygen reaction with PET and PEN.*

## 5.....DISCUSSION

### 5.1 Extent of light penetration

Each of the treatments used in this research involves the use of photons to either directly or indirectly cause a reaction to occur on the polymer. In terms of the direct influence of photons onto the polymers, the absorption spectra must be studied. There are many conditions that influence the absorption of photons such as: light energy and intensity, reactive species used, and the type of environment [12, 33, 51]. The results show that PET and PEN are reactive in the presence of UV light. The formation and destruction of bonds to create and remove different functional groups depend on the energy level of the photons applied. The idea stems from the fact that the materials used are able to absorb and transmit light at certain frequencies. Since the material doesn't transmit light perfectly there are certain calculated average photon penetration depths that are dependent on the photon energy or the wavelength. The photon penetration depth is defined as the location where the  $I_0$ , the initial light intensity, is reduced to  $1/e$  of  $I_0$ . The photon penetration depth is calculated using the Beer-Lambert law along with the experimental transmission spectrum as shown in equation (7) [12, 33].

$$d = \frac{L}{-\ln(I/I_0)} \quad (7)$$

Where  $d$  is the photon penetration depth,  $L$  is the total sample thickness, and  $I/I_0$  is the transmittance ratio. The photon penetration depth of a washed and untreated PET sample used in this research is calculated and plotted using the measured absorptivity coefficient as shown in Fig. 75, along with that of PEN in Fig. 76.

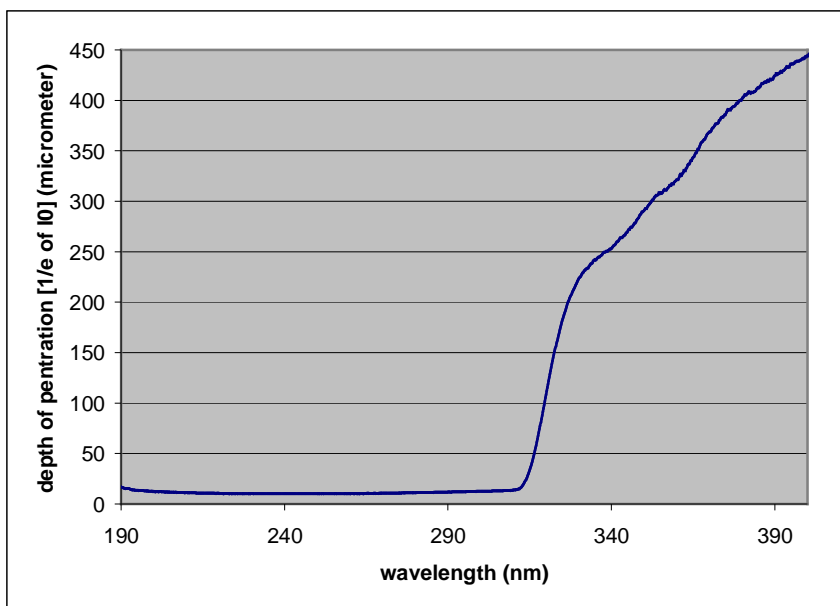


Figure 75: Photon depth of penetration throughout the washed and untreated 0.01mm PET film.

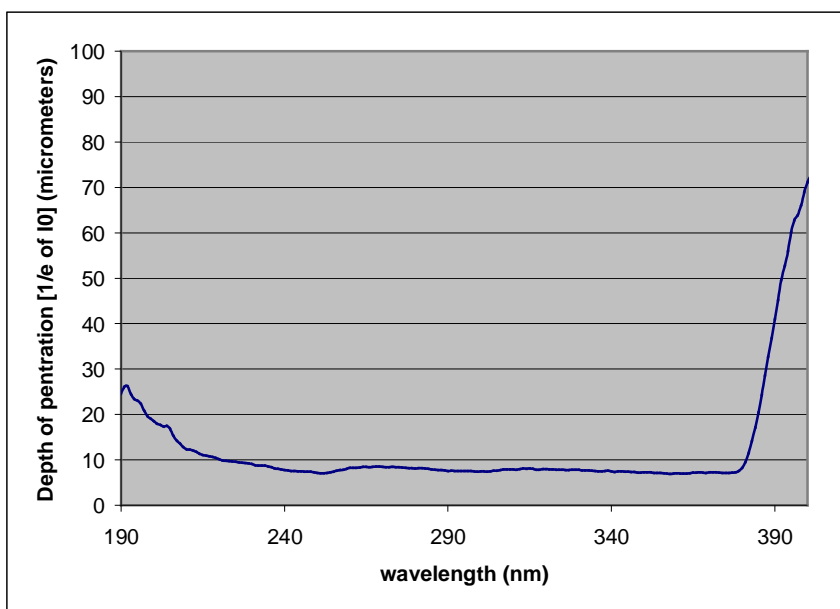
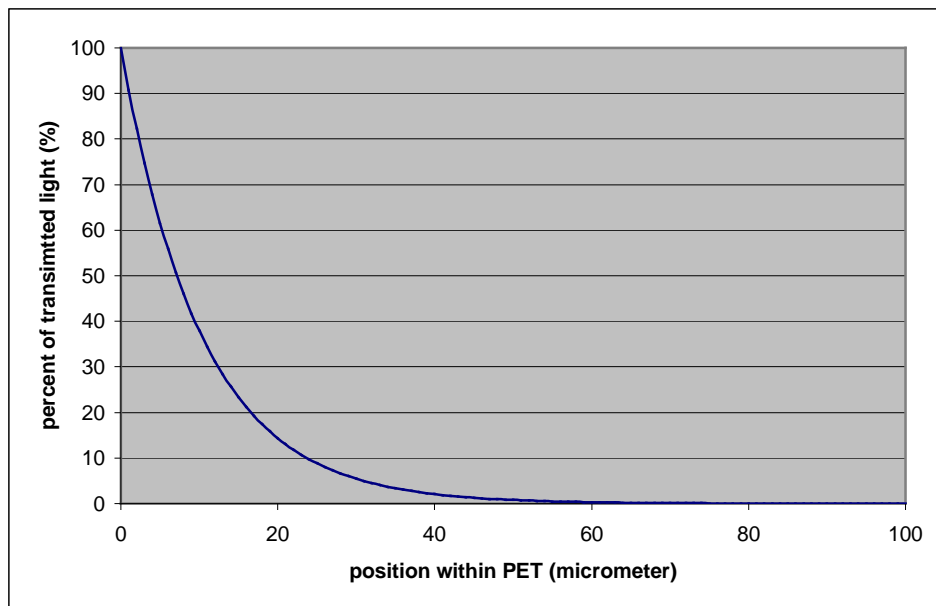


Figure 76: Photon depth of penetration throughout the washed and untreated 0.01mm PEN film.

In quantum mechanics the position of a photon throughout a certain media can be described in terms of probability. The average penetration depth into the PET and PEN is the position described by the probability function where the photon population decays to 1/e of the initial intensity,  $I_0$ . The generic equation that describes the population of the photons throughout the sample is derived from the Beer-Lambert law as shown in (8) [12, 33, 61].

$$\frac{I}{I_0} = e^{-L/d} \quad (8)$$

where  $I/I_0$  is the fraction of the transmitted intensity found at the specified depth,  $d$ , at a total thickness of  $L$ . An example of the displacement plot of photons within the washed and untreated PET sample used in this research is calculated using the measured absorptivity coefficient for the 253.7 nm UV absorption as displayed in Fig. 77. The photon population density for the 253.7 nm photoemission treatment onto PET shows a relatively high percent of photons penetrated all the way up to 40  $\mu\text{m}$ . Since the treatments described in this thesis involves exposure on both sides simultaneously, then a reasonable amount of photons are likely to interact with the inner bulk region of the polymer. Similar absorption coefficients are known for PET and PEN at the radiation wavelength of 184.9, 253.7, 104.8, 106.7, and roughly 300 nm as shown in Fig. 3 at 4.13, 4.89, 6.71, 11.83, and 11.62eV, respectively. The similar absorption coefficients causes the photon penetration depth to behave similar to the 253.7 nm example shown in Fig.77.



*Figure 77: Photon population density as a function of depth within a 253.7 nm UV photoemission treated PET sample.*

## **5.2 Photophysical and photochemical aspects of UV photo-oxidized PET**

### **I. Effect of UV photo-oxidation at the surface**

Since molecular oxygen does not absorb 253.7 nm and the broad band of wavelengths centered around 300 nm (Fig. 6), the initiation step of the treatment at these wavelengths involve interaction of the photons with the surface of the polymer. The XPS elemental analysis of the top 2-5 nm of the 253.7 and 300 nm broad spectrum UV photo-oxidation treated PET samples showed a similar trend. In both cases the atomic percent of oxygen gradually increased as a function of the treatment time as displayed in Tables 3 and 5. The C 1s functional group analysis for each treatment showed an increased formation of carbonyl and anhydride groups as seen in Tables 4 and 6. An increased formation of esters was observed due to the 253.7 nm UV photo-oxidation, while a decrease was detected for the lower energy 300 nm broad spectrum treatment.

The possible photoinitiation mechanisms that can be applied to PET due to this treatment are the Norrish I and II, photo-cycloaddition such as the paterno-buchi reaction, and photoclaissen rearrangement [30, 61]. One of the main classical photodecarbonylation reactions that has been studied on carbonyl-containing species is the Norrish I reaction. The reaction is initiated when the polymer absorbs a photon to push an electron radical from the carbonyl's carbon to the  $\alpha$  position. The particular mechanism can branch into a type IA or IB, based on the applied energy to push the electrons as shown in Fig. 78 [30, 61, 62]. Norrish type IB takes place only with higher energy level photons [62]. The same mechanism maybe applied to PEN by replacing the benzene group with a naphthalene group in Fig. 78.

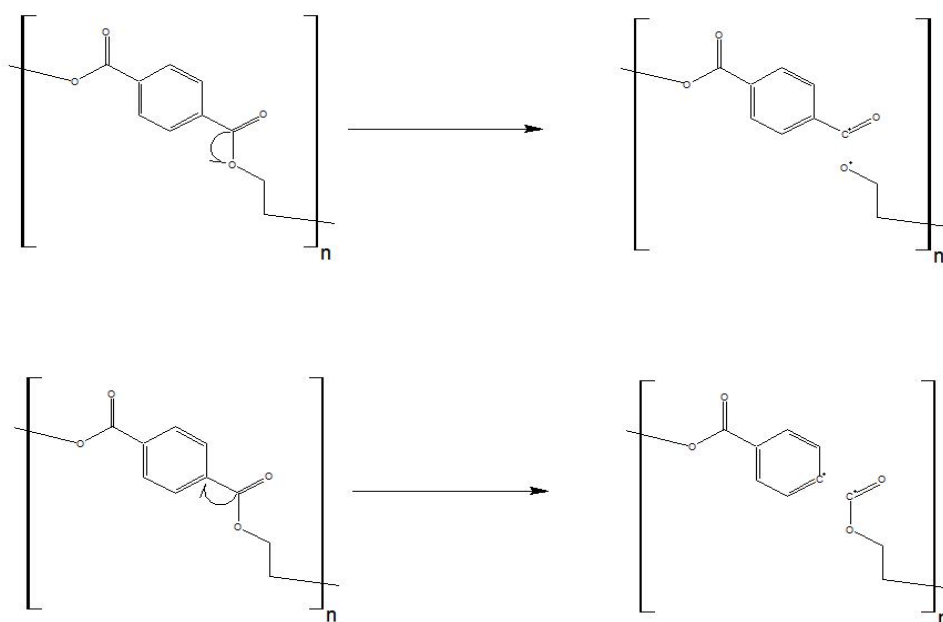


*Figure 78: The Norrish IA(bottom) and IB(top) mechanism applied on PET [30, 62].*

*Note: Same pathway can be applied for PEN by replacing the benzene (1,4 substitution) group with naphthalate (2,6 substitution).*



The initiation of the radical due to the type IB Norrish reaction can resonate across the C-O bond to break at the location between the ester and the ethylene as shown in Fig. 79 [19].

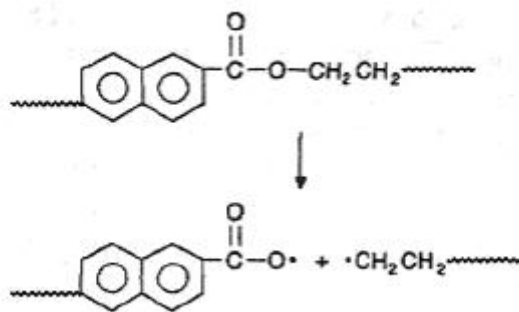


Figure 79: Norrish type I applied to PEN after delocalization of radical across C-O bond [19].

Note: Same pathway can be applied for PET by replacing the naphthalate (2,6 substitution) with benzene (1,4 substitution).

Another similar classical photochemical reaction is the Norrish II, which involves exciting an electrons from the carbonyl's double bond as presented in Fig. 80 [30].

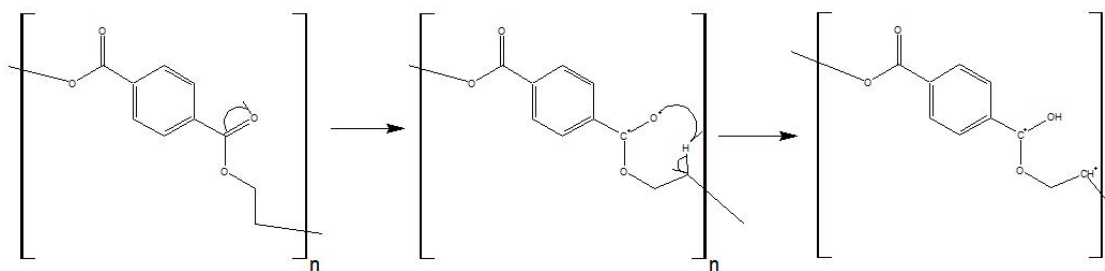


Figure 80: The Norrish II mechanism applied on PET [30].

Note: Same pathway can be applied for PEN by replacing the benzene (1,4 substitution) group with naphthalate (2,6 substitution).

The radical electrons initiated by the Norrish mechanism on the aromatic ring are delocalized which stabilizes them giving them a longer average lifetime [1]. These

radicals may react with the O<sub>2</sub> gas to produce a hydroperoxide, which may break down in the presence of light as shown in Fig. 81 [19].

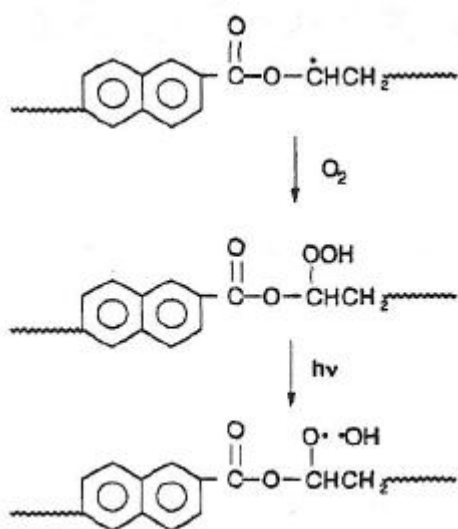
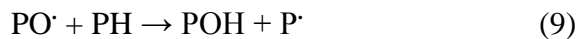


Figure 81: Formation and break down of hydroperoxide on PEN [19].

Note: Same pathway can be applied for PET by replacing the naphthalate (2,6 substitution) with benzene (1,4 substitution).

The radical oxygen groups on the polymer along with the radical hydroxyl group can then abstract hydrogen from a nearby polymer chain for the radical propagation as shown in steps (9)-(10) [61].



The hydroperoxide may break down through several pathways, where a  $\beta$ -scission reaction (Fig. 82) is prominent to produce aldehyde and carbonyl functional groups as was observed by the C 1s analysis for each treatment [19, 61].

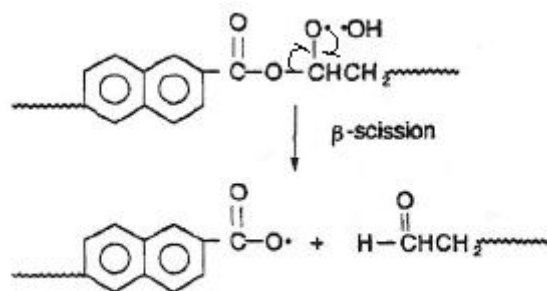


Figure 82: Propagation of the breakdown of the hydroperoxide on PEN [19].

Note: Same pathway can be applied for PET by replacing the naphthalate (2,6 substitution) with. benzene (1,4 substitution).

The breakdown of the hydroperoxide may go a different path to produce anhydrides, such as the cage reaction as shown in the mechanism in Fig. 83 [19].

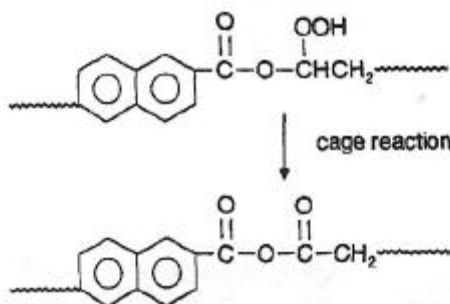
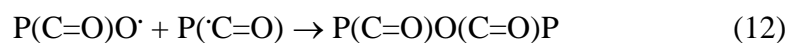


Figure 83: Termination sequence via a cage reaction to produce an anhydride on PEN [19].

Note: Same pathway can be applied for PET by replacing the naphthalate (2,6 substitution) with. benzene (1,4 substitution).

The termination of the Norrish initiated polymers may also combine to form anhydride or carbonate functional groups as shown in steps (11) - (12).



The active radical site on a polymer may also react with the produced hydroxyl radical during the hydroperoxide break down as shown in (13) [61].



The radical esters, produced from the peroxide breakdown, disintegrate to form an aryl and alkyl radical upon the entropy driven evolution of CO<sub>2</sub> as displayed in Fig. 84 [40].

The radical ester, as shown, may also obtain a hydrogen to form carboxylic acid end groups [19, 40].

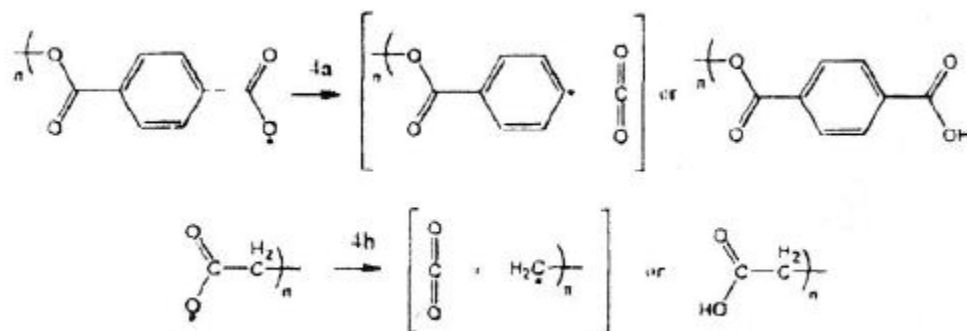


*Figure 84: Carboxylic acid end group formation of PET via dehydrogenation [40].*

*Note: Same pathway can be applied for PEN by replacing the benzene (1,4 substitution) group with naphthalate (2,6 substitution).*

After the photodecarboxylation, extrusion of the CO<sub>2</sub>, the radical electron resonates within the aromatic structures of PET. The Norrish type IA and IB initiated transitional state that was displayed in Fig. 78, can propagate further in the evolution of CO gas as shown in Fig. 85 [30, 61].

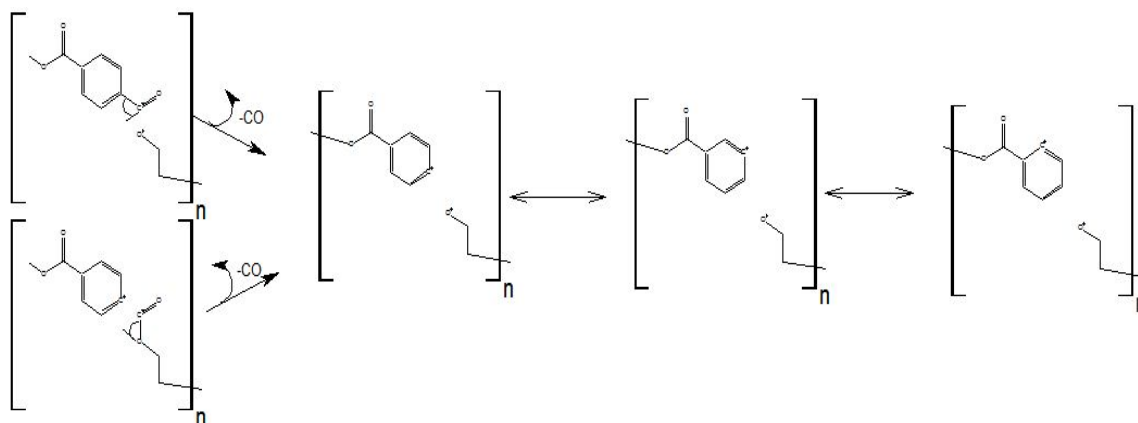


*Figure 85: Propagation and evolution of CO gas from Norrish IA and IB initiated PET [30].*

*Note: Same pathway can be applied for PEN by replacing the benzene (1,4 substitution) group with naphthalate (2,6 substitution).*

As shown in Fig. 85, the radical-containing product of this photodecarbonylation reaction, extrusion of CO, is also able to resonate in the aromatic structures of PET. Since the amount of esters have decreased for the 300 nm UV photo-oxidation treatment, then the termination mechanism, shown in Fig. 86, can take place to form aldehydes and increase the overall observed carbonyls.

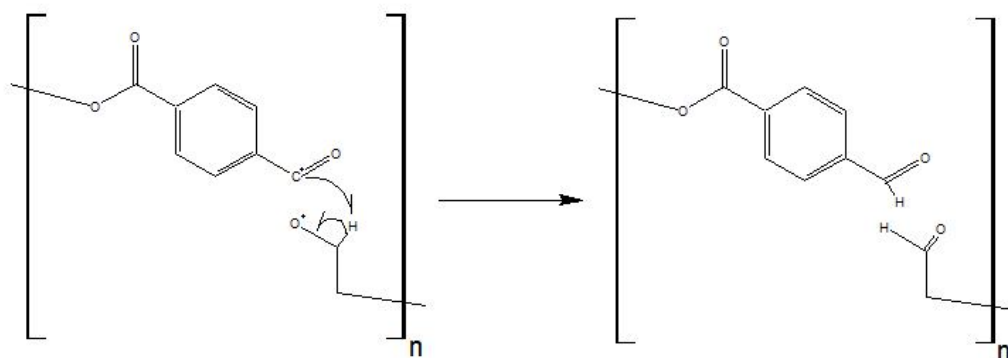


*Figure 86: Termination mechanism of Norrish type IB initiated PET to form aldehydes [30].*

*Note: Same pathway can be applied for PEN by replacing the benzene (1,4 substitution) group with naphthalate (2,6 substitution).*

The termination of the chain via polymer linking, as shown in equation (14), is a generic possibility [61].



The termination of the aryl radicals may take place via the crosslinking mechanism presented in Fig. 87 [19].

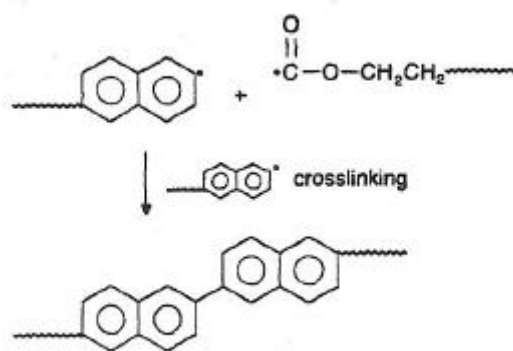


*Figure 87: Crosslinking termination sequence of aryl radical on PEN [19].*

*Note: Same pathway can be applied for PET by replacing the naphthalate (2,6 substitution) with. benzene (1,4 substitution).*

The term photocrosslinking is used in these cases where the presence of light is able to affect the polymer linking characterization. These crosslinking variations (Fig. 88) may lead to crack and grain formation across the surface of the polymer.

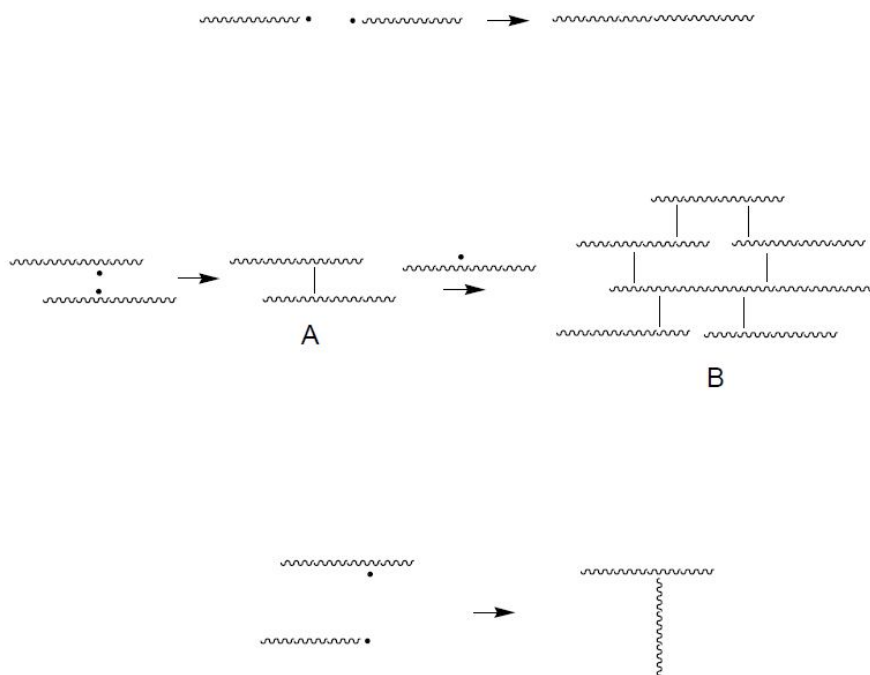


*Figure 88: Photocrosslinking variation that can take place on PET and PEN [61].*

These crosslinking mechanisms are supported by the crack and grain formations observed by the SEM scans of both treatments shown in Figs. 48 and 49. The crosslinked polymer may affect the adsorption of oxygen gas via diffusion. Another concept that may influence the adsorption of these species is photoadsorption, where the presence of photons may affect the adsorption and desorption properties of the polymers being treated [63]. The desorption of Low Molecular Weight Oxidized Materials (LMWOM) has been observed due to the UV and ozone-treated PET [21]. This can cause further reactions to occur on the surface with the LMWOM in the presence of light. The reaction of the polymer surface with these LMWOM can cause the initially smooth surface to become grainy and bumpy. Another possible reason for grain formation is due to photoisomerization, which is defined as the photochemical process that produces an

isomer of the substrate by bond rotation, or skeletal rearrangement or atom/group transfer [63].

The C 1s data (Tables 4 and 6) also showed that both  $sp^2$  and  $sp^3$  carbon groups have decreased due to the 253.7 nm UV photo-oxidation treatment. The decrease in the overall carbon content can be explained by the formation/attachment of LMWOM on the surface. These oxidized species could be from the bulk of the polymer or formed from the photo-oxidation treatment, which would cover the surface thus decreasing the observed carbon content. The amount of  $sp^2$  carbons has decreased while the  $sp^3$  carbons increased due to the 300 nm broad spectrum UV photo-oxidation. This may be explained by photodecarbonylation or photodecarboxylation. Since the 300 nm light has lower energy than the 253.7 nm, then the lower energy entropy driven CO/CO<sub>2</sub> gas extrusion mechanisms would take place more frequently causing the amount of  $Sp^2$  carbonyls to decrease.

The increase in the amount of carbonyls has a direct effect on the decrease in the contact angle as shown in Figs. 36 and 37. The carbonyl groups form a large dipole moment on the surface similar to that of H<sub>2</sub>O, which increases the amount of interaction thus lowering the contact angle or the surface tension [1, 12, 33]. Another explanation for the change in the contact angle could be the variation in the surface morphology due to the treatment, where the liquid-solid interaction could have been altered by the texture of the rougher surface [64].



## II. Effect of UV photo-oxidation at the transitional-bulk layers

The UV absorption spectrum of the PET after treatment showed an overall decreased in the total absorption between 190 to 320 nm as presented in Tables 27 and 28. The change in the absorption spectrum, seen in Figs. 51 and 52, is localized to certain wavelength ranges that prelude the known peaks of the absorption spectrum seen in Fig. 3. The observed peaks in this wavelength range are the ones labeled as I, II, and III in Fig. 3. The increased peak structure in the absorption spectrum can likely be explained by the decrease in the Molecular Weight (MW) of the polymer. The Norrish and scission based mechanisms shown in Figs. 78, 79, and 82, cause general photodegradation to take place. Photodegradation is defined as the transformation of larger molecules into smaller MW fragments [61]. The MW of a polymer has a great significance on the overall energy band gap mixing. The large polymeric species would contain several energy band gaps that mix together as a result of smaller lifetime of excited states due to the increased interaction of components in the system, which leads to a structureless absorption spectrum [14]. As the MW begins to decrease due to photodegradation, the band gaps begin to separate causing the previously available energy levels that existed due to mixing to begin to disappear. As the polymeric mixing band gaps disappear, the absorption at corresponding energy site then begin to decrease to give a more structured shape to the spectrum. The decrease in the polymers' MW can also cause the amount of IR radiation absorbed to increase due to the escalating rotational motion [61]. Therefore besides the change in the functional groups' IR peak signals, the overall increases and decreases in MW due to chain scission and crosslinking patterns must be taken into account when analyzing the IR spectrum. An initial rise in IR absorption is detected for

the 15 min 300 nm UV photo-oxidation treated PET as shown in Fig. 63, which is possibly due to the decrease in MW.

The mechanism shown in Figs. 84 and 89 suggestively take place as observed by the FTIR spectra shown in Figs. 63 and 64 along with Tables 39 and 40, where an increase in vinyl and carboxylic acid end group takes place.

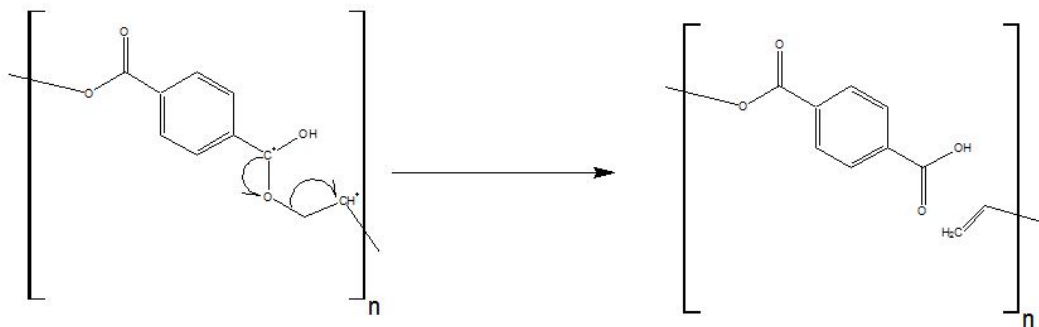


*Figure 89: Photodegradation of Norrish II initiated PET to produce vinyl and carboxylic end groups.*

*Note: Same pathway can be applied for PEN by replacing the benzene (1,4 substitution) group with naphthalate (2,6 substitution).*

A possible explanation for the decrease in the UV absorption is the rise in conjugation by the extrusion of CO/CO<sub>2</sub> as shown in Figs. 84 and 85 followed by crosslinking as was displayed in Fig. 87. The increase in conjugation causes a shift in the energy band gap as was discussed in previous paragraph, which causes an increase in the absorption at higher wavelength and a decrease in the UV region [19]. The observed decrease in the UV absorption spectrum becomes less significant with the increase in treatment time due to the 253.7 nm UV photo-oxidation treatment, indicating that certain chromophores with a higher molar extinction coefficient maybe formed [19]. These groups are most likely ethers and phenols as was observed by the IR spectrum. The formation of ethers can be

explained by the combination of a radical ether with a polymer as generalized in reaction (15) [61].



The termination mechanism of the radical ether with the aryl radical can have a wide range of products due to the resonance on the aromatic ring as shown in Fig. 90.

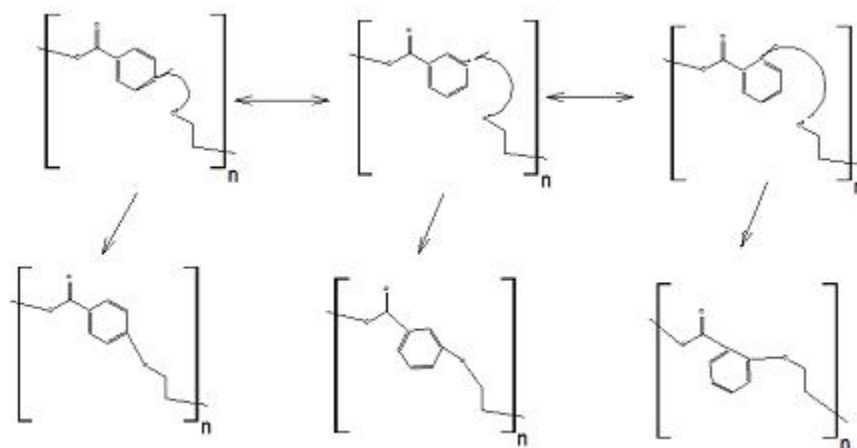


*Figure 90: A possible termination of radical Aryl and ether groups on a PET [30].*

*Note: The pathway can be applied for PEN by: 1) replacing the benzene (1,4 substitution) group with naphthalate (2,6 substitution 2) work through the empty available rearrangements at 1,3-8 substitution pattern possibilities while taking symmetry into account.*

The production of phenol may take place through several mechanistic pathways such as reaction between oxygen and radical aryl groups as displayed in Fig. 91 [40]. The formed aryl peroxide can have ortho-, meta-, or para- substitution.

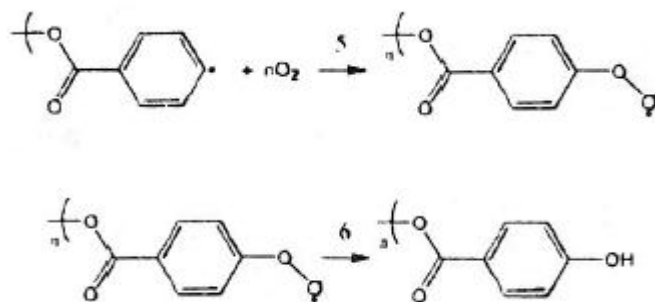


*Figure 91: Propagation of the radical aryl group of PET with oxygen gas, followed by radical peroxide break down along with dehydrogenation to form a phenol end group [40].*

*Note: Same pathway can be applied for PEN by replacing the benzene (1,4 substitution) group with naphthalate (2,6 substitution).*

The other mechanisms utilize the use of ether products such as the photo-Claisen rearrangement which may occurs on aryl ethers as displayed in Fig. 92, or the photo-Fries rearrangement which may also take place on aryl formate reaction products as shown in Fig. 93 [30, 64].

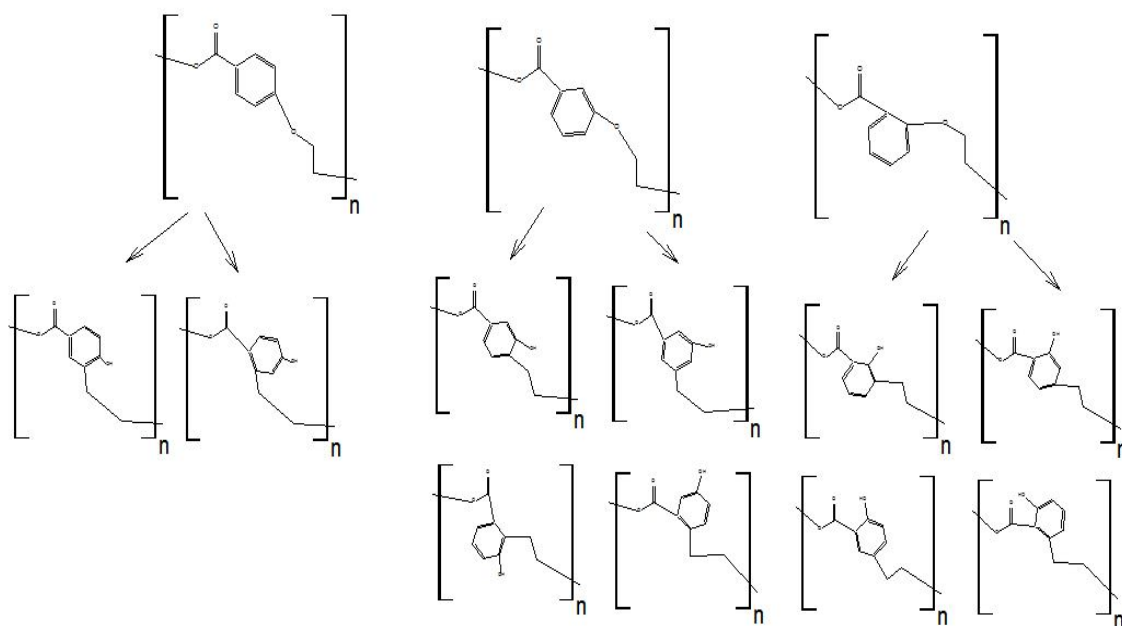


Figure 92: Photo-Claisen rearrangement of a PET aryl ether product [30].

Note: The pathway can be applied for PEN by: 1) replacing the benzene (1,4 substitution) group with naphthalate (2,6 substitution) 2) work through the empty available rearrangements at 1,3-8 substitution pattern possibilities while taking symmetry into account.

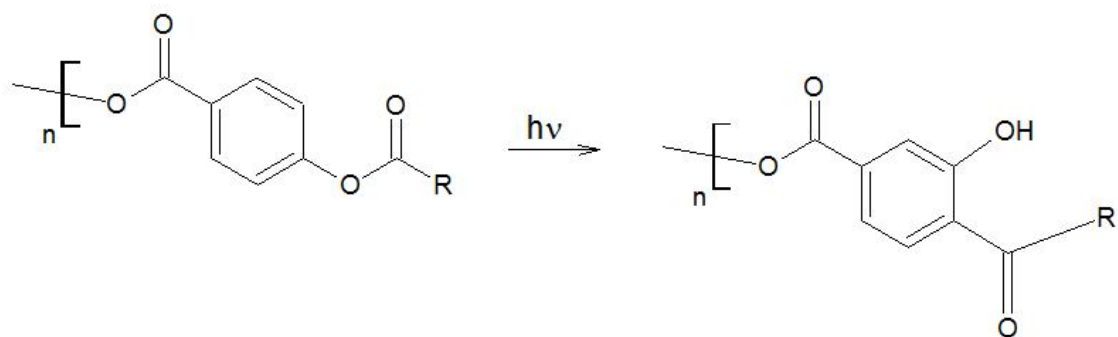


Figure 93: Photo-Fries rearrangement of the aryl formate reaction product of PET [64].

Note: Same pathway can be applied for PEN by replacing the benzene (1,4 substitution) group with naphthalate (2,6 substitution).

### **III. Comparison of the treatments to each other and to the available literature**

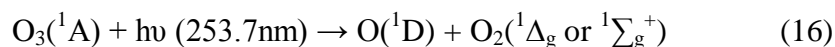
The lower energy 300 nm broad spectrum UV photo-oxidation treatment yielded a higher conjugated products as a result of a lower energy photodecarboxylation and photodecarbonylation reactions. These mechanisms are thermodynamically favored due to its entropy driven CO/CO<sub>2</sub> gas evolution that promotes disorder. The 253.7 nm UV photo-oxidation also allows for the photodecarboxylation and photodecarbonylation to occur, however the higher energy promotes another pathway that forms higher molar absorptivity phenol and/or ether functional groups that increase the UV absorption

The Scheirs and Gardette paper investigated a similar UV photo-oxidation setup applied on PET and PEN [19]. The authors treated PET to a long term vacuum pressure UV photo-oxidation at  $\lambda > 300$  nm. The near-UV and visible absorption spectrum was investigated along with the IR absorbance. The finding was similar to what was investigated by the broad spectrum 300 nm UV irradiation, where chain scission and photocrosslinking took place as was described. Their investigation however did not compare the variation of light energy on the UV photo-oxidation treatment of PET. The researchers' treatment was a long range observation, up to ~750 hours, causing even the more energy demanding mechanistic pathways to be observed. The formation of certain higher absorptivity chromophores was seen which caused photoyellowing of the film after a long period of exposure time [19].

### 5.3 Photophysical and photochemical aspects of atmospheric pressure UV photo-ozonation treated PET

#### I. Effect of UV photo-ozonation at the surface

A gradual increase in the elemental oxygen's percent composition is observed, while a decrease in the atomic carbon is detected at the top 2-5 nm of the treated PET samples as displayed by XPS analysis shown in Table 7. The C 1s analysis (Table 8) shows an increased formation of carbonyl and anhydride/carbonate groups. Ozone is created as was shown in equations (1) and (2) due to the 184.9 nm UV light, which in the presence of the 253.7 nm UV light can produce radical oxygen as shown in reaction (16) [25]. 184.9 nm radiation absorbed by oxygen molecules also dissociates to give O atoms.



The radical oxygen atoms can then initiate several radical mechanisms with the polymer causing a plethora of products that range from dehydration to oxidation. The radical oxygen produced due to highlighted treatments can then react with the polymer removing a hydrogen as seen in Fig. 94 [19].

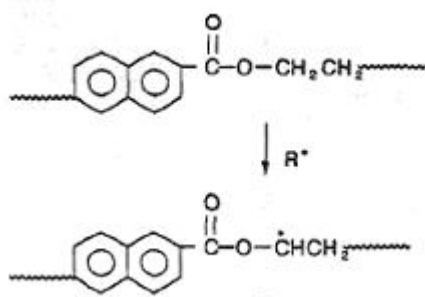


Figure 94: Hydrogen elimination on PEN via radical oxygen atoms [19].

Note: Same pathway can be applied for PET by replacing the naphthalate (2,6 substitution) with benzene (1,4 substitution).

The dehydrogenated PET would then react with oxygen gas to form a peroxide, which then breaks down to form radical esters as displayed in Fig. 95 [40].

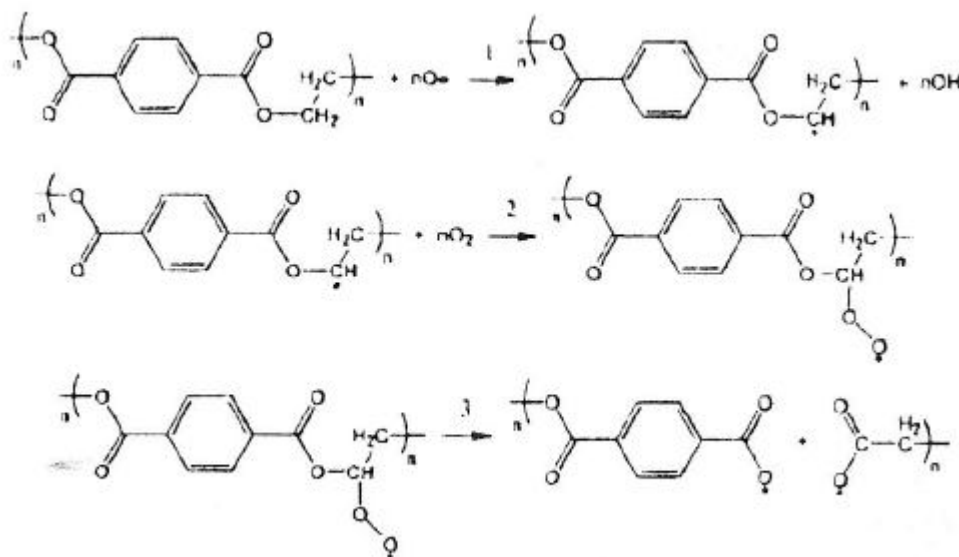


Figure 95: Formation and break down of peroxy radical to form radical esters [40].

Note: Same pathway can be applied for PEN by replacing the benzene (1,4 substitution) group with naphthalate (2,6 substitution).

The increase in the carbonyl and anhydride functional groups may thus be explained by the mechanisms shown in Figs. 83, 86, and 95. The decrease in the detected ester groups is likely due to the Norrish mechanisms breaking them down as shown in Figs. 78 - 80, followed by photodecarbonylation and photodecarboxylation via the evolution of  $\text{CO}/\text{CO}_2$  as presented in Figs. 84 and 85.

The quantity of  $\text{sp}^3$  and  $\text{sp}^2$  carbons have decreased, which can be explained by the formation of new oxide functional groups in the scanned region. The increased ratio of oxidized groups can then decrease the ratio of the carbon based groups. This can also be observed due to the desorption of LMWOM from the surface. The increase in the oxidized functional groups on the surface in turn causes the decrease in the contact angle



due to the increased interaction of water to the more polar surface as shown in Fig. 38. Furthermore the desorption/attachment of the LMWOM to the surface causes it to become rougher and more grainy as displayed in the SEM scans in Fig. 50.

## **II. Effect of UV photo-ozonation at the transitional-bulk layers**

The transitional/bulk regions of the PET were suggestively altered by the treatment as evident by the changes in the IR and UV absorption spectra. This treatment was also tested using the XPS depth profile technique as shown in Fig. 24, which showed a large decrease in the atomic percent of oxygen from the surface to the bulk. This change can be explained by photodecarboxylation and decarbonylation via the mechanisms displayed in Figs. 84 and 85, which increases the population of aryl radical groups that may then undergo crosslinking as shown in Fig. 87. The total UV absorption between 190 to 320 nm is found to immediately decrease due to the treatment by up to 23% as shown in Table 29. This change in absorption caused the spectrum to be more structured (Fig. 56), to the known peaks of PET shown in Fig. 3. The increasing peak structure can be explained by the separation of the energy bands caused by photodegradation as was discussed in the previous section. The IR spectrum (Fig. 32), showed signs of the photodegradation mechanisms shown in Figs. 84 and 89 that produced carboxylic acid and vinyl end groups. The decrease in absorption maybe explained by the rise in conjugation due to photocrosslinking as was observed by the depth profiling XPS scan. The UV absorption spectrum initially decreases significantly then starts to rise with the treatment time which can be explained by the formation of certain functional groups with higher extinction coefficients. A fluctuation of carbonyl functional groups is observed.

The carbonyl formation maybe explained by aldehyde, anhydride, ketone, and esters formations. The formation of these groups may take place through the breakdown of the ester groups via the Norrish reactions to produce radical-based carbonyl compounds as shown in Figs. 78 - 80. The propagation of these groups with other radical aryl or alkyl groups may produce these groups. The formation of ethers and phenol was also observed which may be explained by the mechanisms shown in Figs. 85 and 90; this followed by the photo-Claisen and/or photo-Fries rearrangement to produce phenols as shown in Figs. 92 and 93 along with the breakdown of peroxy radicals in Fig. 91. The possible termination mechanism to the Norrish II initiated radical groups may take several routes that results in photocyclization. This photocyclization may take place via the Norrish-Yang reaction as presented in Fig. 96 [61].

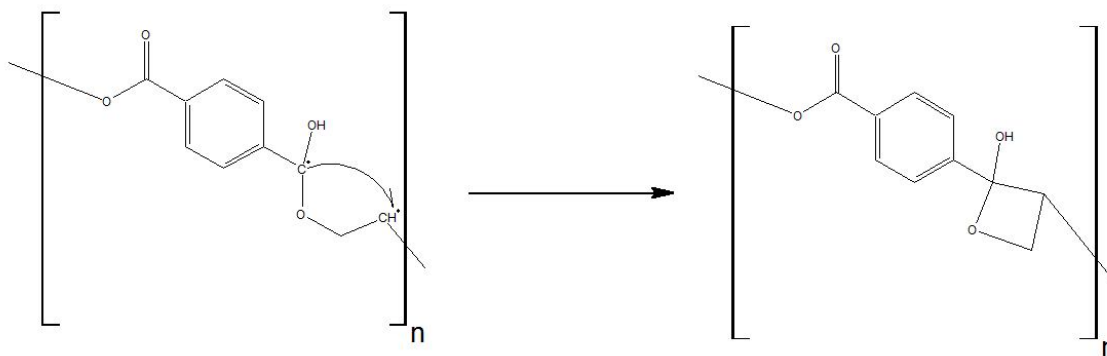


*Figure 96: Photocyclization of PET via the Norrish-Yang reaction [58].*

*Note: Same pathway can be applied for PEN by replacing the benzene (1,4 substitution) group with the naphthalate (2,6 substitution).*

### **III. Comparison of UV photo-ozonation to UV photo-oxidation and to the available literature**

In this thesis, the UV absorption showed a similar trend to the 253.7 nm UV photo-oxidation, where the suggestive increase in conjugation caused it to decrease followed by the production of certain functional groups that showed an increase. The production of phenols and ethers was observed in the same manner, however, a fluctuation in the carbonyl is observed due to the photo-ozonation unlike the decrease observed in the UV photo-oxidation. The production of carbonyls is likely influenced by the ozone and oxygen radicals causing the observation of carbonyls to be more prevalent. The impact on the surface chemistry and physiology was found to be more significant as a result of UV photo-ozonation, this is mainly due to the high energy radical particles that tend to be more reactive causing the sharper rise in the amount of carbonyls.

The available literature on the UV photo-ozonation studied PET was mainly on the surface modification and analysis [21, 25]. The work by Hill and Walzak showed similar results to those observed in this research, where the amount of elemental oxygen was observed to have increased at the surface. The advancing and receding contact angle was also studied to show an overall increase in the surface tension [21, 25]. Another similarity between this research and the literature was the suggested presence of the LMWOM, which contributed significantly to the surface tension and chemistry [21]. The formed functional groups as per the author's observations were carboxylic acid end groups, vinyl end groups, phenols, along with the CO/ CO<sub>2</sub> gas evolution [21]. The results studied by the two articles were more dynamic and rigid in terms of obtaining a precise chemical analysis as compared to the photophysical nature of the irradiation. This thesis however

aims to be able to provide a precise and accurate comparison between the different irradiation techniques along with several suggested mechanistic pathways.

## **5.4 Photophysical and photochemical aspects of atmospheric pressure UV photolysis treated PET in nitrogen**

### **I. Effect of UV photolysis at the surface**

The XPS elemental analysis of the top 2-5 nm of the treated PET films showed a gradual increase in the atomic percent of oxygen and a decrease in the carbon content due to the 184.9/253.7 and 253.7 nm UV photolysis treatments (Tables 11 and 13). The 300 nm broad spectrum irradiation showed very little change at the surface in terms of the elemental composition as displayed in Table 9. The C 1s analysis of each treatment showed an increase in the quantity of carbonyl and anhydride/carbonate groups as displayed in Tables 10, 12, and 14. The increase in these groups is dependent on the light energy applied, where the largest increase is due to the 184.9/253.7 nm and the smallest is the 300 nm broad spectrum UV irradiance. The amount of detected esters is found to have decreased for all treatments. Since no significant oxygen gas is present then the most likely method of radical initiation is from the Norrish mechanisms shown in Figs. 78, 79, and 80. The Norrish I initiated PET may go through several termination sequences with the surrounding polymers to form the anhydride/carbonate functional groups shown in steps (11) - (12). The possible increase in carbonyl can also be account for by the formation of aldehydes as shown in Fig. 86, or by the formation of ketones via the propagation of the Norrish I initiated product with radical aryl or alkyl groups. A decrease in  $sp^2$  carbons and an increase in  $sp^3$  carbons is detected for the 253.7 nm

treatment, which can most likely be explained the increased formation of  $sp^2$  carbonyls at the scanned area. The quantity of  $sp^3$  and  $sp^2$  carbons seem to fluctuate between increasing and decreasing for the 184.9/253.7 and 300 nm broad spectrum UV photolysis. The fluctuations can be explained by the increase in  $sp^2$  carbonyls along with the desorption of LMWOM to the surface, and the CO/CO<sub>2</sub> extrusion to lower the  $sp^2$  carbons and increase the  $sp^3$  carbons. The contact angle is found to have decreased in a direct relation to the increase in the quantity of carbonyls and the light energy emitted as shown in Figs. 39, 40, and 41.

## **II. Effect of UV photolysis at the transitional-bulk layers**

The total UV absorption of PET between 190 to 320 nm after treatment showed a positive change at higher treatment times for the 253.7 and 184.9/253.7 nm treatments (Tables 31 and 32). The 300 nm broad spectrum treatment showed no significant change at lower treatment times, then eventually begin to show signs of decrease as shown in Table 30. The 184.9/253.7 nm treatment showed a decrease in absorption at lower treatment times. The observed change in the UV absorption spectrums (Figs. 54, 55, and 56) showed an increasing peak structure which as discussed in the previous sections may be caused by the decrease in MW by photodegradation. The decrease in absorption detected is likely due to the increase in conjugation via photocrosslinking as shown in Figs. 87 and 88. The polymer's radical initiation likely took place via the Norrish mechanisms like it was discussed for the surface. The 300 nm broad spectrum treatment showed the most significant increased formation of carboxylic and vinyl end groups (Fig. 66) as displayed by the mechanism in Fig. 89.

Since the absorption spectrum showed an increase in the absorption, then some chromophores with a higher extinction coefficient may have been produced at competing rate as the crosslinking. The IR spectrum of the 184.9/253.7 nm UV photolysis treatment (Fig. 68 and Table 44) showed an increase in the amount of carbonyls, which can be explained by the formation of ketones and aldehydes as was discussed in the surface analysis. A fluctuating change in the amount of carbonyls, however, is detected for the 253.7 and 300 nm treatments (Figs 66 & 67, Tables 42 & 43). These fluctuations can be explained by the production of ketones and aldehydes, followed by their break down of via the Norrish mechanisms followed by photodecarboxylation and photodecarbonylation as shown in Figs. 84 and 85. The formation of ethers was observed for each treatment as can be explained by the mechanisms displayed in Fig. 90 and (15). The 300 nm treatment however also showed a decrease in the ethers, which can be explained by the rise in phenols via the photoclaissen and photo fries rearrangement as reveled in Figs. 92 and 93.

### **III. Comparison of UV photolysis to UV photo-oxidation and to the available literature**

The increase in the light energy for UV photolysis causes the production of the chromophores like aldehydes, ketones, anhydrides, and ethers which increase the amount of detected absorption. At the lower light energy, 300 nm broad spectrum treatment, causes the production of phenols. The production of these higher absorptivity functional groups becomes a competing reaction with the production of the more conjugated products. The competition between these two reaction causes the observed changes in the absorption spectrum to be limited, due to the increased and decreased absorption

properties of both species. The rate of oxidized group formations on the surface is dependent on the light energy, which can likely be explained by the energy consumption required by the production of these aldehyde, ketone, and anhydride functional groups.

The UV photo-oxidation treatments predominantly showed a decrease in the absorption due to the amount of energy consumed at the surface via the radical mechanisms involved by the oxygen gas. The lower energy available to the transitional-bulk regions then allows for the lower energy photodecarboxylation and photodecarbonylation reactions to take place and cause photocrosslinking with the aryl groups. Since the produced carbonyls from the UV photo-oxidation and photo-ozonation does not increase the amount of absorption significantly then the extent of the modification within the depth due to the increased concentration of highly reactive oxygen can thus be noted to be mainly a surface effect [19]. This is due to the limited adsorption of these molecules via diffusion needs [19, 61].

A large proportion of the available literature investigates UV photolysis in the VUV and near VUV region (115 and 155 nm) region [31, 32]. The Scheirs and Gardette paper also studied the UV irradiance of PET in the absence of oxygen, however in a vacuum environment at a  $\lambda > 300$  nm [19]. The research also look mildly at different wavelength cutoff points at  $\lambda > 345$  versus 360 nm. The authors drew a similar conclusion to the research in this thesis, where several competing pathways that produce highly conjugated products versus higher absorptivity chromophores. The authors also concluded that a much more significant photoyellowing was observed for the photo-oxidation treatments, which is due to the increased conjugation [19]. Their research also supports the mechanistic pathways suggested by the observed products of this thesis's treatments. The

photodecarboxylation and photodecarbonylation is supported by their observation of CO and CO<sub>2</sub> gas evolution in a vacuum [19].

## **5.5 Photophysical and photochemical aspects of VUV photo-oxidation treated PET and PEN**

### **I. Effect of VUV photo-oxidation at the surface**

The XPS scan of the treated PEN and PET (Tables 15 and 17) showed an increase in the elemental oxygen percent composition and a decrease in the carbon content similar to the UV photo-oxidation. The C 1s functional group analysis (Tables 16 and 18) showed an increase in the quantity of carbonyl and anhydride/carbonate groups for both polymers. The VUV Ar plasma is able to output 104.8 and 106.7 nm UV radiation that is able to produce radical oxygen atoms as shown in equations (3)-(5) [65]. These radical oxygen atoms can then possibly initiate the radical mechanisms on the polymer surface as shown in Fig. 94. The polymer may have also been initiated by the VUV photons through the Norrish reactions (Figs. 78 - 80). The increase in the carbonyl and anhydrides can be explained by a similar mechanistic pathway as the UV photo-ozonation. The formation and breakdown of peroxides due to the radical oxygen may increase the anhydrides as shown in Figs. 81 and 82. The amount of anhydrides/ketones may also be formed via the mechanism shown in Fig. 86 along with the propagation of Norrish initiated products with aryl and alkyl radicals. The anhydride formation may take place through the cage reaction (Fig. 83). Another method of anhydride/carbonate production is via the termination of Norrish I initiated radicals as seen in reaction steps (11) and (12). The breakdown of esters is observed for PET, however an increase in esters is found for the



treated PEN. The increase in the esters may take place through the break down of the peroxides as shown in Fig. 95, followed by the termination with other aryl or alkyl groups. The amount of ethers in the treated PET had decreased, while that of PEN slightly increased. The quantity of  $sp^3$  and  $sp^2$  carbons has decreased for each polymer due to the large increase in the oxidized functional groups within the scanned volume, which effectively lowered the overall ratio of carbon groups. The advancing contact angle decreased for each polymer (Figs. 42 and 43) in response to the rise in the carbonyls. Since PEN showed a much larger increase in the oxide groups on the surface, the decrease in the contact angle is much more significant.

## **II. Effect of VUV photo-oxidation at the transitional-bulk layers**

The total UV absorption of the treated PET between 190 to 320 nm shows an overall decrease as presented in Table 34, while the total absorption of PEN between 190 to 400 nm indicates an increasing trend as shown in Table 33. The changes in the UV spectra with wavelength (Figs. 57 and 58) shows an increase in peak structures of the known PET and PEN peaks (Fig. 3). The increased peak structure is due to photodegradation as discussed in the previous sections. The IR spectrum of PEN (Fig. 69) showed an increase in the carboxylic acid and vinyl end groups as displayed by the mechanism shown in Figs. 84 and 89. The observed decrease in the absorption spectrum of PET is likely attributed to photocrosslinking of aryl groups and the rise in conjugation as was discussed in the previous section by mechanism shown in Fig. 87. The IR spectrum of the treated PET (Fig. 70) shows an increase in the carbonyl and ester groups which can likely be explained by the reaction of radical oxygen with the polymer at the surface (Fig. 95). The

increase in the PEN absorption spectrum, can be explained by the formation of phenols as observed in the IR spectrum. A decrease in the ether signal is also detected which maybe explained by the photo-Claisen and/or photo-Fries rearrangements as shown in Figs. 92 and 93.

### **III. Comparison of the VUV photo-oxidation on each polymer and to the available literature**

The larger naphthalene ring on PEN allows the radical mechanism to be more stable due to the delocalization effects of the more aromatic structure. The stabilization of the radical mechanism allows for the formation of carbonyl functional groups to be formed with more ease. The differences observed between the PET and PEN is due to the aromaticity, which allowed the reactions that required more energy on PET to be formed by the PEN. It is important to note however that the light intensity of the argon plasma is much weaker than that of the UV photolysis/photo-oxidation treatments. Therefore, a large majority of the energy is suggestively lost in the production of oxygen radicals and carbonyl compounds at the surface. The low energy that reached the transitional-bulk region of the PET film caused a small amount of photodecarboxylation and photodecarbonylation to effectively increase the concentration of aryl radicals and increase the conjugation to lower the UV absorption. However the initiated radicals on PEN was stabilized to continue to propagate throughout the polymer to effectively initiate the low energy phenol formation reactions as discussed in the UV photolysis section. The formation of carboxylic acid end groups through the Norrish II mechanism is also a lower

energy requiring reaction, as evident by its formation only on the stabilized PEN structure.

The literature available on the VUV photo-oxidation is mainly onto PET [27-28, 31-32] and no significant data exists for PEN. The data analyzed for the treated PET is via FTIR, XPS, and contact angle [27-28, 31]. The changes detected showed an increased formation of elemental oxygen [27-28, 31]. The same oxide functional groups detected in this research was also found in the literature [28, 31]. The depth of the PET film was studied in the literature, which showed the limited effect of the radical oxygen atoms on the bulk of the polymer [31]. The plasma study in this thesis was mainly focused on the direct comparison of the mechanisms involved and the effect of the structure of PET versus PEN. The research also investigated the chemical effects on the optical properties of each polymer, along with the surface modification and properties due to the treatment.

## **5.6 Photophysical and photochemical aspects of VUV photolysis treated PET and PEN**

### **I. Effect of VUV photolysis at the surface**

The XPS elemental analysis of the treated PET showed a slight decrease in the atomic percent of oxygen and a slight increase in the carbon, however the opposite trend is observed for the PEN samples as presented in Tables 19 and 21. An increase in the quantity of anhydride/carbonate groups for both polymers is detected as presented in the C 1s analysis Tables 20 and 22. Since the photolysis took place in vacuum, then the polymers are likely to have been initiated by the Norrish mechanisms shown in Figs. 78 -

80. The amount of observed carbonyls has increased for PET, which may have been the result of the Norrish I radical products going through a termination sequence with the radical aryl or alkyl groups to produce aldehydes, ketones, and/or anhydrides as shown by reaction steps (11) - (12). The formation of aldehydes may also take place through the mechanism shown in Fig. 86. The PEN showed a decrease in the amount of carbonyls and an increase in the ethers as shown by the mechanisms in Figs. 85 and 90. The quantity of  $sp^2$  carbons is found to have increased and the  $sp^3$  carbons decreased for PET, which can be explained by the rise in the amount of  $sp^2$  carbonyls. The opposite trend was observed for PEN which maybe explained by photodecarboxylation and photodecarbonylation that decreased the amount of  $sp^2$  carbonyls. As seen in Figs. 44 and 45, the contact angle decreases for each polymer as a result of the increasing polarity of the surface due to the increase in the oxide functional groups.

## **II. Effect of VUV photolysis at the transitional-bulk layers**

The change in the total UV absorption for the treated PET between 190 to 320 nm showed a small decrease while PEN showed an increase, between 190 to 400 nm, as shown in Table 35 and 36. The absorption spectrum for each polymer (Figs. 59 and 60) are found to have become more structured due to the treatment where as discussed in the previous section is mainly due to the separation of band gaps. The IR spectra of both polymers (Figs. 71 and 72) showed an increase in the amount of carboxylic and vinyl end groups formed which points to the photodegradation mechanism shown in Fig. 89. The decrease in the UV absorption for the treated PET can also be explained by the increase in conjugation as shown in the crosslinking mechanisms in Fig. 87. The absorption

spectrum of PEN shows a smaller increase in the UV range from 190 - 320 nm, and larger increase from 375 - 400 nm as compared to the UV photo-oxidation. The likely reason for this is the increase in conjugation via photocrosslinking, which decreases the absorption at the UV region and increases at the near UV region. In both polymers an increase in the quantity of ethers and phenols is detected, which can be produced through the photodecarbonylation and radical termination mechanisms shown in Figs. 85 and 90 followed by the photo-Claisen and/or photo-Fries rearrangement (Figs. 91 and 92). The carbonyl signal for the PET is found to decrease due to the treatment, which is explained by the Norrish mechanisms along with photodecarboxylation and photodecarbonylation. However the amount of carbonyls detected for the PEN is found to fluctuate which can be explained by the break down of the ester group to produce aldehydes and ketones as discussed at the surface reactions. The production of aldehydes, ketones, ethers, and phenol are the likely reason for the overall rise in the PEN absorption spectrum.

### **III. Comparison of VUV photolysis on each polymer with the VUV photo-oxidation treatment and to the available literature**

The more stable structure of PEN allowed for certain carbonyl-based compounds to be formed with a higher yield as to significantly alter the optical properties of the film. The VUV photo-oxidation treatment due to the presence of the radical oxygen gas, caused a large proportion of energy to be consumed at the surface in the process of forming the observed carbonyl-based compounds. The VUV photolysis allowed for a higher proportion of energy to be able to reaction the transitional-bulk regions, which caused higher energy demanding reactions to be formed. The formation of phenols,

which is a moderately high demanding energy requiring mechanistic pathway, is more possible for the less aromatic PET structure. The higher energy available allowed for the PEN to be able to form the carbonyl and phenol-based functional groups as well as the more conjugated proposed aryl structure.

The literature found similar results at the surface of the PET due to hydrogen plasma exposure at  $\lambda$  of 112 and 160 nm, where the amount of elemental oxygen decreased due to the treatment as explained by the scission of the ester group and the evolution of CO<sub>2</sub> gas [36]. Another article stated that that mechanism that occurred due to the reaction is crosslinking by radical recombination along with double bond formation [26]. The specific mechanism is stated via the Norrish II reaction taking place to produce oxides, vinyl groups, and phenols [26]. These observations were accurate as detected by the analytical methods used in this research, however the particular mechanism involved was also compared to PEN to set the rough energy requirements. The literature has some available data on some VUV wavelength irradiation of PET, however there is limited data on PEN that provides the mechanism as compared to that of PET.

## **5.7 Photophysical and photochemical aspects of remote oxygen and/or argon reaction with PET and PEN**

### **I. Effect of the remote oxygen and argon at the surface**

The MW discharge of Ar and O<sub>2</sub> is a method used to simulate the same condition as the VUV photo-oxidation without the interaction of the photons with the sample. The extent of the chemical change detected on the surface of each polymer is much greater than any of the other treatment. The XPS elemental analysis showed a very large increase

in the atomic percent of oxygen and a decrease in carbon for both polymers as shown in Tables 23 and 25. The surfaces of the remote argon treated polymers are scanned to establish the Ar plasma's involvement and effects on the remote oxygen reaction treatment. It is a known fact that the Ar plasma has a very short lifetime [66], where the displacement from the microwave plasma cavity to the sample causes the Ar atoms to lose energy and become inert. The XPS elemental survey showed this as displayed in Tables 23 and 25, where no significant change is detected in the atomic percent of polymers.

The C 1s analysis of PET and PEN (Tables 24 and 26) showed an increase in anhydride/carbonate, esters, and carbonyls. In this treatment, the only initiation mechanism that may take place is via the interaction of radical oxygen atoms with the polymer surface. The formation of carbonyl compounds may take place via the mechanism shown in Fig. 95, which would increase the amount of esters anhydride/carbonate through reaction steps (11) - (12). The quantity of  $sp^2$  and  $sp^3$  carbons has been found to have decreased for the treated PEN, which maybe explained by the overall rise in the total oxidized functional group within the scanned area thus lowering the total carbon ratio. Certain fluctuation in the  $sp^3$  and  $sp^2$  carbons is observed for PET, which maybe explained by the increase in the amount of  $sp^2$  carbonyls or the decrease in these carbonyls via the entropy driven decarboxylation or decarbonylation shown in Figs. 84 and 85. The contact angle decreased significantly in response to the massive rise in carbonyl compounds on the surface as shown in Figs. 46 and 47. Some slight changes in the C 1s spectrum is detected for the remote argon treated samples. However, it is important to note that the samples experienced a prolonged exposure to a

vacuum environment for the treatment as well as during the XPS measurements. When the samples are exposed to a prolonged period within a vacuum, out-gassing and bleeding begins to occur [14]. The absorbed atmospheric gases along with washing fluids begin to be released from the sample surface, which shows a slight change. The effect of out-gassing, however, is very slight and falls within the 5% error range associated with the instrumental error.

## **II. Effect of the remote oxygen at the transitional-bulk layers**

The total UV absorption of the treated PET (Table 38) showed a very small and insignificant decrease, while PEN (Table 37) showed a slight increase. The change in the UV absorption spectrum per wavelength of PET showed no significant change to form any observable peaks as shown in Fig. 62. The UV absorption spectrum of PEN (Fig. 61) shows a small increase at the lower UV wavelength region, and a much larger increase at the near UV region. Since no photons were applied directly onto the polymers, then only the surface to transitional region is affected which explains the very low change in absorption. The radicals initiated at the surface continue to propagate throughout the polymers until a termination sequence takes place. Since PEN has a larger aromatic ring, then the radical mechanism becomes more stable and thus able to propagate longer thus explaining the larger rate of change in the absorption. The decrease in the absorption spectrum of PET along with the increase in the near UV absorption of PEN can be explained by photocrosslinking of the aryl groups as shown in Fig. 87. The occurrence of the crosslinked conjugation of the aryl groups is possible due to the breakdown of the ester linkage by decarboxylation as shown in Fig. 84. The IR spectrum of each polymer



(Figs. 73 and 74) supports the observation of XPS on the surface, with the addition of an increase in carboxylic acid, phenols, vinyl and alkyl groups. The formation of carboxylic, vinyl, and alkyl end groups are all products of the discussed radical propagation of oxygen atoms with the polymer as shown in Figs. 84, 91, and 95. The formation of phenols may be explained by the radical propagation and termination of aryl radicals with the oxygen atoms as shown in Fig. 91.

### **III. Comparison of the remote oxygen treatment to VUV photo-oxidation treatment and to the available literature**

These remote oxygen and argon studies were conducted to display the extent of the radical oxygen's effect independent of photolysis. This treatment suggestively proved that the extent of the radical oxygen atoms is mainly at the surface to transitional region. This treatment is to display how the optical properties of the films are mainly dependent on the extent of the oxide modification within the depth of the film. The surface of the polymers also displayed a smaller rise in the oxide formation due to UV or VUV photo-oxidation due to the high concentration of photons being presence on the surface (Fig. 77) thus breaking down the carbonyls, via photodecarboxylation or photodecarbonylation.

There exist certain research papers that have investigated this remote oxygen treatment on PET, however, only a few have thoroughly investigated the mechanisms involved on PET and PEN [40]. These particular mechanisms were studied vigorously to show the chain scission and the resulting rise in the oxide formation at the surface along with the proposed photodecarboxylation method by Gonzalez and his group [40] who studied the remote oxygen reaction at atmospheric pressure which may cause the

occurrence of ozone products. This thesis however aimed to be able to compare the effects of the remote radical oxygen to the effect of VUV and UV photo-oxidation to display the particular comparisons and contrasts.

## **6.....FUTURE WORK**

This research investigated many aspects of the chemical and physical properties of UV and VUV photoreactions on PET and PEN. There are many future techniques that could be used to validate the drawn conclusions from the results obtained. These methods and techniques can be summed up as shown:

- 1) Testing each polymer physical and chemical nature after being exposed to a vacuum environment.
- 2) A molecular weight analysis is needed to validate photodegradation.
- 3) A mass spectrometry testing is needed to monitor the extrusion of gases due to the photochemical reactions.
- 4) A computation study may be needed to clearly indicate the thermodynamic and kinetic tendencies during the photochemical reactions along with the type of mechanism that occurs.
- 5) Study the reaction of ozone with PEN in the presence and absence of UV radiation.
- 6) Investigate the optical properties of PET and PEN in the visible and VUV range for PET and PEN due the applied treatments.
- 7) A deeper depth profile XPS analysis into the bulk region applied for each treatment.

## 7.....CONCLUSION

Several variations of photo-oxidation and photolysis treatments were applied to poly(ethylene terephthalate) (PET) and poly(ethylene 2,6-naphthalate) (PEN). The photophysical and photochemical properties of PET were studied for the atmospheric pressure treatments of 184.9/253.7, 253.7, and 300 nm broad spectrum UV photo-oxidation and photolysis. The effect of VUV (Ar plasma) photo-oxidation, photolysis, and remote oxygen/argon reactions with PEN and PEN were compared and studied.

The PET films showed signs of a decreased UV absorption due to the UV photo-oxidation and UV photo-ozonation treatments. The amount of energy consumed at the surface in the production of oxides from the oxygen may have caused the low energy entropy driven photodecarboxylation and photodecarbonylation to occur at the transitional-bulk region. These reactions would cause the increased concentration of aryl radicals that react to increase the conjugation length of the polymer, which lead to the decreased absorption in the UV region. The PET films however showed signs of an increased absorption due to the UV photolysis, which is indicative of the production of certain higher absorptivity functional groups. These functional groups are most likely formed due to the increased energy available at the transitional-bulk region from the lack of photons consumed at the surface from the oxygen gas. The results also showed that the lower energy photolysis lead to the production of phenol and ether groups, while the higher energy photons lead to the production of carbonyl-containing compounds such as ketones and aldehydes.

The VUV photo-oxidation versus photolysis showed similar results to the atmospheric UV reactions. The PEN structure due to the increased aromaticity over PET, caused the radical-based mechanisms to be stabilized and occur with more vigor. The increased formation of the higher energy demanding aldehyde/ketones or phenol/ethers caused the treatments to increase the amount of UV absorption experienced by the PEN film. Finally the extent of the optical and chemical changes for the remote oxygen radicals was tested, and confirmed it was mainly a surface treatment that had minimal effects on the optical properties.

## REFERENCES

- [1] Silbey, R.J.; Alberty, R.A.; and Bawendi, M.G.. *Physical Chemistry*. 4th edition Hoboken, NJ; Wiley, 2005.
- [2] Adamson, A.W. and Gast, A.P.. *Physical Chemistry of Surfaces*. Hoboken, NJ; Wiley 1997.
- [3] Teare, D.O.H.; Ton-That, C.; and Bradley, R.H. *Surface characterization and ageing of ultraviolet-Ozone-treated polymers using atomic force microscopy and x-ray photoelectron spectroscopy*. Surface and Interface Analysis, 29, 276-283 (2000).
- [4] Mathieson, I. and Bradley, R.H. *Improved adhesion to polymers by UV/ozone surface oxidation*. Int. J. Adhes. Adhes. 1996; 16:29.
- [5] Sheng, E.; Sutherland, L; Brewis, D.M.; and Heath R.J. *Effects of the chromic acid etching on propylene polymer surface*. Adhesion Science and technology. 1995; 9:47.
- [6] France, R.M. and Short, R.D. *Plasma treatment of polymers effects of energy transfer from an argon plasma on the surface chemistry of poly(styrene), low density poly(ethylene), poly(propylene) and poly(ethylene terephthalate)*. Chemical Society, Faraday Trans. 1997; 93:3173.
- [7] Strobel, M.; Walzak, M.J.; Hill, J.M.; Lin, A.; Karbasheski E.; and Lyons, C.S. *A comparison of gas-phase methods of modifying polymer surfaces*. Adhesion Science and technology. 1995; 9: 365.

- [8] Mutel, B.; Dessaux, O.; Goudmand P.; Gengembre L.; and Grimblot J. *Energy consumption and kinetic evolution of nitrogen fixation on polyethylene terephthalate by remote nitrogen plasma: XPS study*. Surface interface Analysis. 1993; 20: 283.
- [9] Strobel, M; Lyons, C.S.; Strobel, J.M.; and Kapaun, R.S. *Analysis of air-corona-treated polypropylene and polyethylene terephthalate films by contact angle measurements and XPS*. J. Adhesion Science and Technology. 1992; 6: 429.
- [10] Onyiriuka, E.C. Adhesion Science and Technology. *Electron beam surface modification of polystyrene used for cell cultures*. 1994; 8(1): p.1-9.
- [11] Guruvenket, S.; Mohan Rao, G.; Komath, M.; and Raichur, A.M. *Plasma Surface Modification of Polystyrene and Polyethylene*. Applied surface science. 2004; Elsevier.
- [12] Callister, W.D. and Rethwisch, D.G. *Materials Science and Engineering and Introduction*. 8th Edition. Hoboken, NJ; Wiley, 2010.
- [13] Kutz, M. *Applied plastics Engineering Handbook*. 1st Edition. Oxford, UK; Elsevier, 2011.
- [14] Painter, P.C. and Coleman, M.M. *Fundamentals of Polymer Science*. 2nd edition. Boca Raton, FL; CRC Press LLC, 2000.
- [15] Tabankia, M.H. and Gardette, J.L. *Photo-chemical degradation of polybutyleneterephthalate: part 1-photo-oxidation and photolysis at long wavelengths*. Polymer Degradation and Stability, 1986, 14, 351.
- [16] Selke, S.E.M. *Plastic Packaging Technology*. Cincinnati, OH; Hanser/Gardner, 1997.
- [17] O'Regan, M.; Hildner, M.; Prakash, S.; Sellars, M.; and Wessel, R. *Plastic Displays: Recent Developments at Dupont Displays*. Proc. of SPIE Vol. 5214.

- [18] Shuto, T.; Wantanabe, N.; Ikeda, A.; Higashimachi, T.; and Asano, T. *Microjoining of LSI chips on poly(ethylene naphthalate) Using compliant Bump*. Japanese Journal of Applied Physics 50 (2011) 06GM05.
- [19] Scheirs, J. and Gardette, J.L. *Photo-oxidation and photolysis of poly(ethylene naphthalate)*. Polymer Degradation and stability. Northern Ireland, 56(1997) 339-350.
- [20] Davenas, J.; Boiteux, G.; Seytre, G.; and Jardin, C. *Role of the structure on the photo and cathodo-luminescence of poly(ethylene naphthalate): PEN*. Synthetic Metals 115 (200) 83-87.
- [21] Hill, J.M.; Karbasheski, E.; Lin, A.; Strobel, M.; and Walzak, M.J. *Effects of aging and washing on UV and Ozone-treated poly(ethylene terephthalate) and polypropylene*. Polymer Surface Modification: Relevance to Adhesion. (1995) pp. 273-289
- [22] Ouchi, I.; Hosoi, M.; and Matsumoto, F. *Photodegradation of poly(ethylene 2,6-Naphthalate) Films*. Applied Polymer Science. Vol. 20, 1983-1987 (1976).
- [23] Teyssedra, G.; Mary, D.; and Laurent, C. *Electroluminescence and photoluminescence of UV-aged poly(ethylene naphthalate) films*. IEE, proc.-Sci. Meas. Technol., Vol. 150, No. 2, March 2003.
- [23] Mary, D.; Teyssedra, G.; and Laurent, C. *UV-induced degradation of poly(ethylene naphthalate) films from the standpoint of electrical and luminescence properties*. 2001 annual report conference on Electrical Insulation and Dielectric Phenomena.
- [24] Allen, N.S.; and McKellar, J.F. *Photochemical Reaction in commercial poly(ethylene 2,6-naphthalate)*. Applied Polymer Science, Vol.22, 2085-2092 (1978).



- [25] Walzak, M.J.; Flynn, S.; Foerch, R.; Hill, J.M.; Karbaszewski, E.; Lin, A.; and Strobel, M. *UV and ozone treatment of polypropylene and poly(ethylene terephthalate)*. polymer surface modification: relevance to adhesion, pp.253-272 (1995).
- [26] Hollander, A.; Kelmberg-Sapieha, J.E.; and Wertheimer, M.R. *The influence of Vacuum-Ultraviolet Radiation on Poly(ethylene terephthalate)*. Polymer science: Part A: polymer chemistry, Vol.34, 1511-1516 (1996).
- [27] Gupta, B.; Plummer, C.; Bisson, I.; Frey, P.; and Hilborn, J. *Plasma-induced graft polymerization of acrylic acid onto poly(ethylene terephthalate) films: characterization and human smooth muscle cell growth on grafted films*. Biomaterials 23 (2002) 863-871.
- [28] Ouchi, I.; Nakai, I.; and Kamada, M. *Anisotropic absorption spectra of polyester films in the ultraviolet and vacuum ultraviolet regions*. Nuclear Instruments and Methods in Physics Research B 199 (2003) 270-274.
- [29] Ouchi, I. *Anisotropic Absorption and Reflection Spectra of Poly(ethylene terephthalate) Films in Ultraviolet region*. Polymer Journal, Vol. 15, No.3, pp 225-243 (1983).
- [30] Braslavsky, S.E. *Pure and Applied Chemistry*. 2007, Vol. 79, p. 293.
- [31] Cho, K.; Setsuhara, Y.; Takenaka, K.; Shiratani, M.; Skine, M.; and Hori, M. *Effects of photoirradiation in UV and VUV regions during plasma exposure to polymers*. Thin Solid Films 519 (2011) 6810-6814.
- [32] Cho, K.; Takenaka, K. ; Setsuhara, Y.; Shiratani, M.; Skine, M.; and Hori, M. *Effects of Photon irradiation in UV and VUV regions during plasma processing of organic materials*. Transactions of JWRI, Vol.39 (2010), No. 2.

- [33] Harris, D.C. *Quantitative Chemical Analysis*. W.H. Freeman and company; New York, NY (2007).
- [34] Grace, J.M.; Zhuang, H.K.; Gerenser, L.J.; and Freeman, D.R. *Time-resolved investigation of the surface chemical modification of poly(ethylene naphthalate) by nitrogen plasma treatment*. Vacuum Science and Technology. A21(1), Jan/Feb 2003.
- [35] Gerenser, L.J.; Grace, J.M.; Apai, G.; and Thompson, P.M. *Surface Chemistry of nitrogen plasma-treated poly(ethylene-2,6-naphthalate): XPS, HREELS and static SIMS analysis*. Surface and Interface Analysis, 29, 12-22 (2000).
- [36] Hollander, A. and Behnisch J. *Vacuum-ultraviolet photolysis of polymers*. Surface and Coating Technology 98 (1998) 855-858.
- [37] Peng, G.; Yang, D.; and He, S. *Effects of VUV Radiation on Properties and Chemical Structure of Polyethylene Terephthalate Film*. J.I. Kleiman (ed.). Protection of materials and structures from space environment. 225-232 (2006) Springer.
- [38] Foerch, R. and Hunter, D.H. *Remote nitrogen plasma treatment of polymers: polyethylene, nylon 6,6, poly(ethylene vinyl alcohol), and poly(ethylene terephthalate)*. Polymer Science. 1992, A30, 279-286.
- [39] Grace, J.M. and Gerenser, L.J. *Plasma Treatment of Polymers*. Rochester, NY; Dispersion Science and Technology. Vol.24, Nos. 3&4, pp.305-341, 2003.
- [40] Gonzalez II, E.; Barankin, M.D.; Guschl, P.C.; and Hicks, R.F. *Remote Atmospheric-Pressure Plasma Activation of the surfaces of Polyethylene Terephthalate and Polyethylene Naphthalate*. Langmuir 2008, 24, 12636-12643.
- [41] WHO. *The World Health Report*. 2012, [http://www.sodis.ch/index\\_EN](http://www.sodis.ch/index_EN). (accessed August 2012).

- [42] Wegelin, M.; Canonica, S.; Alder, A.C.; Marazuela, S.; Suter, M.J.F.; Bucheli, Th.D.; Haefliger, O.P.; Zenobi, R.; McGuigan, K.G.; Kelly, M.T.; Ibrahim, P.; and Larroque, M. *Does Sunlight change the materials and content of polyethylene terephthalate (PET) bottles?*. Water Supply: Research and Technology-Aqua, 50.3, 2001.
- [43] Han, H. and Mayer, J.W. *Band gap shift in the indium-tin-oxide films on polyethylene naphthalate after thermal annealing in air*. Applied physics 100, 083715 (2006).
- [44] Guedri, L.; Ben Amor, S.; Gardette, J.L.; Jacquet, M.; and Rivaton, A. *Lifetime improvement of polyethylene naphthalate) by ZnO adhesive coatings*. Polymer Degradation and Stability 88 (2005) 199-205.
- [45] Kryszak, M.; Jayasekar, A.; Parekh, B.; Oliveira, L.; Debies, T.; Santhanam, K.S.V.; DiLeo, R.A.; Landi, B.J.; Raffaele, R.P.; and Takacs, G.A. *Gas-Phase Surface Functionalization of Carbon Nanotubes With UV Photo-Oxidation*. Polymer Surface Modification: Relevance to Adhesion, Vol. 5 (2009).
- [46] Rayonet. *Southern New England Ultra Violet company*.  
<http://www.rayonet.org/graphscharts.htm> (accessed October 25)
- [47] Feichtinger, J.; Kerres, J.; Schulz, A.; Walker, M.; and Schumacher, U. *Plasma modification of membranes for PEM fuel cells*. New Mat. Electrochem. Systems. 2002, 5, 155.
- [48] Okabe, H. *Photochemistry of Small Molecules*, John Wiley & Sons, New York, 1978.
- [49] Huffman, R.E. *Absorption cross-sections of atmospheric gases for use in aeronomy*. Can. J. Chem. 47, 1823-1834 (1969).

- [50] Lu, F. *Gas-Phase Surface Modification of Single-walled Carbon Nanotubes and Polymers*. MS. Thesis, Rochester Institute of Technology, Rochester, NY, 2010.
- [51] Skoog, D.A.; Holler, F.J.; and Crouch, S.R. *Principles of Instrumental Analysis*. 6th Edition. Belmont, CA. Thomson Brooks/Cole (2007).
- [52] Beamson, G. and Briggs, D. *High Resolution XPS of Organic Polymers*. Chichester, West Sussex: John Wiley, 1991.
- [53] Shimadzu Corporation. *ISR-2200 Integrating Spherical Attachment Manual*. 1996 p/n 206-61600.
- [54] Van Horn, B.L. and Winter, H. *Conoscopic Measurement of Birefringence and Orientation in Biaxially Stretched Polymer Films and Sheets*. *Macromolecules* 2003, 36, 8513-8521.
- [55] Holland, B.J. and Hay, J.N. *The thermal degradation of PET and analogous polyesters polyesters measured by thermal analysis-Fourier transform infrared spectroscopy*. *Polymers* 43 (2002) 1835-1847.
- [56] Krimm, S. *Infrared Spectra of High polymers*. *Fortschr. Hochpolym.-Forsch.*, Bd.2, S.51-172 (1960).
- [57] Laskarakis, A.; Gravalidis, C.; and Logothetidis, S. *FTIR and Vis-FUV real time spectroscopic ellipsometry studies of polymer surface modifications during ion beam bombardment*. *Nuclear Instruments and Methods in Physics Research B* 216 (2004) 131-136.
- [58] Wu, G.; Li, Q.; and Cuculo, J.A. *Fiber structure and properties of poly(ethylene-2,6-naphthalate) obtained by high-speed melt spinning*. *Polymer* 41 (2000) 8139-8150.

- [59] Wade Jr., L.G. *Organic Chemistry*. 7<sup>th</sup> edition. Upper Saddle River, NJ. Prentice Hall (2010).
- [60] Mittal, K.L. *Contact Angle, wettability and Adhesion*. Vol. 6. Hotei publishing; Leiden, The Netherlands (2009).
- [61] Malanowski, P. *Weathering of aromatic polyester coatings*. Ph.D. Dissertation, Eindhoven University of Technology, Universiteitsdrukkerij, 2009.
- [62] Conforti, P.F.; Yingling, Y.G.; and Garrison, B.J. *Computational studies of ultraviolet ablation of poly(methyl methacrylate)*. Journal of Physics: conference series 59 (2007) 322-327.
- [63] Rosario, R.; Gust, D.; Garcia, A.A.; Hayes, M.; Taraci, J.L.; Clement, T.; Dailey, J.W.; and Picraux, S.T. *Lotus Effect Amplifies Light-Induced Contact Angle Switching*. J. Phys. Chem. B (2004)., 1976, 46, 71.
- [64] Verhoeven, J.W. *Pure and Applied Chemistry*, 1996, Vol. 68, p.2223.
- [65] Inagaki, N.; Tasaka, S.; Narushima, K.; and Mochizuki, K. *Surface Modification of Tetrafluoroethylene-perfluoroalkyl Vinyl ether copolymer (PFA) by Remote Hydrogen Plasma and Surface Metallization with Electroless Plating of Copper Metal*. Macromolecules 32, 8566 (1999).
- [66] Vujnovic, V. and Wiese W.L. *A Critical Compilation of Atomic Transition Probabilities for Singly Ionized Argon*. J. Phys. Chem. Ref. Data, Vol.21, No.5, 1992.